NTNU
Norwegian University of
Science and Technology

Modelling a Multiphase Subsea Separation System

Torstein Alexander Bishop

Chemical Engineering and Biotechnology
Submission date: June 2016
Supervisor: Johannes Jäschke, IKP
Co-supervisor: Tamal Das, IKP

Norwegian University of Science and Technology
Department of Chemical Engineering

Norwegian University of Science and Technology
NTNU

Department of Chemical Engineering

Associate Prof. Johannes Jäschke

Modelling a Multiphase Subsea Separation System

Master's thesis

by
Torstein Bishop

Co-supervisor: Tamal Das

Trondheim, 10. juni 2016

Abstract

With the oil and gas industry changing rapidly and new oil-fields becoming less accessible, the demand for new technology and innovative thinking is increasing. With these challenges in mind a possible solution could be to further exploit the possibilities that lies within subsea processing and separation. In this thesis the main objective has been to develop a model for a Gas-Liquid Cylindrical Cyclone separator (GLCC-separator) for control and optimization purposes.

The model for the GLCC-Separator was created by splitting the separator into three parts; an inlet area, an upper part of the separator and a lower part of the separator. The inlet area determines the composition of the inlet flow to the separator by using an entrainment correlation, while the upper and lower part determines the separator performance. The models estimating the separator performance are based on an average droplet/bubble velocity estimated by the centrifugal and drag forces by assuming Stokes' law.

The GLCC performance was not validated with experimental data, but was tested against varying flow rates and inlet gas volume fractions in order to get a tentative understanding of how these factors affect the separation performance. The GLCC was then combined with a deliquidizer model to form a separation system. This system was optimized for inlet gas fractions and flow rates, with respect to the gas fraction in the outlet gas stream and the oil fraction in the outlet oil stream. The optimization variable was the ratio between the product streams of the deliquidizer.

The results from the simulations show that the performance of the GLCC is highly dependent on the inlet gas volume fraction and the inlet flow

rate. High flow rates and inlet gas volume fractions around 0.5 were found to yield poor performance. The simulations also revealed that the entrainment model overestimates the entrainment of gas into the liquid stream at certain combinations of inlet gas fractions and flow rates, thus reducing the operational boundaries of the model. It was also revealed that the entrainment model removed the possibility to explicitly control the outlet flow streams of the separator, which can make control and optimization problematic. The optimization of the separation system did however show that the deliquidizer manage to yield acceptable values for the gas fraction in the outlet gas stream and the oil fraction in the outlet oil stream.

Sammendrag

Olje og gass industrien er i stadig forandring og nye olje og gass felt blir stadig mindre tilgjengelige. Industrien tvinges dermed til å tenke nytt og komme opp med nyskapende teknologi for å overkomme disse problemene. En mulig løsning kan være å dra fordel av mulighetene innenfor subsea prosessering og seperasjon. Målet for dette arbeidet har vært å utvikle en model for en gass-væske sylindrisk syklon separator (GLCC-separator) med hensyn til optimaliserings og regulerings formål.

Modellen for GLCC-separatoren var utviklet ved å dele separatoren inn i tre fokusområder; innløpet til separatoren, den øvre delen og nedre delen av separatoren. Innløpet til separatoren beregner sammensetningen av strømmene inn i separatoren ved å bruke eksperimentelle korrelasjoner for gas- og væskemedrivning. Den øvre og nedre delen av separatoren beregner separatorens separasjonseffektivitet. Separasjonseffektiviteten er basert på gjennomsnittelige dråpestørrelser og dråpehastigheten er beregnet fra sentrifugal- og friksjonskraften gitt fra Stokes' lov.

Modellen ble ikke validert ved sammenligning med eksperimentelle data, men ble tested mot variendre strømningshastigheter og gassfraksjoner. Modellen for GLCC-separatoren ble så kombinert med en modell av en deliquidizer for å danne et subsea separasjonssystem. Dette systemet ble optimalisert med hensyn på å maksimere gassfraksjonen i gass strømmen og oljefraksjonen i oljestrømmen ut av systemet. Optimaliseringsvariabelen var forholdet mellom utstrømmene fra deliquidizeren.

Resultatene viser at separasjonsgraden i stor grad avhenger av instrømmene og gassfraksjonen i innløpsstrømmen, og gir dårligest separasjon ved en gassfraksjon på 0.5 og ved høye innløpstrømmer. Simuleringene

avslørte også at korrelasjonen for medrivning overestimerte medrivningen av gass inn i oljestrømmen, noe som reduserer modellens bruksområder. Det ble også avdekket at utløpstrømmene ikke kan eksplisitt bestemmes grunnet medrivningsmodellen. De optimaliserte driftsbetingelsene ga akseptable verdier av olje og gass i de respektive utløpsstrømmene.

Preface

This Master's thesis was written as the final part of my degree in chemical engineering at the Norwegian University of Science and Technology (NTNU).

I would like to thank my supervisor Johannes Jäschke for guidance, advice and valuable discussions during my work. I would also like to thank my co-supervisor, Ph.D candidate Tamal Das for help and feedback when writing this thesis. The Process Systems Engineering group at the Department of Chemical Engineering has let us take part in their work and meetings, which has been very educational and inspiring, and for that I am grateful.

I am also grateful to all my friends at NTNU. All that we have been through and experienced together is something I will cherish and never forget. The frequent coffee breaks and irrelevant discussions my friends have provided me with during the course of this thesis have been vital and for that I thank you!

Declaration of Compliance

I declare that this thesis is an independent work in agreement with the exam regulations of the Norwegian University of Science and Technology (NTNU).

Torstein Bishop, Trondheim, 10.06.2016.

Contents

List of Figures

List of Tables

List of Symbols

Latin letters

Symbol	Description	Unit
A_d	Projected droplet/bubble area	m^2
A_P	Inlet pipe cross-sectional area	m^2
A_N	Inlet nozzle cross-sectional area	m^2
a_c	Centrifugal acceleration	$m\ s^{-2}$
B_r	Radial location of maximum tangential velocity	-
C_D	Drag coefficient	-
C_{decay}	Decay factor for decreased vortex momentum	-
c	Droplet size correlation intercept	m
c_{eq}	Equality constraints	-
c_{in}	Inequality constraints	-
D_s	Separator diameter	m
d	Droplet diameter	m
d_{32}	Sauter-mean droplet diameter	m
E_l	Entrainment of liquid	-
E_g	Entrainment of gas	-
F_b	Gravitational buoyancy force	N
F_f	Frictional force	N
FS	Flow split	-
FS_{opt}	Optimal flow split	-
f	Frictional coefficient	$kg\ s^{-1}$
GR	Gas recovery	-
g	Gravitational acceleration	$m\ s^{-2}$

Symbol	Description	Unit
J	Cost/Objective function for optimization	-
k_{re-en}	Re-entrainment proportionality constant	m^2
L	Separator length	m
L_{DL}	Deliquidizer length	m
L_L	Length of lower part of GLCC separator	m
L_U	Length of upper part of GLCC separator	m
M_m	Molar mass	kg $mole^{-1}$
M_T	Total momentum flux	N s
M_t	Tangential momentum flux	N s
m	Droplet size correlation slope	h m^{-2}
p	Pressure	Pa
p_c	Critical pressure	Pa
q_B	Volumetric flow rate to bottom of GLCC from inlet	m^3 s^{-1}
q_g	Volumetric flow rate of gas	m^3 s^{-1}
q_{HPO}	Volumetric flow rate through heavy phase outlet	m^3 s^{-1}
$q_{HPO,DL}$	Volumetric flow rate through HPO of deliquidizer	m^3 s^{-1}
$q_{HPO,GLCC}$	Volumetric flow rate through HPO of GLCC	m^3 s^{-1}
$q_{HPO,S}$	Volumetric flow rate through HPO of system	m^3 s^{-1}
q_{in}	Inlet volumetric flow rate	m^3 s^{-1}
q_{LPO}	Volumetric flow rate through light phase outlet	m^3 s^{-1}
$q_{LPO,GLCC}$	Volumetric flow rate through LPO of GLCC	m^3 s^{-1}

Symbol	Description	Unit
$q_{LPO,S}$	Volumetric flow rate through LPO of system	$m^3\ s^{-1}$
q_o	Volumetric flow rate of oil	$m^3\ s^{-1}$
q_{re-en}	Volumetric re-entrainment flow rate	$m^3\ s^{-1}$
q_T	Volumetric flow rate to top of GLCC from inlet	$m^3\ s^{-1}$
q_{TL}	Total flow rate to the lower part of the GLCC	$m^3\ s^{-1}$
q_{TU}	Total flow rate to the upper part of the GLCC	$m^3\ s^{-1}$
R_c	Radius of vortex core with solid body rotation	m
Re	Reynolds number	-
R_{gc}	Universal gas constant	$J\ mole^{-1}\ K^{-1}$
R_i	Radius of gas-extraction pipe	m
R_{in}	Radius of GLCC inlet pipe	m
R_s	Separator radius	m
R_{gas}	Radius of gas core	m
R_{cap}	Capture radius is the same as R_{gas}	m
r	Radial coordinate	m
r_d	Droplet radius	m
r_{in}	Radial position for droplet at inlet	m
T	Temperature	K
T_c	Critical temperature	K
T_m	Maximum moment of tangential velocity	-
T_r	Reduced temperature	-
t	Time	s

Symbol	**Description**	**Unit**
u	Degree of freedoms	-
V_d	Volume of particle	m^3
V_m	Molar volume	m^3 mole
v	Velocity	m s^{-1}
v_g	Gas velocity	m s^{-1}
$v_{l,in}$	Inlet velocity in inlet pipe	m s^{-1}
v_r	Radial velocity	m s^{-1}
v_t	Tangential velocity	m s^{-1}
$v_{t,L}$	Tangential velocity in lower part of GLCC	m s^{-1}
$v_{t\,n}$	Tangential velocity at inlet nozzle	m s^{-1}
$v_{t,U}$	Tangential velocity in upper part of GLCC	m s^{-1}
v_t^{max}	Maximum tangential velocity	m s^{-1}
v_t^0	Initial tangential velocity	m s^{-1}
v_z	Axial velocity	m s^{-1}
$v_{z,L}$	Axial velocity in lower part of GLCC	m s^{-1}
$v_{z,U}$	Axial velocity in upper part of GLCC	m s^{-1}
W_f	Mass flow rate of annular liquid film	kg s^{-1}
W_l	Total liquid mass flow rate	kg s^{-1}
Wt_g	Weighting coefficient for gas	-
Wt_o	Weighting coefficient for oil	-
$\mathbf{x}$	State variables of separation system	m
Z	Compressibility factor	-
z	Spatial coordinate	m

Greek letters

Symbol	Description	Unit
α_{HPO}	Gas volume fraction in heavy phase outlet	-
α_{in}	Inlet gas volume fraction	-
$\alpha_{in\,L}$	Gas fraction entering lower part of GLCC	-
α_{LPO}	Gas fraction in light phase outlet	-
$\alpha_{LPO,GLCC}$	Gas fraction in LPO out of GLCC	-
$\alpha_{LPO,S}$	Gas fraction in LPO out of system	-
$\alpha'_{o,HPO}$	Oil fraction in HPO before re-entrainment	-
$\alpha'_{o,LPO}$	Oil fraction in LPO before re-entrainment	-
$\alpha_{o,HPO}$	Oil fraction in HPO	-
$\alpha_{o,HPO,S}$	Oil fraction in HPO out of system	-
$\alpha_{o,LPO}$	Oil fraction in LPO	-
$\alpha_{o,in\,U}$	Oil fraction entering upper part of GLCC	-
β	Smoothing parameter	-
Δ	Difference in the variables that follows	-
η_{Split}	Split efficiency	-
λ	Length scale	m
μ_c	Viscosity of continuous phase	Pa s
μ_g	Viscosity of gas	Pa s
μ_o	Viscosity of oil	Pa s

Symbol	**Description**	**Unit**
Ω	Swirl intensity decay number	-
ω	Acentric factor	-
π	Ratio of a circles circumference to diameter	-
π_1	Dimensionless gas velocity	-
Φ	Swirl number	-
ρ	Density	kg m^{-3}
ρ_c	Density of continuous phase	kg m^{-3}
ρ_d	Droplet density	kg m^{-3}
ρ_g	Gas density	kg m^{-3}
ρ_l	Liquid density	kg m^{-3}
σ	Surface tension	N m^{-2}
τ	Residence time	s
θ	Inclination angle of inlet pipe	rad
θ_v	Angle of vanes on swirl element to z-direction	rad

List of Acronyms

Acronym	**Description**
DL	Deliquidizer
GLCC	Gas-Liquid cylindrical cyclone separator
GVF	Gas volume fraction
HPO	Heavy phase outlet
LPO	Light phase outlet
LVF	Liquid volume fraction

1 Introduction

The oil and gas industry is changing rapidly, with unstable oil and gas prices, demand for more environmentally friendly operations plus oil and gas fields becoming less accessible. With these challenges in mind, the industry has an increasing demand for innovative thinking and new technology. One possible solution for these challenges can be further development of subsea technology and especially subsea separation. Where the oil and gas industry has previously relied heavily on conventional topside vessel-type separation technology, a technology that has not changed substantially over the recent years, the compact subsea separation systems offer a new and innovative technology. The conventional separators are bulky and heavy with expensive operating costs, however a compact separation system is a simple low-cost system with smaller dimensions that can be an economically attractive alternative to the conventional separation system [19]. Subsea separation technology offers increased oil and gas recovery, reduced topside facility costs and increased accessibility to remote oil fields [10, 25, 38]. This may then increase the economical lifetime of a field as well as allowing fields with lower economic potential to be developed. The use of subsea systems will also make it possible to have a viable production from smaller fields that can be tied together and fed back to a host facility for processing [38].

There are, however, also downsides, issues and challenges that has to be overcome when using compact subsea separation systems. Maintenance is more tedious and expensive compared to topside processing facilities due to the remote and deep locations of the system [28]. In order to reduce the probability of system malfunction that will lead to expensive maintenance

work, it is important to operate the system at its operational optimum. Optimization of the compact separation system therefore becomes important and this requires simple but accurate models that describes the system.

1.1 Objective of Master Thesis

The purpose of this thesis is to develop a model describing the separation performance of a Gas-Liquid Cylindrical Cyclone (GLCC) separator for control and optimization purposes. This model will then be combined with an already existing model of a deliquidizer to form a hypothetical compact subsea separation system that is optimized for different inlet gas fractions and flow rates. The main idea is that the GLCC separator will perform a bulk separation of an inlet stream to the system, where centrifugal forces will be the driving force behind separation process. The gas-rich stream will then be sent to the deliquidizer and further purified by separating out the oil-residue.

1.2 Previous Work

The thesis is a continuation of the specialization project completed in the fall of 2015. In this project a deliquidizer was modelled based on the models developed by Tyvold[41] based on first principles and using few empirical correlations. This deliquidizer is, as mentioned above, connected to the GLCC to form a compact separation system and therefore some of the contents in the specialization project report is reused in this thesis.

2 Literature Review

In order to make a model for a Gas-Liquid Cylindrical Cyclone(GLCC) separator to predict the separation efficiency for control and optimization purposes, a literature review was conducted to get an overview of the field of study on the GLCC's. Even though the first experiments started up in the mid 90's, the compact separators are still a developing technology for the oil and gas industry and therefore few studies are available on experimental data and on performance. The reason for this being the lack of knowledge on the complex multiphase hydrodynamics inside the separator. The main areas of research have been on how bubble/particle trajectory and droplet size affect the separation and how the geometry affects the performance. Mechanistic models of the flow have also been developed and studies on the flow fields inside the separator have been conducted. In the following sections a main overview of the research done in these areas will be presented.

2.1 Bubble Trajectory

Marti et al.[23] analysed the gas carry-under in a GLCC and attempted to generate a bubble trajectory model that predicts this phenomena and the separation efficiency of the separator in 1996. The model can thus calculate the trajectory of a bubble and determine whether it gets separated or not. The models developed were tested towards CFD simulations, which showed a good agreement with the model.

In 1998, Mantilla[22] improved the model for predicting gas carry-under presented by Marti et al.[23], in his master thesis. The model presented by

Marti et al. in 1996 only included a force balance in the radial direction, while the model presented by Mantilla included a force balance in the axial direction as well as the force balance in the radial direction. Mantilla also used improved correlations for the hydrodynamics in the separator. Comparisons between the old model, the modified model and CFD simulations showed that the improved model had a better agreement with the CFD simulations compared to the old model.

Molina et al.[27] presented a model in 2008 that predicted the liquid carry-over in a GLCC. The model builds on the models presented by Marti et al.[23] by determining the trajectory of the droplet in the upper part of the separator. The simulations from the model were compared against experimental data obtained from test rigs and the model showed a good agreement with the experimental data. The GLCC used for this model is somewhat modified compared to the GLCC's used in the previous models since it has an installed device, above the inlet, called an annular film extractor (AFE). The AFE consists of an opening in the separator wall that extracts the liquid from the upper part of the separator and a liquid boot where the liquid is collected before the liquid is sent to the liquid outlet stream through a return pipe.

In 2013 Gao et al.[11] studied the effects droplet size and droplet breakup have on the separation efficiency of a GLCC separator. The governing equation for the droplets in a flow field was described by the Reynolds stress turbulence model (RSM) while the droplet breakup was described by the Taylor analogy breakup model (TAB). The models were validated by experimental data from a test rig. The models and the experiment did show that the size of a droplet is highly dependent on the inlet velocity and has a great effect on the separation efficiency.

2.2 Geometry Effects

Movafaghian et al.[30] conducted both experimental and theoretical studies on how the inlet geometry, fluid properties and pressure affect the hydrodynamics of the GLCC separator. The hydrodynamics govern the equilibrium liquid level, zero-net liquid flow hold-up and the operational envelope for liquid carry-over. The results show that for high superficial gas velocities (> 7 m/s) a dual-inlet configuration is superior to the single-inlet configurations, however at lower superficial gas velocities the results for a dual-inlet and a single-inlet configuration are similar.

In 2013 Hreiz et al.[17] conducted a study on how the design of the nozzle effects the performance of the GLCC separator. The study was done by using three different nozzles and the results show that a reduction of the inlet nozzle highly affects the performance of the GLCC. With an insufficient or too severe area reduction liquid carry-over will occur, proving that the nozzle design has a huge impact on the separator performance.

2.3 Mechanistic Modelling

Taitel and Dukler[39] presented in 1976 models that determined the flow regime transitions in a two-phase gas-liquid flow. These models are based on physical concepts and also take into account the effect that pipe size, fluid properties and angle of inclination have on the flow regime. The flow regimes considered are intermittent, stratified smooth, stratified wavy, dispersed bubble and annular-annular dispersed liquid flow.

In 1995 Kouba et al.[19] studied the design and performance of the GLCC separators. Initial mechanistic models for the flow behaviour and bubble

trajectory were presented and compared with experimental data. These models were, at the time, the state-of-the-art for design and predicting the performance of a GLCC separator, as well as fundamental for future research.

Arpandi[2] improved the mechanistic model presented by Kouba et al.[19] in 1995, for predicting the flow behaviour in a GLCC separator. The model consists of sub-models describing important properties such as the gas-liquid interface shape, equilibrium liquid level, the zero-net liquid hold-up as well as a procedure to calculate the operational envelope for the liquid carry-over. The models were verified by comparison with experimental data and showed a good agreement.

In his master thesis in 1998 Gomez[13] presented an improved mechanistic model for the flow behaviour and bubble trajectory inside a GLCC separator. The models that were improved are the models from Kouba et al.[19] and Marti et al.[23]. The model improvements were done by including an extensive nozzle analysis of the GLCC, an analytical model for the vortex interface shape and a unified particle trajectory model for bubbles and droplets. Gomez also developed a state-of-the-art GLCC computer simulator with respect to design purposes for the industry.

In 2004 Gomez et al.[14] developed a mechanistic model that describes the flow inside a GLCC separator. This model includes a sub-model for the swirl intensity decay that predicts the decay of the swirl throughout the separator, as well as a sub-model for the swirling flow velocity distribution. This is sub-model calculates the distribution for the tangential, radial and axial velocity throughout the separator.

Rosa et al.[35] presented in 2001 a model for design purposes with respect to liquid carry-over and gas carry-under of a new modified cyclone

separator. This separator consists of three sub-separators. The first sub-separators, called the primary separator, consists of a chamber with an inlet and resembles a traditional separator. The second sub-separator, called the secondary separator, is a long helix-channel while the third sub-separator is a liquid pool that uses the concept of gravity separation in order to separate out the remaining gas bubbles

2.4 Flow Field

By using a Laser Doppler Anemometer (LDA) system, Millington and Thew[26] reported in 1987 axial and tangential velocity profiles inside a cylindrical separator. They made an important discovery that the vortex inside a cylindrical separator is a forced vortex and that the axial distance between the liquid exit and the inlet plays a crucial role in determining the carry-under performance and design specifications for the separator.

Algifri et al.[1] studied in 1988 turbulence measurements in decaying swirl flow in a pipe by using a hot-wire probe and air as the working fluid. The results from this study suggested that the tangential velocity, except in the vicinity of the wall, can be approximated as a Rankine vortex.

The gas core stability and configuration were studied by Bandyopadhyay et al.[5] in 1994. The results from this study shows that the gas core configuration in the center of the cylindrical separator is sensitive to the relative angle between the inlet and outlet and the aspect ratio of the cylinder.

Chang and Dhir[7] conducted in 1994 single-phase swirling flow measurements with air as working fluid. From the results they concluded that the axial velocity shows an existence of a flow reversal region in the central

part of the cylinder. The results also showed that the velocity increases towards the wall and that the tangential velocity is a combination of a free and forced vortex and the swirl intensity decays in an exponential manner.

In 1996, Kurokawa & Ohtaki[21] studied the flow characteristics in a cyclone separator and its effect on the gas-separation efficiency. From this study the existence of a complex velocity profile was confirmed. The study highlights three regions in the vortex flow, namely, a forced vortex that generates a jet region in the center of the pipe with an extremely high swirl velocity, a free vortex towards the walls of the separator and a transition region with high swirl velocity.

Hreiz et al.[16] studied in 2014 the swirl flow in a GLCC separator and the flow field was first characterized qualitatively by flow visualizations and the findings were then confirmed quantitatively by LDA measurements. From this study it is shown that the vortex core presents complex hydrodynamics and is characterized by an alternation between a laminar and a turbulent state. The laminar state is associated by flow in one direction while the turbulent state induces velocities in opposite directions. The study also concludes that double flow reversal, contrary to previous hypothesis, yields good separation performance in the cyclone and that the use of multiple inlets will favour the double flow regime.

2.5 Summary

It is clear that the focus on the GLCC has been to study and determine the characteristics of the flow field inside the separator as well as generating models to describe the flow. Droplet trajectory inside the separator has

also had a large focus as well as how the geometry of the separator and inlet nozzle affects the flow and trajectory inside the GLCC. There is however scarce amounts of literature on the efficiency of a GLCC separator in order to determine the quality of the outlet gas and liquid streams. This sets the foundation for this thesis, where the objective is to model a GLCC so the performance can be analysed and efficiency determined as well as the model is suited for control and optimization.

3 Theory

The basic theory for the separation process is presented in this chapter. The main phenomena that can affect the separation are sedimentation, coalescence and diffusion. However in this thesis only sedimentation is considered and the theory is presented in Section 3.1. The parameters used to evaluate the separation performance of the separators are presented in Section 3.2

3.1 Sedimentation

Droplets or bubbles of a dispersed phase in a colloidal dispersion that has a density that differs from the density of the continuous phase will sediment or cream due to gravitational forces. The rate at which the particles will sediment or cream are mainly given by the size and density of the particle. A particle with a volume V_d and density ρ_d dispersed in a continuous phase with density ρ_c, will be exposed to the gravitational buoyancy force, F_b, expressd as [29]:

$$F_b = V_p(\rho_d - \rho_c)g \tag{3.1}$$

where g is the gravitational acceleration and the main driving force behind the sedimentation process. When $F_b < 0$ the particle will rise and creaming will occur and when $F_b > 0$ the particle will sink as sedimentation occurs. Due to a frictional force, F_f, caused by the viscosity of the continuous phase the motion of the particle will retard. The velocity of the droplets will initially increase rapidly, but the friction force is proportional to the velocity, v, and therefore the particle will nearly instantaneously

reach its terminal velocity [29]. The frictional force can be expressed as [18]:

$$F_f = -\frac{1}{2} C_D \rho_c A_d v|v| \tag{3.2}$$

where A_d is the projected area of the particle, C_D is the drag coefficient and v is the relative velocity of the particle to the surrounding fluid. The drag coefficient is dependent on the relative velocity of the particle to the surrounding fluid and if laminar flow is assumed the drag coefficient can be given by Stokes' law [29]:

$$C_D = \frac{24}{\mathrm{Re}} \tag{3.3}$$

If the particle is assumed to be spherical the Reynolds number, Re, can be expressed as [18]:

$$\mathrm{Re} = \frac{2 r_p \rho_c v}{\mu_c} \tag{3.4}$$

where r_d is the diameter of the particle and μ is the viscosity of the fluid. By inserting Equations 3.4 and 3.3 into 3.2 and equating Equations 3.2 and 3.1, an explicit expression for the terminal velocity of the particle can be expressed by:

$$v = \frac{2\, r_d^2\, (\rho_d - \rho_c) g}{9 \mu_c} \tag{3.5}$$

3.2 Separation Efficiency

It is necessary to define measures of separation efficiency in order to evaluate the performance of a separator and the measures for separation efficiency used in this thesis will be the gas recovery and split efficiency. These measures are the same as the ones used in the specialization project during fall 2015 [6] and they are adapted from the measures used by Tyvold in his Master's thesis [41]. If a separator with an inlet stream, light phase outlet (LPO) and a heavy phase uutlet (HPO) is considered, gas recovery is defined as the fraction of gas that is kept in the LPO and can be expressed as:

$$GR = \frac{\alpha_{LPO}\, q_{LPO}}{\alpha_{in}\, q_{in}} \tag{3.6}$$

where α_{LPO} and q_{LPO} are the gas volume fraction and volumetric flow in the LPO and α_{in} and q_{in} are the gas volume fraction and volumetric flow into the separator. From Equation 3.6 it is clear that the gas recovery is one of there is no gas in the heavy phase Outlet and zero if there is no gas in the light phase outlet.

The split efficiency is a measure of how much of the oil and gas that exits through its desired outlet and is defined as:

$$\eta_{Split} = 1 - \frac{(1-\alpha_{LPO})\, q_{LPO} + \alpha_{HPO} q_{HPO}}{q_{in}} \tag{3.7}$$

where α_{HPO} and q_{HPO} are the gas volume fraction and volumetric flow in the heavy phase outlet. From Equation 3.7 it is clear that the efficiency is one if the HPO is pure liquid and the LPO is pure gas.

4 Description of Model

In this chapter the models for the entire separation system are presented as well as the assumptions behind them. The hypothetical separation system that is studied in this thesis is presented in Section 4.1, while the models for the GLCC separator and deliquidizer are presented in Sections 4.2 and 4.3 respectively.

In order for the model to produce any output it will need input variables and parameters. The inputs needed are fluid properties such as density, viscosity, surface tension as well as separator dimension and empirical parameters. The inputs needed for the simulations are described and presented in Section 4.4.

In this thesis there has been assumed no pressure drop through the separators, meaning that any density differences for the gas phase has been neglected and that all flows are considered as volumetric flows.

4.1 Separation System

The hypothetical separation system studied in this thesis is presented in Figure 4.1. A multiphase stream from an oil/gas well will enter the system at the GLCC, where a bulk separation of the stream will happen. The gas stream will leave the GLCC through the light phase outlet stream, $q_{LPO,GLCC}$, while the oil stream will leave the GLCC through the heavy phase outlet stream, $q_{HPO,GLCC}$. The deliquidizer will then further purify the gas stream from the GLCC by separating out any oil residue the GLCC failed to separate. The gas stream will leave the deliquidizer through the light phase outlet, $q_{LPO,S}$, where it will be sent to topsite facilities. The

oil will leave the deliquidizer through the heavy phase outlet, $q_{HPO,DL}$, where it will be mixed with the oil stream from the GLCC separator and sent for further treatment or processing.

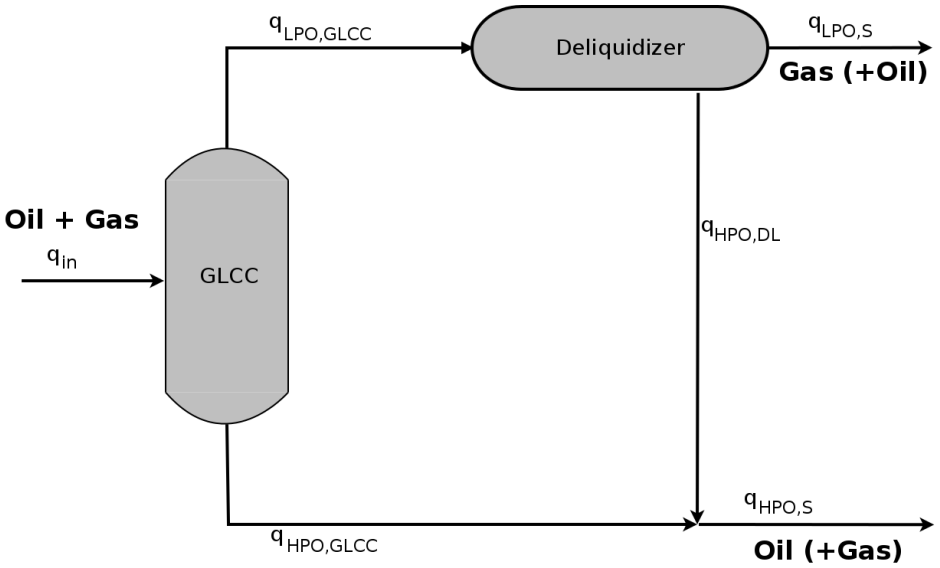

Figure 4.1: Flow diagram for the separation system that consists of two separators. The GLCC separator is designed to perform bulk separation while the deliquidizer is a swirl separator designed for a continuous gas phase and will separate out the oil residue from the GLCC separator.

It is also possible to include a degasser in a system presented here, which will further purify the oil stream from the GLCC by separating out gas residue. However, modeling such a separator is outside the scope of this Master Thesis and Kristiansen et al.[20] showed that such a separator will be redundant for some operating conditions.

4.2 Gas-Liquid Cylindrical Cyclone Separator

The model for the GLCC separator is based on centrifugal forces acting on oil droplets and gas bubbles. The size of the the droplets and bubbles are given by average sizes. An entrainment correlation is used to determine the inlet conditions to the separator.

The inlet to the GLCC is inclined and fitted tangentially, which will generate a vortex inside the separator, see Figure 4.2. Due to the density difference between oil and gas, oil will be pushed towards the separator walls and flow downwards, while gas will travel towards the centre of the separator and flow upwards. Since gas will be flowing upwards and oil will be flowing downwards, gas will be the continuous phase in the upper part, while in the lower part oil will be the continuous phase, see Figure 4.3.

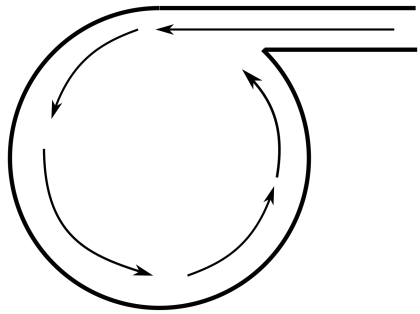

Figure 4.2: A top-down view of the GLCC separator highlighting how a vortex is formed as a result of the tangential inlet.

The angle of attack when developing a model for the GLCC has been to split up the separator into three areas; the inlet area, the upper part and

the lower part of the separator. The inlet area is used to determine the amount of flow flowing upwards and downwards in the separator, while the upper and lower part of the separator are considered as separate swirl separators. Thorough descriptions of the inlet area, lower and upper part of the separator along with major assumptions are given in Sections 4.2.1, 4.2.6 and 4.2.7 respectively.

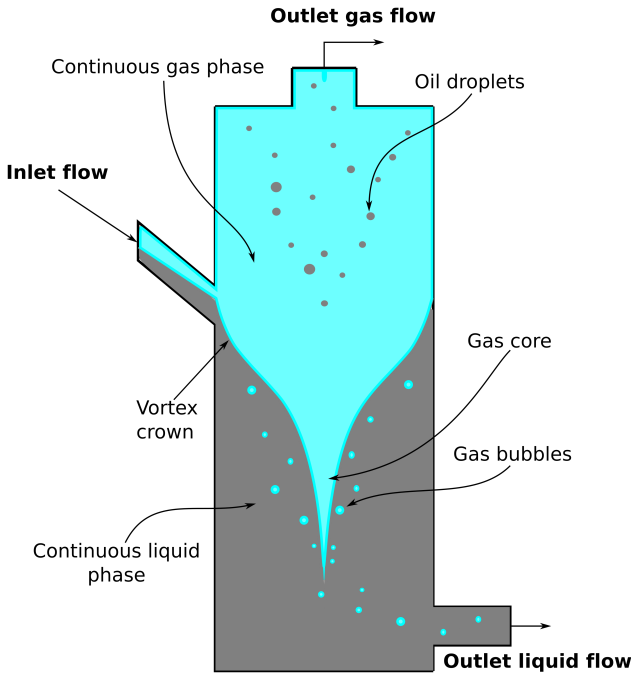

Figure 4.3: Illustration of the GLCC separator, with the inlet pipe, lower part with a continuous liquid phase and dispersed gas bubbles and the upper part with continuous gas phase and dispersed oil droplets.

4.2.1 Inlet Area Analysis

Due to the varying complex flow patterns that occur in the inlet, obtaining an analytical expression for the conditions inside the inlet becomes a demanding task. However, since the inlet area determines the incoming gas-liquid distribution in which the GLCC performance is highly dependent on, performing an analysis of the inlet conditions becomes critical[13].

The inlet pipe is, as mentioned earlier, inclined, which has been proven to increase the performance of the separator[19]. The inclination of the inlet pipe causes the liquid stream to spiral below the inlet, which will prevent liquid in blocking the inlet flow of gas into the upper part of the separator. However, the inclined and tangentially fitted inlet can, under certain flow conditions, promote droplet formation in the upper part and bubble entrainment in the lower part of the separator. At the end of the inlet pipe there is a reduced area nozzle, through which the flow enters the separator chamber, see Figure 4.4. The area at the inlet is reduced in order to accelerate the inlet flow, which will increase the tangential velocity, resulting in better separation performance[15].

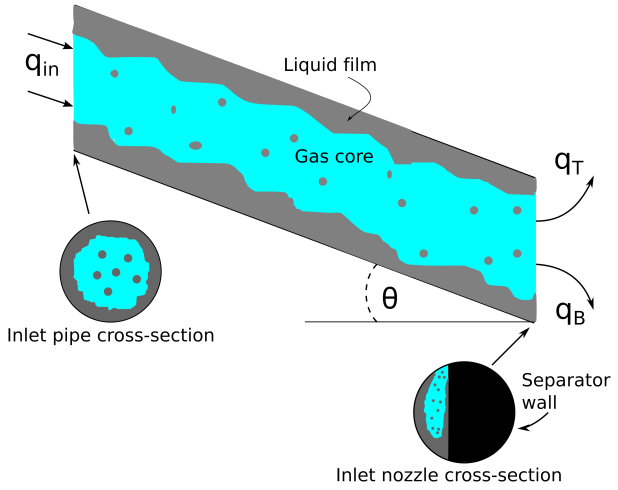

Figure 4.4: Schematic of the inlet pipe with an inclination angle, θ. The pipe has an inlet flow, q_{in} and two outlet flows. q_B flows down to the lower part of the GLCC and consists mainly of liquid and q_T flows to the upper part and consists mainly of gas. The flow is assumed to be annular, with a liquid film around the wall and gas core with entrained liquid droplets.

Flow patterns at the inlet of the GLCC are typically stratified, slug, dispersed bubble or annular flow, however in this thesis the inlet flow is assumed to be annular. Annular flow can be described as a liquid film moving along the pipe wall and a fast moving gas core that will contain entrained liquid droplets, see Figure 4.4. By assuming annular flow, the entrainment of liquid droplets into the gas phase can be defined as[43]:

$$E_l = \frac{W_l - W_f}{W_l} \tag{4.1}$$

where W_l is the total liquid mass flow and W_f is the liquid mass flow in

the film along the wall. Paleev and Fillippovich[32] defined the following empirical equation in order to calculate the amount of liquid in the film along the wall:

$$\frac{W_f}{W_l} = 0.985 - 0.44 \log\left(\pi_1 \times 10^4\right) \tag{4.2}$$

where π_1 is a dimensionless gas velocity. Inserting Equation 4.2 into the definition of entrainment, Equation 4.1, yields the following equation for calculating the liquid entrainment:

$$E_l = 1 - \left(0.985 - 0.44 \log\left(\pi_1 \times 10^4\right)\right) \tag{4.3}$$

where π_1 is given from Wallis' entrainment correlation[44]:

$$\pi_1 = \frac{v_g \mu_g}{\sigma} \left(\frac{\rho_g}{\rho_l}\right)^{1/2} \tag{4.4}$$

In Equation 4.4 v_g is the gas velocity, μ_g is the viscosity of the gas, σ is the surface tension between gas and liquid, ρ_g is the gas density and ρ_l is the liquid density.

Due to the scarcity of correlations estimating the amount of dispersed gas bubbles in the liquid flow to the lower part of the separator, it has been assumed in this thesis that the entrainment of gas into the downwards liquid flow is the same as the entrainment of liquid into the upwards gas flow $E_g = E_l$.

By having an estimate for the amount of liquid flowing upwards and the amount of gas flowing downwards, the downwards flow, q_B, and the upwards flow, q_T, can be calculated from:

$$q_T = \alpha_{in}\, q_{in}(1 - E_g) + E_l\,(1 - \alpha_{in})q_{in} \tag{4.5}$$

$$q_B = (1 - \alpha_{in})\, q_{in}(1 - E_l) + \alpha_{in}\, E_g\, q_{in} \tag{4.6}$$

where q_{in} is the inlet volumetric flow and α_g is the inlet gas fraction. The gas volume fraction in the flow to the lower part of the separator, $\alpha_{in\,L}$, and the oil volume fraction in the gas flow to the upper part of the separator, $\alpha_{o,in\,U}$, can be calculated from:

$$\alpha_{in\,L} = \frac{\alpha_{in} E_g\, q_{in}}{q_B + q_o} \tag{4.7}$$

$$\alpha_{o,in\,U} = \frac{E_l\,(1 - \alpha_{in})q_{in}}{q_T + q_g} \tag{4.8}$$

q_o is the flow rate of oil that has been separated in the upper part of the separator and is flowing down to the lower part. Likewise q_g is the flow rate that has been separated in the lower part of the separator and is flowing up to the upper part of the separator. Due to the combined nature of the upper and lower part of the separator that result in computational difficulties, these values will be neglected when calculating the residence time and the axial velocity of the separator. These flows will also be small compared to q_B and q_T, and this assumption is thus considered not to have a large affect on the results.

4.2.2 Axial Velocity

Axial Velocity

The swirling motion and tangential velocity inside the lower part of a GLCC separator promotes pressure gradients in an axial direction, which in turn will influence the flow field and yield complex flow phenomena inside the separator. The swirl intensity has a large impact on the flow regime inside the separator, where low intensities results in a forward flow across the cross-sectional area of the separator. High swirl intensities will, on the other hand, result in flow reversal near the centre of the separator[22]. The swirl intensity inside a GLCC separator is usually high, which means that the axial flow will usually be of the latter. Chang and Dhir[7] studied the flow field inside tubes and showed that from the centre and towards the wall, the velocity will increase to a maximum followed by a decrease towards the wall. Close to the centre, at the interface between the liquid and gas core, at R_{gas}, flow reversal will occur, see Figure 4.5.

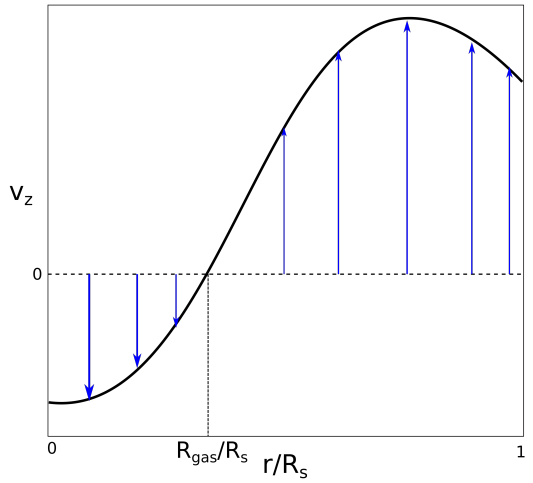

Figure 4.5: Axial velocity, v_z, as a function of the radial position in the lower part of a GLCC separator with radius R_s. The profile illustrates the area of flow reversal, $r/R_s < R_{gas}/R_S$, as well as increase of velocity towards a maximum before decreasing towards the wall, for $r/R_s > R_{gas}/R_s$.

The axial velocity for the liquid in the lower part of the GLCC separator has been somewhat simplified by assuming an annular plug flow. This implies that there is no friction between the separator walls and the fluid, nor between the plug flow and the gas flow in the gas core moving in the opposite direction. The assumption also implies that the axial velocity will be unaffected by the swirling motion in the fluid and that there is no back mixing of the fluid. Turbulence is also neglected by using time-averaged velocities. The axial velocity for the lower part of the GLCC separator is illustrated in Figure 4.6a) and is given by:

$$v_{z,L} = \frac{q_B}{\pi(R_s^2 - R_{gas}^2)} \tag{4.9}$$

where q_B is the volumetric flow rate to the lower part of the separator from the inlet pipe, R_s is the separator radius and R_{gas} is the radius of the gas core and given in Equation 4.24.

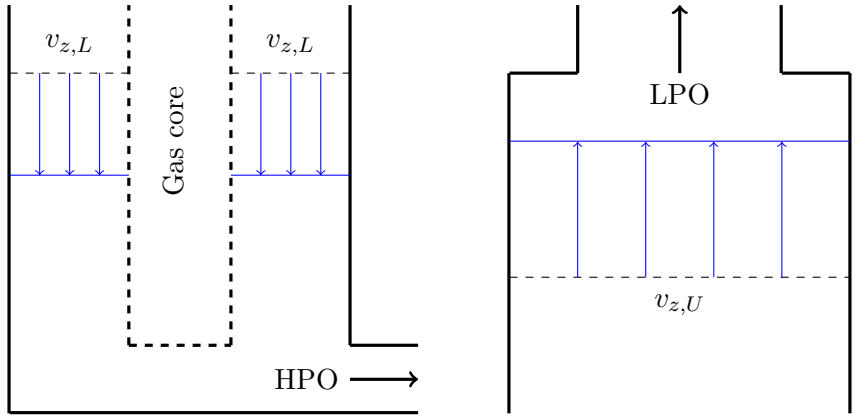

(a) Lower Part of GLCC. (b) Upper Part of GLCC.

Figure 4.6: Axial velocity profile for the lower part, a), and for the upper part, b), of the GLCC separator.

For the upper part of the separator, where gas is the continuous phase, there will also be swirling motions that will lead to complex flow phenomena. However, the axial velocity for the upper part will also be simplified by assuming an annular plug flow, with the same assumptions described above for the axial velocity for the lower part. The axial velocity for the upper part of the GLCC separator is illustrated in Figure 4.6b) and is given by:

$$v_{z,U} = \frac{q_T}{\pi R_s^2} \tag{4.10}$$

where q_T is the volumetric flow rate to the upper part of the separator

from the inlet pipe.

Even though the velocity profiles are a simplification of what is realistic inside such a separator, it is expected to be sufficient for this case. The reason being that the aim is to estimate the separator performance and the axial velocity mainly affects the performance by determining the residence time of the droplets and bubbles as well as the tangential velocity, in which case the average velocity is assumed to be sufficient. For optimization and control purposes it is desirable to control the axial velocities and the outlet flows of an separator by using a flow split. This will, however, not be possible in this model because the entrainment analysis determines the split and by using a flow split the system would become over-specified.

4.2.3 Tangential Velocity

The tangential inlet to the GLCC separator generates a vortex inside that will be the driving force behind the separation process. The centrifugal acceleration from the vortex forces the denser fluid towards the separator wall, while the lighter fluid will travel towards the separator center. The centrifugal acceleration is defined as:

$$a_c(r) = \frac{v_t(r)^2}{r} \tag{4.11}$$

where $v_t(r)$ is the tangential velocity of the fluid. Through experiments, the vortex in the lower part of the separator can be described as a Rankine Vortex[1, 7, 21, 26]. A Rankine vortex has a velocity profile that can be divided in two regions, one inner region with a solid body rotation, also known as a forced vortex, and an outer region with a free vortex[12]. The Rankine vortex is illustrated in Figure 4.7.

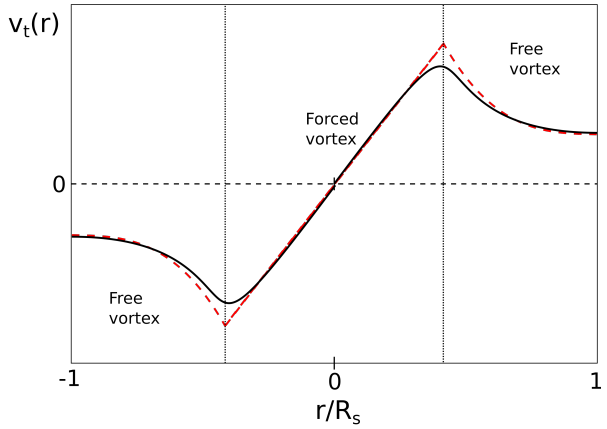

Figure 4.7: Tangential velocity, v_t, as a function of the radial position inside the GLCC separator with radius R_s. The dashed line represents the velocity of a Rankine vortex, while the solid line represents the used equation for the tangential velocity. The figure also illustrates the areas of forced and free vortex.

The tangential velocity can be expressed by the following equation proposed by Algifri et al.[1]:

$$v_{t,L}(r) = \frac{T_m}{\frac{r}{R_s}} \left(1 - \exp\left[-B_r \left(\frac{r}{R_s} \right)^2 \right] \right) \cdot v_{z,L} \tag{4.12}$$

where T_m is related to the maximum moment of the tangential velocity and B_r is related to the radial location of the maximum tangential velocity. Based on experimental data, Mantilla[22] presented the following correlations to determine the values of T_m and B_r:

$$T_m = 0.9\,\Omega - 0.05 \tag{4.13}$$

$$B_r = 3.6 + 20\exp\left(-\frac{\Omega}{0.6}\right) \tag{4.14}$$

where Ω is the swirl intensity decay number that takes into account the decay of the vortex from momentum loss due to stress from the pipe wall. Chang and Dhir suggested the following correlation for the swirl intensity decay number[7]:

$$\Omega = 1.48\left(\frac{M_t}{M_T}\right)^{0.93}\exp\left[-0.113\left(\frac{M_t}{M_T}\right)^{0.35}\left(\frac{z}{D_s}\right)^{0.7}\right],\ \text{for } z/D_s \geq 2 \tag{4.15}$$

where z is the axial location inside the separator and D_s is the diameter of the GLCC. The reason for the condition $z/Ds \geq 2$ is because at axial positions close to the inlet, the swirl decays at a much lower rate and the swirl intensity is nearly constant over a small distance downstream from the inlet[7]. M_t/M_T is the ratio between the tangential momentum flux and the total momentum flux at the inlet and is given by[14]:

$$\frac{M_t}{M_T} = \frac{v_{t\,n}}{v_z} \tag{4.16}$$

where $v_{t\,n}$ is the tangential velocity of the liquid at the inlet nozzle and can calculated from[23]:

$$v_{t\,n} = v_{l,\,in} = \frac{A_P}{A_N}\cos(\theta) \tag{4.17}$$

where $v_{l,in}$ is the liquid velocity in the inlet pipe, A_P is the cross-sectional area of the inlet pipe and A_N is the cross-sectional area of the inlet nozzle.

For the upper part of the GLCC separator the tangential velocity can be represented as a forced vortex, which has a linear relationship with the radial location and can be expressed as[27]:

$$v_{t,U}(r) = v_t^{max}(z)\left(\frac{r}{R_s}\right) \tag{4.18}$$

where v_t^{max} is the maximum tangential velocity, which occurs at the wall of the separator, and is given as[15]:

$$v_t^{max}(z) = \frac{3}{2}\, v_{z,U}\Omega \tag{4.19}$$

Ω is the swirl intensity decay number and is given in Equation 4.15. However in this case the 1.48 constant in front of the exponential expression is changed to 0.01. This is done based on the fact that gas will have a lower momentum than being the case for the liquid vortex, thus adjusting the equation for a gas vortex.

4.2.4 Radial Velocity

As mentioned in Section 4.2.3 the centrifugal acceleration is expected to be the driving force behind the separation process inside the separator. If the fluid is assumed to be in the Stokes' regime, Equation 3.5 can be rewritten by inserting Equation 4.11, which will give the following equation for the radial velocity, v_r, of an droplet or bubble:

$$v_r(r,z) = \frac{2\,r_d^2\,(\rho_d - \rho_c)}{9\mu_c}\frac{v_t^2(r,z)}{r} \tag{4.20}$$

where r_d is the droplet/bubble radius, μ_c is the viscosity of the continuous phase, ρ_d and ρ_c are the densities of the dispersed and continuous phase respectively. The radial velocity in Equation 4.20 is the relative velocity of the droplet/bubble to the continuous phase, but in this thesis any radial motion in the fluid is neglected, thus the radial velocity to the droplet/bubble is approximated as the absolute radial velocity. This assumption is expected to be acceptable, since the radial velocity of the fluid has been reported to be three orders of magnitude smaller than the tangential and axial velocity inside such separators[7, 14]. Other mass transfer phenomena, like diffusion, are not taken into account for the radial velocity, because it is expected that the centrifugal acceleration will affect the droplets/bubbles to a much larger extent than other transfer laws.

4.2.5 Droplet Size

The size of the droplets/bubbles affects the separation process, as can be seen from Equation 4.20. The droplets/bubbles are assumed to be formed in the annular flow in the inlet pipe by waves that form on the surface of the liquid film[40]. The formation of bubbles/droplets are expected to occur predominantly due to the velocity, surface tension and density of the phases. For annular flows the Sauter-mean diameter, d_{32}, is expected to represent the droplet/bubble size and can be expressed as[33]:

$$d = d_{32} = \left(\frac{1}{v_g}\right)\left(\frac{0.14\,\lambda\,\sigma}{\rho_g}\right)^{0.5} \tag{4.21}$$

where λ is a length scale presented by Azzopardi[3] and is expressed as:

$$\lambda = \left(\frac{\sigma}{\rho_l \, g} \right)^{0.5} \tag{4.22}$$

Equations 4.21 and 4.22 are expressed for determining the droplet size. In order to calculate the size of bubbles it is assumed that the same equations can be used, but with swapped indices for velocity and density.

4.2.6 Equation of Motion: Lower Part

As mentioned in the introduction to this chapter, the angle of attack when modeling a GLCC separator was to consider the upper and lower part as two separate swirl separators. The lower part of the separator is thus considered as a swirl separator with liquid being the continuous phase and gas bubbles being the dispersed phase. The lower part will consist of swirling liquid with a swirling gas core in the centre of the separator. The liquid level, or vortex crown, will touch and rise somewhat upwards the walls due to the centrifugal forces, see Figure 4.3 for an illustration.

The goal of the model is to calculate the separation efficiency of the GLCC separator. This is done by determining the radial inlet position, r_{in}, of a gas bubble that enters the lower part from the inlet nozzle and will travel sufficiently enough towards the separator centre to reach the gas core just before the outlet, see Figure 4.8. This analysis is done by integrating the radial velocity, given by Equation 4.20, and the axial velocity, given by Equation 4.9, from $t = 0$ to $t = \tau$. τ is the residence time of the bubble in the separator and can be expressed as:

$$\tau = \frac{\pi(R_s^2 - R_{cap}^2)L_L}{q_b} \tag{4.23}$$

where L_L is the length of the lower part of the separator.

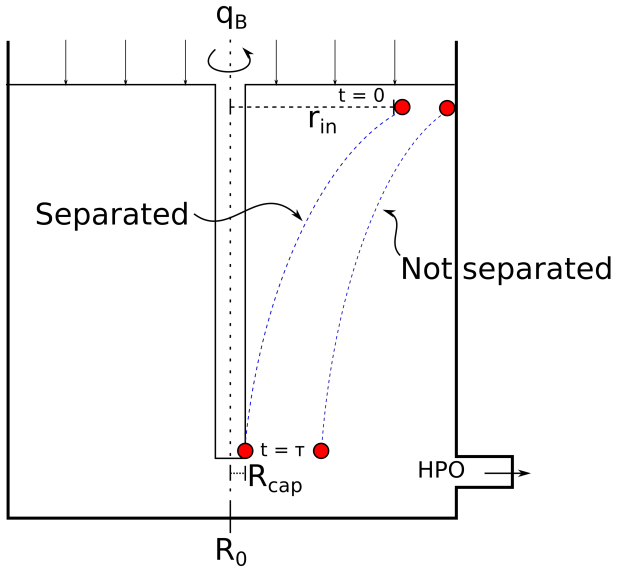

Figure 4.8: Gas bubbles entering the lower part at $r < r_{in}$ at $t = 0$ will reach the gas core, R_{cap}, at $t = \tau$ or before and be separated. Bubbles entering at $r > r_{in}$ will not be separated and leave through the HPO.

In Equation 4.23 R_{cap} is the "capture" radius or the radius of the gas core and is given by[22]:

$$R_{cap} = 0.5 - \frac{0.65}{e^{0.6\Omega}} \tag{4.24}$$

The gas core radius will in reality decrease downwards the separator, but

is assumed to be constant through out the length of the lower part of the separator in this thesis. Another assumption is that the liquid level of the rotating liquid is assumed to be flat instead of rising upwards the walls. Even though these assumptions differ from reality, they are made in order to reduce the computational time while integrating in order to make the model more suited for optimization and control.

The integration of the radial and axial velocity is done in MATLAB with the fourth order explicit Runge-Kutta integrator with constant time steps. The integral time is divided into 10 equal time-steps, $h = \tau/10$, and the radial and axial position for the bubble at r_{n+1} and z_{n+1} is calculated from the previous position, r_n and z_n. The set up for the integrator is[8]:

$$
\begin{aligned}
r_{n+1} &= r_n + \frac{h}{6}(k_1 + 2k_2 + 2k_3 + k_4) \\
k_1 &= v_r(t_n, r_n) \\
k_2 &= v_r(t_n + \frac{h}{2}, r_n + \frac{k_1}{2}) \\
k_3 &= v_r(t_n + \frac{h}{2}, r_n + \frac{k_2}{2}) \\
k_4 &= v_r(t_n + h, r_n + k_3)
\end{aligned}
\tag{4.25}
$$

$$
\begin{aligned}
z_{n+1} &= z_n + \frac{h}{6}(l_1 + 2l_2 + 2l_3 + l_3) \\
l_1 &= v_z(t_n, z_n) \\
l_2 &= v_z(t_n + \frac{h}{2}, z_n + \frac{l_1}{2}) \\
l_3 &= v_z(t_n + \frac{h}{2}, z_n + \frac{l_2}{2}) \\
l_4 &= v_z(t_n + h, z_n + l_3)
\end{aligned}
\tag{4.26}
$$

where $v_r(t, r)$ and $v_z(t, z)$ are the radial and axial velocity of the bubble respectively. The details of the MATLAB function can be found in Appendix E.3.1.

Since the inlet radial position, r_{in}, is unknown and the outlet radial position is known, R_{cap}, the inlet radial position is used by integrating the axial and radial velocity backwards. In other words, integrating from $t = \tau$ to $t = 0$ to find the inlet radial position for a bubble that will manage to reach the gas core just before reaching the outlet. Forward integration of the velocities could have been done by using the *shooting method*, however due to the nature of the radial velocity, $\rho_d < \rho_c$ in Equation 4.20, the velocity will be negative, which will cause implications for the integrator if negative radii are obtained.

When the inlet radial position, r_{in}, is found the gas volume fraction (GVF) in the heavy phase outlet (HPO) can be found. This is found by assuming that all gas bubbles entering the lower part of the separator at $r > r_{in}$ will leave the separator through the heavy phase outlet. Correspondingly it is assumed that all bubbles entering at $r < r_{in}$ will reach the gas core and be separated. It is also assumed that re-entrainment of gas into the oil phase does not occur, the bubble distribution at the inlet to the lower part is uniform in radial and tangential phase as well as droplet trajectories does not cross each other. The gas volume fraction in the HPO can then be calculated from Equation 4.27. The expression is derived in Appendix A.

$$\alpha_{HPO} = \alpha_{in\,L} \left(\frac{R_s^2 - r_{in}^2}{R_s^2 - R_{cap}^2} \right) \frac{q_{TL}}{q_{HPO}} \tag{4.27}$$

where α_{HPO} is the GVF in the HPO, $\alpha_{in,L}$ is the gas volume fraction into the lower part of the separator and q_{HPO} is the volumetric flow rate

out through the HPO. q_{TL} is the total flow flowing downwards in the separator and is the sum of the downwards flow from the inlet pipe, q_B, and the liquid flow flowing down from the upper part of the separator, q_o. The oil fraction in the HPO can then be found from:

$$\alpha_{o,HPO} = 1 - \alpha_{HPO} \tag{4.28}$$

4.2.7 Equation of Motion: Upper Part

Just like the lower part, the upper part of the GLCC separator can be considered as a swirl separator, with gas being the continuous phase and being forced towards the centre and oil droplets as the dispersed phase being forced to the separator walls due to the centrifugal forces. The liquid volume fraction (LVF) and the gas volume fraction in the light phase outlet (LPO) can be found with the same approach as for the lower part of the GLCC separator. In this case it is desirable to find the inlet radial position, r_{in}, of an oil droplet entering the upper part, that will travel sufficiently enough in the radial direction to reach the separator wall just before the outlet, see Figure 4.9. The droplets are assumed to be separated when reaching the separator wall, and even though there will in reality be a liquid film on the wall with a given thickness, this thickness will be neglected in this thesis.

Finding the inlet radial position is done by integrating the radial velocity, Equation 4.20, and the axial velocity, 4.10, from $t = 0$ to $t = \tau$, where the residence time, τ, in this case will be given by:

$$\tau = \frac{\pi R_s^2 L_U}{q_T} \tag{4.29}$$

where L_U is the length of the upper part of the separator.

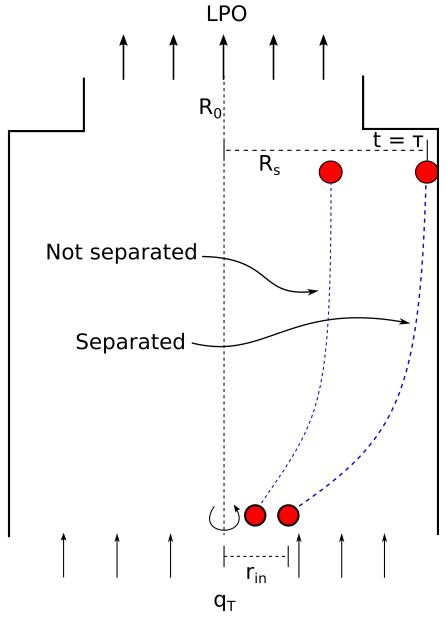

Figure 4.9: Oil droplets entering the upper part at $r > r_{in}$ at $t = 0$ will reach the separator wall at $t = \tau$ and be separated. Droplets entering at $r < r_{in}$ will not be separated and leave through the LPO.

The integration of the radial and axial velocity is done in MATLAB with the fourth order Runge-Kutta integrator as described in Section 4.2.6 and given by Equations 4.25 and 4.26. Unlike the lower part, the boundary value problem, presented by the unknown inlet radius but known separator radius, will in this case be solved by the *shooting method*. The *shooting method* uses the Newton-Raphson method in order to find an inlet radial position, r_{in}, that will yield the wanted separator radius, R_s [8]. The MATLAB function for the *shooting method* is given in Appendix E.3.2.

When the inlet radial position, r_{in}, is found the LVF in the LPO can be found by assuming that all oil droplets entering the separator at $r < r_{in}$ will not be separated and will leave the separator through the LPO. By assuming uniform droplet distribution in the radial and tangential plane at the inlet as well as the droplet trajectory does not cross, the liquid volume fraction can be found by Equation 4.30. The expression is derived in Appendix A.

$$\alpha_{o,LPO} = \alpha_{o,in\,U} \left(\frac{r_{in}^2}{R_s^2} \right) \frac{q_{TU}}{q_{LPO}} \tag{4.30}$$

where $\alpha_{o,LPO}$ is the oil fraction in the LPO, $\alpha_{in,\,U}$ is the gas volume fraction into the upper part of the separator and q_{LPO} is the volumetric flow rate out through the LPO. q_{TU} is the total upwards flow in the separator and is the sum of the upwards flow from the inlet pipe, q_T, and the gas flow from the lower part of the separator, q_g. The GVF in the LPO can then be found from:

$$\alpha_{LPO} = 1 - \alpha_{o,LPO} \tag{4.31}$$

4.3 Deliquidizer

Even though the model for the deliquidizer was developed during the specialization project in the fall of 2015[6], the deliquidizer will be used when optimizing the hypothetical separation system and a brief introduction to the model and main ideas are therefore included in this thesis. The model of the deliquidizer is based on the work of Tyvold[41].

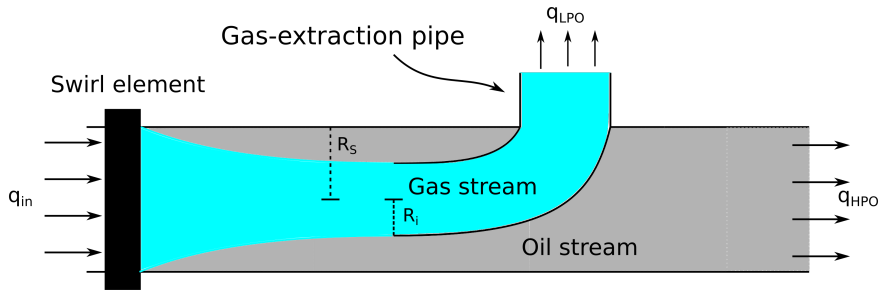

Figure 4.10: An illustration of the deliquidizer where a vortex is generated by the swirl element and the flow is thus separated to the light phase outlet (LPO) and heavy phase outlet (HPO).

The model for the deliquidizer is, just as the GLCC separator, based on centrifugal forces acting on the oil droplets, due to the swirl generated by a static swirl element, see Figure 4.11. The size of the droplets are given by average sizes. The inlet stream enters the deliquidizer axially and will pass through a swirl element which will induce a vortex in the flow. The centrifugal forces that arises from the vortex will force the oil droplets towards the separator walls. At the end of the separator there is a gas-extraction pipe, with radius $R_i < R_s$, where the light phase is extracted. The flow outside of this pipe will exit through the heavy phase outlet, see Figure 4.10.

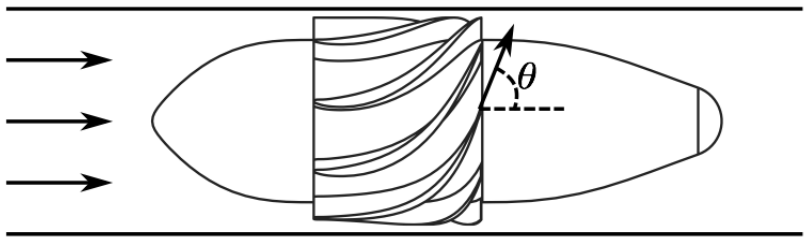

Figure 4.11: An illustration of the swirl element, where the flow is from the left to the right. The vortex is induced by the vanes that have an angle θ to the axial direction. Figure from Tyvold[41].

4.3.1 Axial Velocity

By using using valves on either side of the separator, the outlet streams can be manipulated. The flow split (FS) is defined as the ratio between the light phase outlet stream, q_{LPO}, and the inlet stream, q_{in}, and can be expressed as:

$$FS = \frac{q_{LPO}}{q_{in}} \tag{4.32}$$

The flow split can be used as a separator tuning parameter for the separation performance. The axial velocity inside the separator will be affected by the difference in the outlet flow rates, resulting in that the velocity in the outer part of the pipe may be faster or slower than the inner part of the pipe. The axial velocity inside the separator is therefore assumed to be split into two regions, each having a constant velocity, see Figure 4.12. One region is for $r > R_i$ and the other region is for $r \leq R_i$ and the velocity is given by Equation 4.12. The assumptions and simplifications for the axial velocity in the deliquidizer are the same as mentioned in Section

4.2.2.

$$v_z(r) = \begin{cases} \frac{q_{LPO}}{\pi R_i^2} & 0 \leq r \leq R_i \\ \frac{q_{HPO}}{\pi\left(R^2 - R_i^2\right)} & R_i < r \leq R_s \end{cases} \tag{4.33}$$

where R_s is the radius of the deliquidizer.

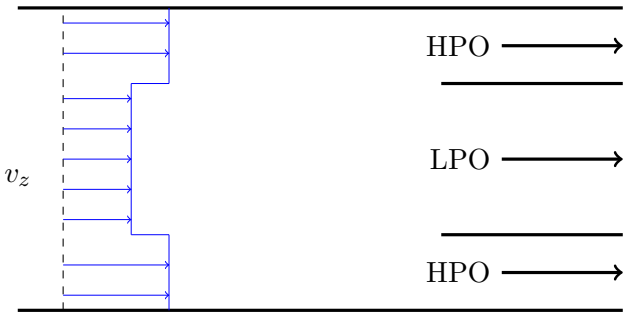

Figure 4.12: Velocity profile in the separator illustrating the velocity differences between the regions. Figure adapted from Tyvold[41].

4.3.2 Tangential Velocity

The vortex generated by the swirl element will be the driving force behind the separation inside the deliquidizer. The centrifugal acceleration that arises from this vortex will force the denser oil droplets towards the wall, just like in the GLCC separator, and is given in Equation 4.11. Experiments conducted by Dirkzwager[9] and van Campen[42] show that the vortex can be described as a Rankine vortex, just like in the GLCC. However in this separator the outer region of the deliquidizer is assumed to be constant and Figure 4.13 illustrates the velocity profile and the boundary between the regions at a radius R_c.

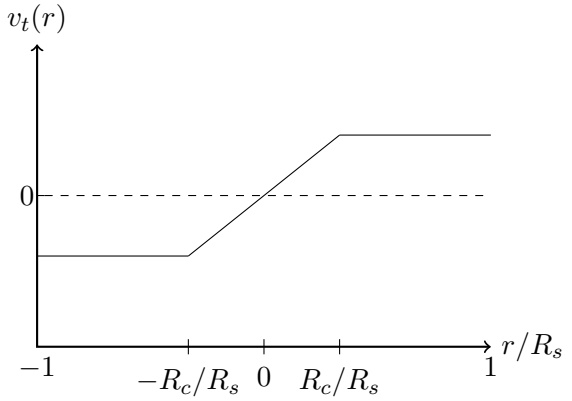

Figure 4.13: Profile of the tangential velocity, v_t, for a Rankine vortex with inside a separator with radius R_s.

From the assumptions above, the tangential velocity immediately downstream of the swirl element can thus be given by Equation 4.34[41]:

$$v_t^0(r) = \begin{cases} v_t^{max} \frac{r}{R_c} & ,0 \leq r \leq R_c \\ v_t^{max} & ,R_c < r \leq R_s \end{cases} \tag{4.34}$$

Where v_t^{max} is the maximum velocity and is assumed to be proportional to the velocity in the axial direction, v_z:

$$v_t^{max} = \Phi \, v_z \tag{4.35}$$

Φ is a proportionality constant and is referred to as the *swirl number* and can be calculated from either the geometry or determined experimentally. The swirl inside the separator is expected to lose momentum due to stress from the walls and a decay factor, C_{decay}, is introduced to take into account

the momentum loss. The tangential velocity can then be expressed as[9, 41]:

$$v_t(r,z) = v_t^0(r)\ \exp(\frac{-C_{decay}\ z}{2R}) \tag{4.36}$$

where C_{decay} is 0.04 [9].

The critical inlet radius of an oil droplet, r_{in}, that is expected to travel to the edge of the gas-extraction pipe, R_i, is expected to travel across the tangential velocity regions since $R_i > R_c$. The expression for the tangential velocity, Equation 4.34, is discontinuous at R_c, which will cause problems for the integrator. This problem is solved by using a smoothing approximation by Balakrishna and Biegler[4]:

$$\max\left(f(x),0\right) = \frac{1}{2}\ \left[\left(f(x)^2+\beta^2\right)^{1/2} + f(x)\right] \tag{4.37}$$

where β is the smoothing parameter. By rewriting Equation 4.34 and applying the smoothing function, the tangential velocity, v_t^0 can be smoothed as follows[41]:

$$v_t^0 = v_t^{max} - \max\ \left(v_t^{max}\ \left[1-\frac{r}{R_c}\right], 0\right) \tag{4.38}$$

The critical radius is set to be $R_c = 0.25R_s$ and the smoothing parameter is set to 1.

4.3.3 Radial Velocity

The radial velocity to the oil droplets in the deliquidizer follow the same assumptions as described in Section 4.2.4. The radial velocity for an oil

droplet is therefore given from Equation 4.20 in Section 4.2.4.

4.3.4 Droplet Size

van Campen[42] stated that the acceleration of a dispersed system can lead to a droplet breakup, and it is therefore reasonable to assume that the droplet size in the deliquidizer is dependent on the inlet flow into the separator. The relationship between the droplet size and the inlet flow is given in Equation 4.39:

$$d = m\, q_{in} + c \tag{4.39}$$

$$\tag{4.40}$$

where $m = -0.6 \cdot 10^{-6}$ and is the slope and $c = 0.0002$ and is the intercept. The Equation is an empirical relationship between the inlet flow and droplet size and was fitted towards experimental data by Matovu[24].

4.3.5 Equation of Motion

Just like the GLCC separator, the goal of the model of the deliquidizer is to estimate the separation efficiency. This is done by finding the inlet position of an oil droplet, r_{in}, that will travel sufficiently enough in the radial direction to reach the gas-extraction pipe, R_i, at the exit of the deliquidizer, see Figure 4.14. The radial position in of the droplet at the deliquidizer exit is found by integrating Equation 4.20 from $t = 0$ to $t = \tau$. The residence time, τ, is the time the droplet has in the separator, from entering at $z = 0$, until leaving at $z = L_{DL}$, and is in this case given by:

$$\tau = \frac{\pi \, R_i \, L_{DL}}{FS \cdot q_{in}} \tag{4.41}$$

L_{DL} is the length of the deliquidizer between the swirl element and the start of the gas-extraction pipe.

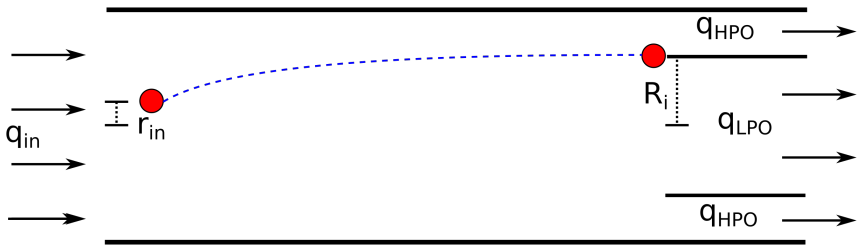

Figure 4.14: Oil droplet entering the deliquidizer at $r = r_{in}$ at $t = 0$ and exits the deliquidizer at $r = R_i$ at $t = \tau$.

The integration of the radial velocity is done with a fourth order explicit Runge-Kutta integrator, Equation 4.25, and the boundary value problem is solved with the shooting method, see Section 4.2.6 for description.

When the inlet radial position, r_{in}, is found it is assumed that all oil-droplets entering above this position ($r > r_{in}$) will exit the separator through the heavy phase outlet, while all droplets entering below this position ($r < r_{in}$) will leave the separator through the light phase outlet. If the assumptions are the same as described for the lower and upper part of the GLCC, Sections 4.2.6 and 4.2.7, the liquid volume fraction (LVF) in the HPO can be found from[41]:

$$\alpha'_{o,HPO} = (1 - \alpha_{in}) \frac{(1 - FS) R_i^2 + FS \left(R_i^2 - r_{in}^2\right)}{(1 - FS) R_i^2} \tag{4.42}$$

The LFV in the LPO is derived from component mass balance and given as:

$$\alpha'_{o,LPO} = \frac{1}{q_{LPO}} \left[(1 - \alpha_{in}) q_{in} - \alpha'_{o,HPO} q_{HPO}\right] \tag{4.43}$$

4.3.6 Re-Entrainment

The axial flow presented in Section 4.3.1 is divided into two regions, each with constant velocities and no net flux across the boundary between the region. This is is an oversimplification of what is realistic and in reality it is expected that, if for example the pressure in the LPO is lower than in the HPO, some fluid will be pulled across the boundary and exit through the LPO and vice versa, see Figure 4.15. To compensate for this oversimplification, re-entrainment is included[41].

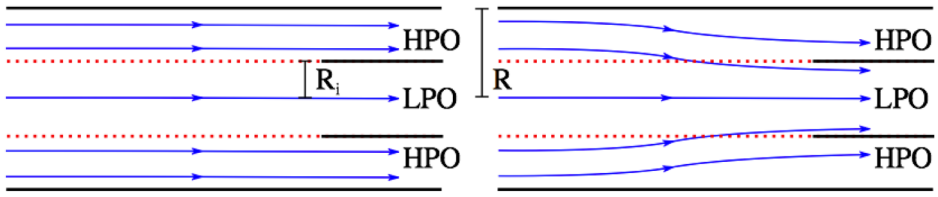

Figure 4.15: **Left:** Streamlines (blue) according to the model with no net flow across boundary, the pressure is lower at the LPO than in the HPO. **Right:** Streamlines with the re-entrainment concept included and a flow going inwards. Figure from Tyvold[41].

Re-entrainment implies that some oil that was initially separated from the gas will be re-entrained with the LPO for high flow splits and the opposite will be the case for low flow splits between the outlet streams. The re-entrainment rate is assumed to be dependent on the difference in the axial velocities for LPO and HPO and is given as[41]:

$$q_{re-en} = k_{re-en}\,\Delta v \tag{4.44}$$

where Δv is the velocity difference between the inner (LPO) and the outer (HPO) region and k_{re-en} is a proportionality constant and set to be $2{\cdot}10^{-4}$ and is determined from experimental data.

By introducing the re-entrainment concept, Equation 4.43 can be written as[41]:

$$\alpha_{o,LPO} = \frac{1}{q_{LPO}}\left[\alpha'_{o,LPO}\,(q_{in} - q_{re-en}) + \alpha'_{o,HPO}\,q_{re-en}\right] \tag{4.45}$$

From Equation 4.45 it is possible to determine the GVF in the LPO and HPO from:

$$\alpha_{LPO} = 1 - \alpha_{o,LPO} \tag{4.46}$$

$$\alpha_{HPO} = \frac{1}{q_{HPO}}\left[\alpha_{in} q_{in} - \alpha_{LPO}\,q_{LPO}\right] \tag{4.47}$$

4.4 Model Input

In the models described in the above sections, there are a lot of parameters that need to be defined in order for the model to produce any output.

These inputs are the dimension of the separator, Section 4.4.1, and the fluid properties, Section 4.4.2, including the density and viscosity. The majority of the input is taken from the work of Kristiansen et al.[20] and the rest of the input are taken from Tyvold[41] and Matovu[24]. Input that are needed but not found in literature are adjusted in order for the models to converge.

Inlet volumetric flow, gas volume fraction and flow split are also considered as model inputs but will not be discussed in this chapter since the simulations conducted are run over a range of these values.

4.4.1 Separator Dimensions

GLCC Separator

The dimensions for the GLCC separator is given in Table 4.1. The dimensions, such as separator length, separator radius, and inlet radius are from Kristiansen et al.[20], the remaining dimensions are given values that are reported to be optimum in literature.

Table 4.1: Dimensions for the GLCC separator.

Parameter	**Value**
Separator length, L_s	5 [m]
Separator radius , R_s	0.10 [m]
Inlet height	2.5 [m]
Inlet radius , R_{in}	0.10 [m]
Inlet nozzle area, A_N	0.0081 [m^2]
Inlet inclination angle, θ	27°

The inlet inclination angle is put to 27° since it has been reported to be the optimum inclination angle[19]. The inlet nozzle area has been chosen so that the ratio between the inlet nozzle area and cross-sectional area of the inlet pipe is 0.25, which is the recommended ratio from literature[15]. The height at which the inlet pipe enters the GLCC separator is, due to scarce information from literature, chosen to give equal lengths of the upper and lower parts of the separator.

Deliquidizer

The dimensions for the deliquidizer are given in Table 4.2. The length and radius of the separator (outer pipe) are taken from Matovu[24], while the other two parameters are calculated and estimated.

Table 4.2: Dimensions for the deliquidizer.

Length L_s [m]	Outer pipe radius R_s [m]	Inner pipe radius R_i [m]	Swirl number Φ [-]
1.5	0.075	0.067	0.1

The radius of the inner pipe, R_i, was calculated in order to minimise re-entrainment at a flow split of 0.8. The axial flow rates in the LPO and HPO were therefore set to be equal when determining this radius.

Φ is the swirl number and relates the vortex to the geometry of the swirl element. This parameter was assigned to 0.1 in order give a reasonable swirl intensity for the gas continuous flow inside the separator. Since the flow inside the deliquidizer consists of a gas continuous, the swirl number is therefore lower than what Tyvold[41] used and what is reported on the work on liquid-liquid systems from Dirkzwager[9] and van Campen[42]. It

is however reasonable to expect a lower swirl number for a system where the gas will be the continuous phase. This is because there will be a large density difference between the liquid droplets and the continuous gas phase meaning smaller centrifugal forces are necessary for any separation to occur.

4.4.2 Fluid Properties

The fluid properties are one of the most important inputs to the model in order to analyse the performance of the separation system. In this system the gas is considered to be pure methane while the liquid will be crude oil. The properties, which are presented in Table 4.3, are from the experiments conducted by Kristiansen et al.[20].

Table 4.3: Properties of the oil and methane gas used in the model.

Fluid	**Density** $[kg/m^3]$	**Viscosity** $[mPa \cdot s]$	**Surface Tension** $[mN/m]$
Crude Oil	881	8.8	15.5
Methane	31.6	0.0127	-

The density for the gas is calculated by using the Soave-Redlich-Kwong Equation of State, which presented in Section 4.4.3. Through this equation the gas density is dependent on the operational conditions for pressure and temperature. In this thesis the operating pressure and temperature is set to be $p = 50$ bar and $T = 50°\text{C}$ respectively.

Equation 4.20 shows that the radial velocity of a bubble/droplet is inversely proportional to the viscosity of the mixture. However, measuring and obtaining data on the viscosity of a gas-liquid mixture is extremely hard, so to overcome this problem, the viscosity used in Equation 4.20 will

be the viscosity of the continuous phase, see Figure 4.16. In other words the viscosity in a gas-in-oil mixture will be the viscosity of the oil, μ_o, and the viscosity in an oil-in-gas mixture will be the viscosity of the gas μ_g.

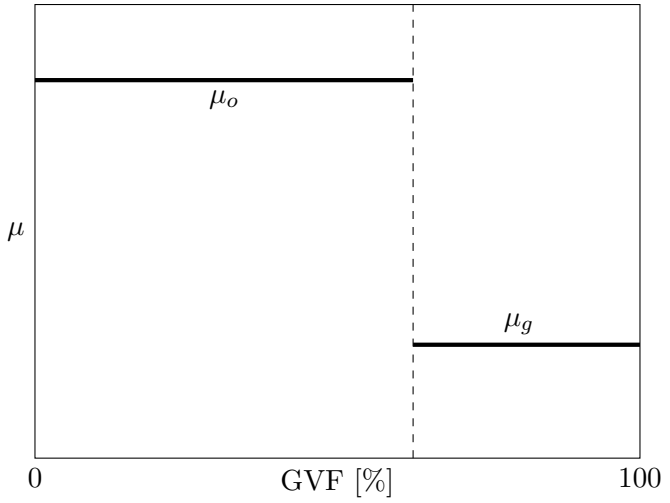

Figure 4.16: Illustration of the viscosity profile as a function of the gas volume fraction, GVF, where μ_o is the viscosity of the oil and μ_g is the viscosity of the gas. The dashed line marks the phase inversion.

The assumption of using the viscosity of the continuous phase in Equation 4.20 is expected to be reasonable due to the fact that there will be low fractions of the dispersed phase in the mixture. The amount of dispersed phase is also not expected to have a large affect on the viscosity.

4.4.3 Soave-Redlich-Kwong Equation of State

Gasses are highly compressible fluids and their properties are highly dependent on the state at which the gas is. Since the hypothetical separation

system presented above is thought to operate at different conditions than standard pressure and temperature ($p = 1$ bar & $T = 25°$C), it is desirable to have a relationship between the state of the gas and its properties. The Soave-Redlich-Kwong Equation of State (SRK-EOS)[37], given in Equation 4.48, is used to calculate the gas density as a function of the temperature and pressure.

$$p = \frac{R_{gc}T}{V_m - b} - \frac{a\,\alpha}{V_m(V_m + b)} \tag{4.48}$$

where R_{gc} is the universal gas constant and V_m is the molar volume. The parameters α, a and b are defined as[37]:

$$a = \frac{0.42747\,R_{gc}^2 T_c^2}{p_c} \tag{4.49}$$

$$b = \frac{0.08664\,R_{gc}T_c}{p_c} \tag{4.50}$$

$$\alpha = \left(1 + \left(0.480 + 1.574\omega - 0.176\omega^2\right)\left(1 - T_r^{1/2}\right)\right) \tag{4.51}$$

$$T_r = \frac{T}{T_c} \tag{4.52}$$

where p_c is the critical pressure, T_c is the critical temperature, T_r is the reduced temperature and ω is the acentric factor.

Equation 4.48 can be rewritten as[37]:

$$Z^3 - Z^2 + Z\left(A - B - B^2\right) - AB = 0 \tag{4.53}$$

where Z is the compressibility factor and:

$$V_m = Z\frac{R_{gc}T}{p} \tag{4.54}$$

$$A = \frac{a\,p}{R_{gc}^2 T^2} \tag{4.55}$$

$$B = \frac{b\,p}{R_{gc}T} \tag{4.56}$$

Equation 4.53 can then be solved for Z and from Equation 4.54 the molar volume can be found. The density of the gas, ρ_g, can then be calculated from:

$$\rho_g = \frac{M_m}{V_m} \tag{4.57}$$

where M_m is the molar mass of the gas. The full details of the MATLAB code used to solve the cubic SRK is given in Appendix E.3.3. The values for the acentric factor, critical temperature and pressure were found in *The Properties of GASES and LIQUIDS*[34].

5 Optimization

The models presented in Chapter 4 were combined to form a separation system, which will be optimized in order to maximize the gas volume fraction in the light phase outlet and the liquid volume fraction in the heavy phase outlet of the system. The cost function and constraints for the optimization procedure are given in Sections 5.1 and 5.2 respectively.

5.1 Cost Function

In an optimization problem it is desirable to maximize or minimize a cost/objective function J subject to the equality, c_{eq}, and inequality constraints, c. An optimization problem can thus be formulated as[31]:

$$\begin{aligned} \min_{u} J(u, x) \\ \text{s.t } c_{eq}(u, x) = 0 \\ c_{in}(u, x) \geq 0 \end{aligned} \tag{5.1}$$

where x represents the state and u is the steady state degrees of freedom of the system. The equality constraints, c_{eq}, represents the model equations and the inequality constraints, c_{in} represents the constraints on for example gas/liquid fractions between zero and one and non-negative flows.

For this system it is desirable to maximize the amount of gas in the light phase outlet of the system, $q_{LPO,S}$, as well as maximizing the amount of oil leaving the heavy phase outlet of the system, $q_{HPO,S}$ in Figure 4.1. This is done by formulating the following cost function.

$$J(FS, \boldsymbol{x}) = Wt_g\, \alpha_{LPO,S} + Wt_o\, \alpha_{o,HPO,S} \tag{5.2}$$

where Wt_g is the weight coefficient of the gas fraction and set to 2. Wt_o is the weight coefficient of the oil fraction and is set to 1. The higher value of the weight coefficient for gas indicates that when the optimizer solves the problem, the gas volume fraction should be emphasized. Further on $\alpha_{LPO,S}$ is the gas fraction in the light phase outlet and $\alpha_{o,HPO,S}$ is the oil fraction in the heavy phase outlet. FS is the deliquidizer flow split and the only degree of freedom in the system, while $\boldsymbol{x}$ is the states that describe the separation system. This cost function can be motivated by considering that the flow in the LPO of the system could be sent to a compressor and that the flow in the HPO of the system could be sent to a pump. It is therefore desirable to obtain as pure gas and liquid streams as possible to reduce compressor and pump deterioration. The weighting coefficient can then be used to describe how sensitive the compressor or pump is towards liquid and gas respectively, thus indicating what stream should be the purest. In this case it is thought that the compressor is more sensitive towards liquid than the pump is sensitive towards gas and the weighting coefficient for the gas is therefore given a larger value than the coefficient for the oil.

The solver used to maximize the cost function is the MATLAB optimizer *fmincon*, which finds the minimum of a given function. This means that the cost function in Equation 5.2 has to be rewritten and the optimization problem can be formulated as:

$$\min_{FS} -(Wt_g\,\alpha_{LPO,S} + Wt_o\,\alpha_{o,HPO,S}) \tag{5.3}$$
$$\text{s.t} \quad c_{eq}(FS, \boldsymbol{x}) = 0$$
$$c_{in}(FS, \boldsymbol{x}) \geq 0$$

Here c_{eq} is the equality constraints of the separation system and will be the model equations while c is the inequality constraints, which will be constraints related to the physics of the system. The constraints will be further elaborated in the next section. The algorithm used in the *fmincon* optimizer to solve the optimization problem is the *Sequential Quadratic Programming* algorithm.

5.2 Constraints and Boundaries

Constraints are a useful tool to make sure that the optimizer searches for a solution within the boundary of where the model is valid and physically feasible. The constraints used in this problem will be a set of non-linear equality and inequality constraints. The equality constraints will be given by the models describing the separation system while the inequality constraints will concern volume fractions, flow rates and the flow split. The volume fractions are physically constrained between zero and one, which will also be the case for the flow split. Flow rates are defined as positive, meaning that lower constraints for the flow rates will be zero. An upper constraint for the flow rates are set to be the value of the inlet flow rate to the system. This implies that there cannot be a higher flow rate inside or out of the system than what actually entered it. In addition, two of the variables have been assigned more explicit constraints due to model

limitations and insight and are given in Table 5.1.

Table 5.1: Specified inequality constraints for GVF in the LPO of the GLCC, $\alpha_{LPO,GLCC}$, and the flow split, FS. The remaining constraints are given by the model.

Variable	**Min Constraint**	**Max Constraint**
$\alpha_{LPO,GLCC}$	0.6	1
FS	0.6	0.95

The gas volume fraction in the light phase outlet of the GLCC, $\alpha_{LPO,GLCC}$, has been assigned a minimum constraint of 0.6. The reason being that this is the flow that enters the deliquidizer and the deliquidizer is designed for a gas-continuous system. If the fraction of gas is below 0.5 the flow will be oil-continuous and the model will not be valid. The lower constraint on the flow split is based on the fact that the deliquidizer model gives inaccurate results for a flow split below 0.6 [6]. The upper constraint is assigned to make sure that all the flow is not sent through the separator and that no separation occurs.

6 Results & Discussion

The results from the simulations and optimization are presented and interpreted in this chapter. The simulation results from the GLCC separator is presented in Section 6.1, while the optimization results are presented in Section 6.2. Simulations for the deliquidizer were not run in this thesis because the deliquidizer was modeled and the results were interpreted in the specialization project during the fall of 2015[6]. The results and any discussions of the results are therefore not included in this chapter, however, plots for the performance of the deliquidizer are given in Appendix D for the readers convenience.

All the simulations and optimization procedures are done in MATLAB and the scripts are given in Appendix E.

6.1 GLCC Separator

The GLCC separator has been simulated in order to examine the performance of the GLCC and how the performance is affected by varying inlet flow rates and inlet gas volume fractions. Due to the scarcity of experimental data, it has not been able to compare the performance of the separator against such data and thus verify the model. The interpretation of the results has rather been to analyse the performance to see if the characteristics of the separator is in compliance with what is expected from the model.

The effect of inlet gas fraction and the inlet flow rate are analysed and interpreted in Sections 6.1.1 and 6.1.2 respectively.

6.1.1 Inlet Gas Fraction Analysis

The aim of this section is to analyse and interpret how the GLCC separator performs with varying inlet gas volume fractions, α_{in}. By having a knowledge about how the inlet gas volume fraction affects the performance, the separators robustness towards such disturbances will be highlighted, as well as areas where the model breaks down. The performance of the separator as a function of the inlet gas volume fraction, α_{in}, was simulated for four different values of the inlet flow stream, q_{in}, namely 85 m^3/h, 150 m^3/h, 200 m^3/h and 300 m^3/h.

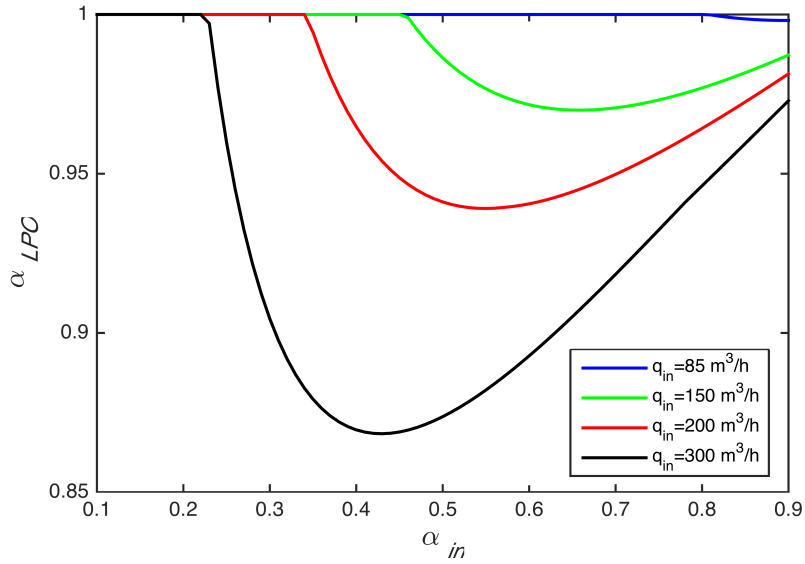

Figure 6.1: The gas volume fraction in the light phase outlet, α_{LPO}, as a function if the inlet gas volume fraction, α_{in}, at four different inlet flow rates, q_{in}.

From Figure 6.1 it is observable that at low inlet gas volume fractions

(GVF) there is 100% gas, α_{LPO}, in the light phase outlet (LPO). This is because at these low gas fractions there will be no entrainment of gas into the liquid flow going downwards and entrainment of liquid into the gas flow going upwards, see Figure C.1 in Appendix C. As the inlet gas volume fraction increases the amount of gas in the system will increase, which will result in increasing gas velocities, see Figure C.5 in Appendix C. The entrainment is dependent on the gas velocity, and at a certain inlet gas volume fraction the gas velocity will be large enough for entrainment to occur. When entrainment occurs liquid will contaminate the gas stream going to the upper part of the separator, which will decrease the GVF in the LPO. The decrease of GVF in the LPO is caused by three phenomena, the first being that the entrainment of liquid increases rapidly at low inlet gas fractions, see Figure C.1. The second phenomena that causes the decrease of GVF in the LPO is that at low inlet gas fractions the tangential velocity in the upper part of the separator might not be sufficient enough to force the oil droplets towards the separator wall. The droplet size is the third phenomena causing the decrease of GVF in the LPO. The droplet size is dependent on the gas velocity, as given in Equation 4.21, and as the inlet gas fraction increases, the gas velocity will increase. This will result in a decreasing droplet size that will reduce the redial velocity of the droplet through Equation 4.20.

The GVF in the LPO decreases with increasing inlet gas fraction to a minimum that coincides with the maximum entrainment of liquid for the given inlet flow rates. When the inlet gas fraction increases further, the purity in the LPO will also start to increase. The reason behind this tendency might be that even though the gas velocity increases, which should imply that the entrainment rate of liquid increases, the liquid fraction in the upwards flow actually decreases since the overall liquid content in the

separator is being reduced. Also at larger inlet gas fractions the tangential velocity will be a lot higher and thus force the droplets to the separator wall and therefore have a positive effect on the separation in the upper part of the separator.

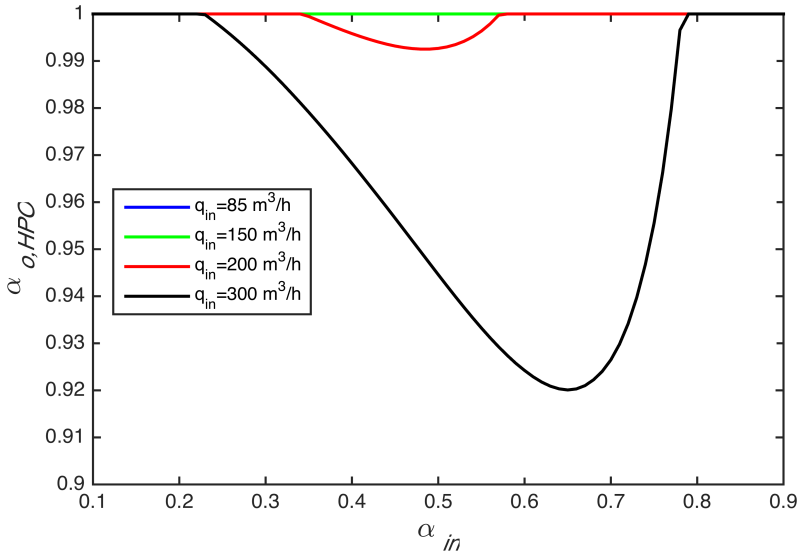

Figure 6.2: The liquid volume fraction in the heavy phase outlet, α_{HPO}, as a function if the inlet gas volume fraction, α_{in}, at four different inlet flow rates, q_{in}.

From Figure 6.2 it is possible to observe that the liquid volume fraction (LVF) in the heavy phase outlet (HPO), $\alpha_{o,HPO}$, show the same trend as the gas volume fraction in the LPO, α_{LPO}, when the inlet gas fraction varies. The oil content in the HPO is 100% until, depending on the inlet flow rate; the inlet gas fraction becomes high enough for entrainment of gas bubbles to occur. However, the rate at which the LVF decreases with increasing inlet gas fraction, is not as large as for the GVF with increasing

inlet gas fraction. This can be described by that at low inlet gas fractions, there will be more oil in the system, thus giving high liquid velocities, Figure C.5. The high liquid velocities generate high tangential velocities that will separate out the gas bubbles, thus reducing the rate at which the LVF decreases. The liquid fraction will continue to decrease with increasing inlet gas fraction until a minimum. This minimum comes as a result of an equilibrium between the factors effecting the separation in the lower part of the separator. Even though, at the minimum, the liquid velocity is decreased, which decreases the tangential velocity, the decrease in liquid velocity has increased the residence time of the bubble in the separator. With increased residence time, the bubble has a longer time to travel the radial distance and reach the gas core to be separated, which may make up for the reduced tangential velocity. The size of the droplet will also increase with decreasing liquid velocity, see Figure C.6, thus affecting the separation process and the equilibrium between the factors. The LVF will then increase again with increasing inlet gas fractions, mainly due to increasing bubble sizes and increasing residence time, due to the decreasing liquid velocity.

It is however worth noting from Figure C.3 that above an inlet gas fraction of approximately 0.75 (for an inlet flow rate of 300 m^3/h) the amount of entrained gas in the downwards liquid flow exceeds 50%, meaning that the separator model breaks down. The reason for this is that the lower part of the GLCC separator is considered a gas-in-oil separator with oil as the continuous phase. With gas content above 50% it indicates that this is not the case, yielding inaccurate calculations. This also indicates that the entrainment model exceeds its operational boundaries when a combination of high inlet flow rates and high inlet gas fractions occurs.

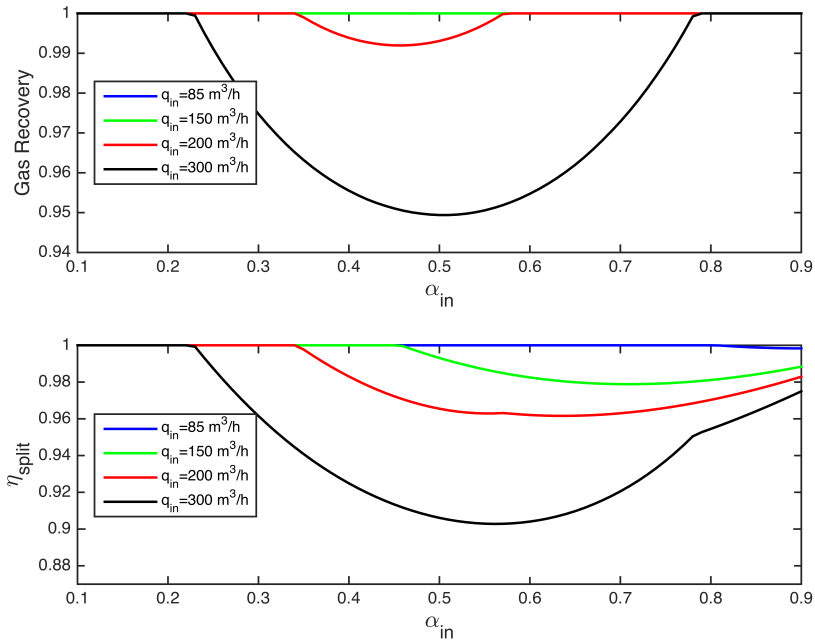

Figure 6.3: The gas recovery, GR, and the split efficiency, η_{split}, as a function of the inlet gas volume fraction, α_{in}, for four different inlet flow rates, q_{in}

The plots for gas recovery, GR, and split efficiency, η_{split}, in Figure 6.3 correlates as expected with the values for the gas volume fraction in the LPO, α_{LPO}, and the liquid volume fraction in the HPO, $\alpha_{o,HPO}$. This means that the gas recovery equals one when hundred percent oil is obtained in the HPO and that the split efficiency equals one when hundred percent separation is obtained. The reduction in both the gas recovery and the split efficiency at an inlet gas fraction of about 0.5 comes as consequence that the GVF in the LPO and the LVF in the HPO is not 100%. The discontinuity at about 0.8 for a flow rate at 300 m^3/h for the split

efficiency comes as a result that the LVF in the HPO becomes 100% and thus the slope will therefore change.

6.1.2 Inlet Flow Rate Analysis

The aim of this section is to analyse and interpret how varying inlet flow rates, q_{in}, affects the performance of the GLCC separator. This analysis will give a good insight in how the separator handles disturbances through varying flow rates as well as indicating areas at which the model will break down. The performance of the separator as a function of the inlet flow rate, q_{in}, was simulated for four different values of the inlet gas volume fraction, α_{in}, namely 0.1, 0.4, 0.5 and 0.7.

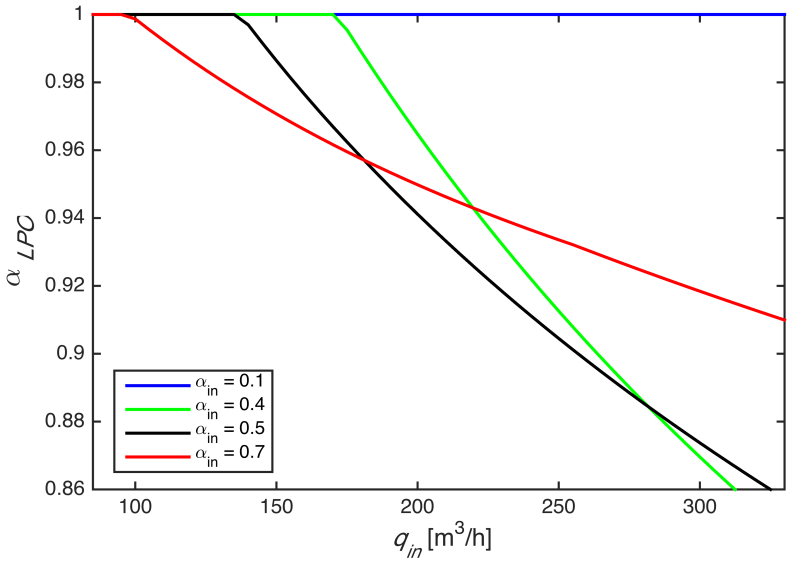

Figure 6.4: The GVF in the LPO, α_{LPO} as a function if the inlet flow rate, q_{in}, at four different values of inlet gas volume fraction, α_{in}

From Figure 6.4 it can be noted that at low flow rates the light phase outlet is a pure gas stream. However, when the inlet flow rate increases the purity will, depending on the inlet gas fraction, start to decrease as the flow rate reaches a certain value. The reason for this is that at a certain value of the inlet flow rate, the gas velocity in the separator will be high enough to yield entrainment of liquid in the gas stream flowing upwards. A higher inlet gas fraction will give a higher initial gas velocity in the system resulting in a lower initial flow rate needed for entrainment to occur compared to a low inlet gas fraction. This is the reason for the difference in the inlet flow rates at which the entrainment occurs for the different inlet gas fractions. Further increase of the inlet flow rate will result in a further decrease in the gas volume fraction in the LPO. This can be explained by that the entrainment increases for increasing flow rates, see Figure C.2 C and it is clear that the entrainment of liquid is the main reason behind oil contamination in the LPO.

It is also observable from Figure 6.4 that the rate at which the GVF in the LPO decreases is smaller for higher inlet gas fractions compared to lower inlet gas fractions. The reason behind this tendency can be that even though the inlet flow rate increases, which should result in an increased entrainment rate, the overall liquid content in the system is small when the gas fraction is large. This means that less liquid will actually be entrained in the gas flow. This will thus reduce the contamination in the LPO stream, thus resulting in a lower rate at which the LVF in the LPO decreases.

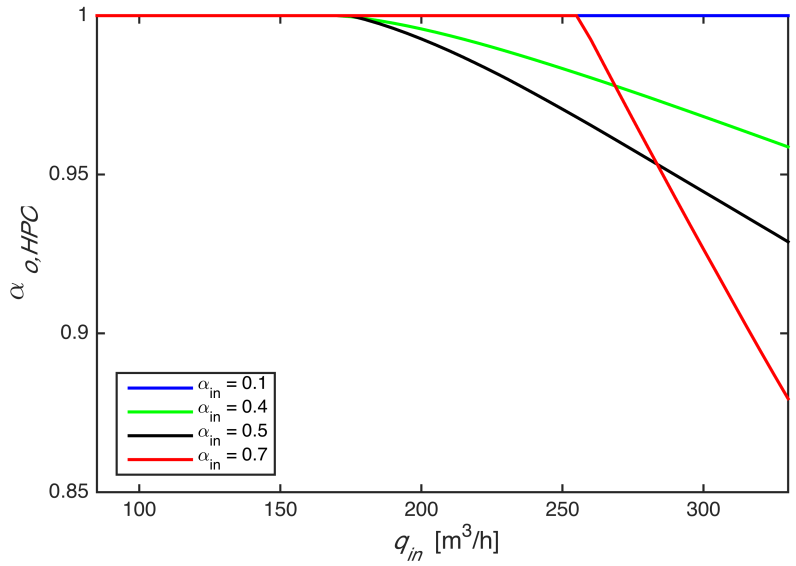

Figure 6.5: The LVF in the HPO, $\alpha_{o,HPO}$ as a function if the inlet flow rate, q_{in}, at four different values of inlet gas volume fraction, α_{in}

From Figure 6.5 it can be seen that the volume fraction of oil the HPO, $\alpha_{o,HPO}$, is one at low inlet flow rates. This can be explained by the fact that at low flow rates no entrainment of gas into the liquid stream will occur, which gives perfect separation. For an inlet gas volume fraction above 0.4, the liquid fraction in the HPO will continue to be one even though the flow rate has exceeded the velocity needed for entrainment to occur. This is because the tangential velocity increases as a result of the increasing liquid velocity due to the increase of inlet velocity, see Figure C.5, which will force the gas bubbles towards the gas core. For an inlet gas fraction of 0.4 and below, the oil fraction in the LPO starts to decrease as entrainment occurs. This can be explained by that once the entrainment occurs for the case with low gas fractions, the liquid velocity is so large

that, even though the tangential velocity is large, the gas bubbles are so small that not all bubbles manage to travel sufficiently enough in the radial direction to reach the gas core, see Figure C.6. Also at low inlet gas fractions, the residence time for the bubble will be smaller, giving the bubble a shorter time to separate, compared to higher inlet gas fractions. As the flow rate then increases the purity of oil in the HPO will start to decrease for inlet gas fractions above 0.4. This decrease is caused by the decreased bubble sizes and residence time in the separator and these effects are larger than the effect of the increased tangential velocity from the increased flow rate.

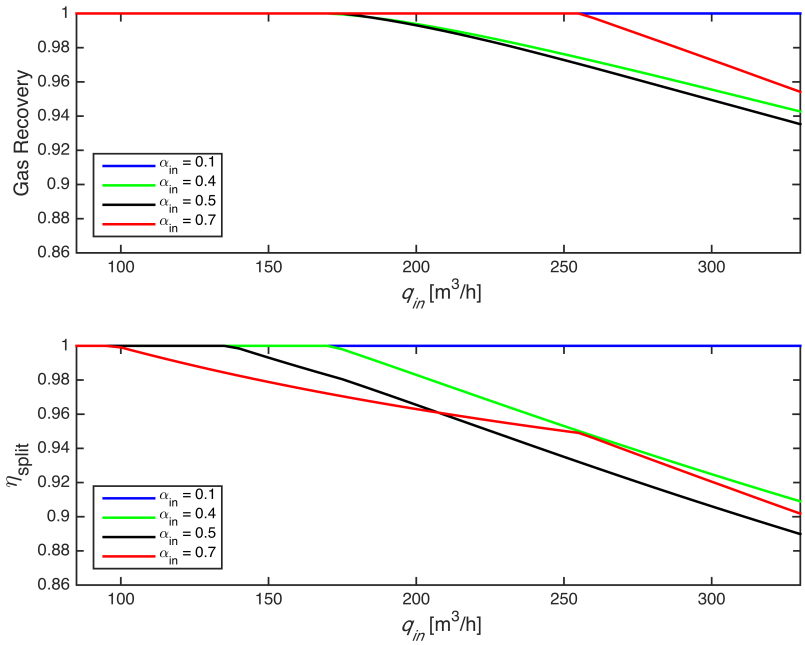

Figure 6.6: The gas recovery, GR, and the split efficiency, η_{split}, as a function of the inlet flow rae, q_{in}, for four different inlet gas volume fractions, α_{in}

The profiles for the gas recovery, GR, and the split efficiency, η_{split}, in Figure 6.6 correlates as expected with the values of GVF in the LPO, α_{LPO}, and the LVF in the LPO, $\alpha_{o,HPO}$. This means that the gas recovery and split efficiency follow the same trends as the profiles for α_{LPO} and $\alpha_{o,HPO}$. The discontinuity in the split efficiency slope of an inlet gas fraction of 0.7 at about 250 m^3/h occurs since this is the point where the LVF in the HPO will start to decrease. This will result in a change in the slope for the split efficiency and give the discontinuity observed.

6.1.3 Factors Affecting the Performance

When developing the model for the GLCC separator, there have been made assumptions and simplifications to the model that will have an affect on the overall separation performance. The major assumptions include the entrainment model, constant gas core radius, flat liquid level, force balance on droplet/bubble and no pressure drop inside the separator and it is therefore important to understand how they affect the separation performance of the separator.

From Sections 6.1.1 and 6.1.2 it is clear that the entrainment model has a large effect on the performance and it is therefore important to have a realistic and accurate model for the entrainment in order to minimize the error in the separator. The entrainment model was included to give a description of how much gas is expected to flow down with the liquid flow and how much liquid was expected to be entrained in the gas flow and flow upwards. This turned out to be the most challenging part of the modeling, because the entrainment correlations stated in the literature are all empirical and mostly deducted from experiments conducted in air-water systems, which will have slightly different properties than a

methane-oil system, which will then give inaccurate entrainment rates for said methane-oil system.

Another factor is that the used entrainment correlation predicts the entrainment of liquid in the gas flow at annular flows and not the entrainment of gas into the liquid stream. This issue was solved by putting the entrainment rate of gas into the liquid stream equals the entrainment rate of liquid into the gas stream, as explained in Section 4.2.1, due to scarce information on this matter. As seen from Figures C.3 and C.4 in Appendix C, at a given inlet gas fraction and inlet flow stream the fraction of entrained gas into the downwards liquid stream exceeds 0.5, which causes the model to break down, due to flow then being gas-continuous. This trend makes sense when thinking of how the model of the entrainment rate is defined, since the gas entrainment is equals to the liquid entrainment and the entrainment of liquid is dependent on the gas velocity. This does however give inaccurate results and decreases the operational area of the model. There are two solutions to this that could be considered for further work and the first solution could be to put the entrainment of gas equal to a given fraction of the liquid entrainment so that the gas entrainment is reduced. The other solution, considered the better solution, is to make the entrainment of gas into the liquid stream dependent on the liquid stream. Due to the lack of correlations for this prediction, this could be done by swapping the subscripts in Equation 4.4 from gas to liquid and vice-versa.

For control and optimization applications it is desirable to control the flow split between the outlet flows from the separator. However, due to the definition of the entrainment model this degree of freedom is lost since the split is determined when calculating the entrainment. This is highly unfortunate and an improvement to the model could overcome this

problem. A first thought could be to determine the outlet flow rates from the flow split and make the entrainment of gas and liquid a function of the flow split. This would result in an entire new model for entrainment but unfortunately due to time limitations, no further investigation could be put into this subject.

The model is believed to overestimate the separation performance and especially for the lower part of the GLCC separator. A major contribution to this overestimation may come from the assumption that the gas core has a constant radius. In reality the radius of the gas core will reduce as the distance from the inlet increases due to momentum loss in the vortex. A result of the decreasing radius is that the gas bubbles will have to travel a further distance in order to reach the gas core and be considered as separated. This will result in a reduced separation performance since more of the bubbles will not manage to reach the gas core and instead leave the separator out through the HPO. This assumption was made due to computational considerations, however making the gas core radius a function of the length of the lower part of the separator could improve the estimation of the separation performance. The liquid level was assumed to be flat and this may also have had an impact on the performance estimation. The liquid will in reality climb somewhat up the separator walls due to the vortex, which will also have effect on the distance the bubble has to travel. Another assumption that is thought to have an effect on the performance of the separator is that there is no pressure drop inside the separator. Gasses are highly compressible and a pressure increase or decrease will alter the density of the gas and this will then result in alterations in the radial velocity for the droplets/bubbles, see Equation 4.20 in Section 4.2.4. Such alterations in the velocity will then have an impact whether or not a gas bubble/oil droplet manages to travel

sufficiently enough in the radial direction in order to be separated.

A force balance on the droplets and bubbles were only conducted in the radial direction and the velocity of the droplet/bubble in the axial direction is therefore given by the bulk velocity of the continuous fluid. A model improvement could be to include a force balance in the axial direction, which will have an impact on the axial velocity of the bubble/droplet. By including an axial force balance and affecting the axial velocity, the residence time of the droplet/bubble in the separator will change, thus yielding more accurate separation results.

6.2 Optimization

The hypothetical separation system described in Section 4.1 was optimized as described in Section 5. The objective of the optimization procedure was to maximize the gas volume fraction in the light phase outlet stream and the liquid volume fraction in the heavy phase outlet stream by using the flow split at the deliquidizer.

The system was optimized and analysed for two different cases; the first case with a varying inlet gas fraction, Section 6.2.1, and the second case with a varying inlet flow rate, Section 6.2.2.

A full overview of the optimal values for each variable for the two cases are given in Appendix B.

6.2.1 Inlet Gas Fraction

The systems optimal operating points were tested towards a variance in the inlet gas volume fraction, α_{in}. The interval of inlet gas fractions was

chosen based on the results provided in Section 6.1.1 and to make sure that the system was optimized in areas where entrainment occurred. From the results in Section 6.1.2, the GLCC separator shows poor performance for inlet gas fractions between 0.4 and 0.6 and it might therefore be interesting to examine the optimal operating points of the system when the GLCC separator performance is at its worst. The inlet flow rate is $q_{in} = 265$ m^3/h and based on the design flow rate for Statoil's GLCC[20], where the dimensions for the GLCC in this thesis are taken from.

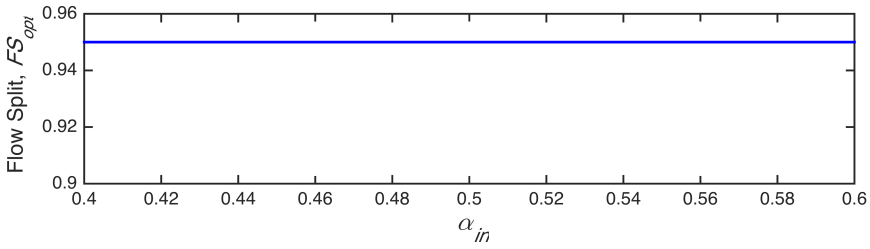

Figure 6.7: The optimal flow split, FS_{opt}, at the deliquidizer as a function of the inlet gas volume fraction, α_{in}. The inlet flow rate is 265 m^3/h.

In Figure 6.7 the optimal deliquidizer flow split, FS_{opt}, is presented as a function of the inlet gas volume fraction, α_{in}. As it can be seen the flow split operates at its maximum constraint over the entire interval of the inlet gas volume fraction meaning the constraint on the flow split always will be active. By having such a high flow split, the majority of the inlet flow to the deliquidizer will be sent out through the light phase outlet (LPO). This results in that some of the oil residue in the flow also will flow out through the LPO, however with an gas volume fraction of about 0.9 in the flow entering the deliquidizer, see Table B.1 in Appendix B, the oil contents is low and will not have the largest affect on the purity of gas in the LPO. There is also a trade-off here, because if the flow split is

lower, more flow will leave out through the HPO of the deliquidizer. Since the flow entering the deliquidizer has a large fraction of gas, more gas will then leave through the HPO and lower the liquid volume fraction in the HPO of the system.

The fact that the constraint on the flow split is always active, may indicate that optimizing the system using only one flow split (=degree of freedom) is hard and not a robust way of controlling the system. The optimal way would be to have a flow split on the outlet flows from the GLCC separator, but the way the model is put together this is not possible, as discussed in Section 6.1.3. This means that there is no split that will directly control the amount of oil in the heavy phase outlet of the system, which could make optimization and control of the system problematic. A possible solution to this issue could be to introduce a degasser, which will separate gas residue from the oil stream, thus giving an extra flow split that could be used to control the amount of oil in the HPO of the system.

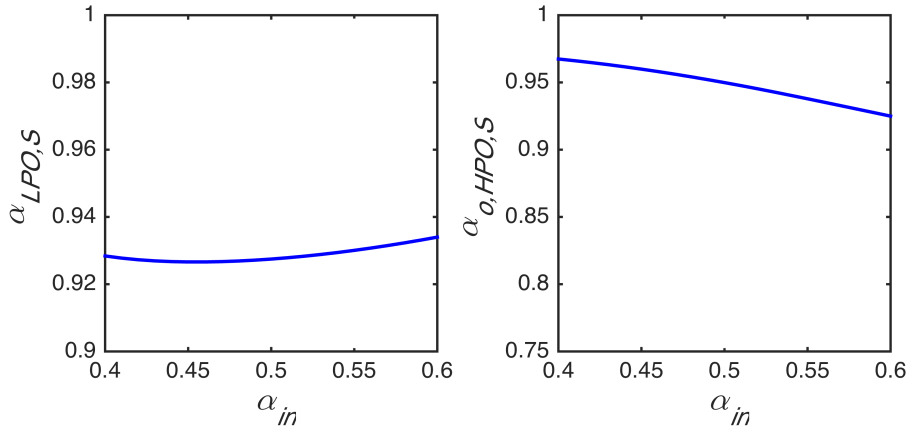

Figure 6.8: Gas volume fraction in the light phase outlet of the system, $\alpha_{LPO,S}$, and the liquid volume fraction in the heavy phase outlet of the system, $\alpha_{o,HPO,S}$, as a function of the inlet gas volume fraction, α_{in}, for the optimized flow split. The inlet flow rate is 265 m^3/h.

The GVF in the LPO of the system, $\alpha_{LPO,S}$, and the LVF in the HPO of the system, $\alpha_{o,HPO,S}$, are given in Figure 6.8. It is clear that the optimized flow split of the deliquidizer manages to provide a light phase outlet of the system with a GVF of around 0.93. It is also observable that as the inlet gas fraction increases the GVF decreases to a minimum before increasing again with increased inlet fraction. This can be explained by the trend the performance of the GLCC shows when the inlet gas fraction is increased. The performance of the GLCC has a large drop at inlet gas fractions around 0.4 before reaching a minimum and then increasing as the gas fraction increases. It is therefore expected that this response propagates to the behaviour of the GVF in the LPO of the system. The deliquidizer does experience improved performances with increasing inlet gas volume fractions and this performance will therefore somewhat dampen the drop

in performance of the GLCC and still yield a high gas purity in the LPO of the system.

The optimized value for the deliquidizer flow split also manages to maintain a relatively high value for the liquid volume fraction in the heavy phase outlet, $\alpha_{o,HPO,S}$. At such a high optimal value of the flow split, which results in a small flow out through the HPO of the deliquidizer, the liquid volume fraction in the HPO of the system will to a large extent be determined by the performance of the GLCC. It is observable from Figure 6.8 that the liquid fraction decreases as the inlet gas volume fraction increases. The GLCC also shows the same response for increasing inlet gas volume fraction; however, the performance of the GLCC does reach a minimum and starts to increase again with an increasing inlet gas volume fraction. The continued decrease of the liquid volume fraction in the HPO of the system can be a result of the fact that as the inlet gas fraction increases; the fraction of gas entering the deliquidizer will increase. Due to the large amounts of gas entering the deliquidizer, the fraction of gas leaving the deliquidizer out through the HPO will be relatively high, thus contaminating the HPO of the system and further lowering the liquid volume fraction in this flow.

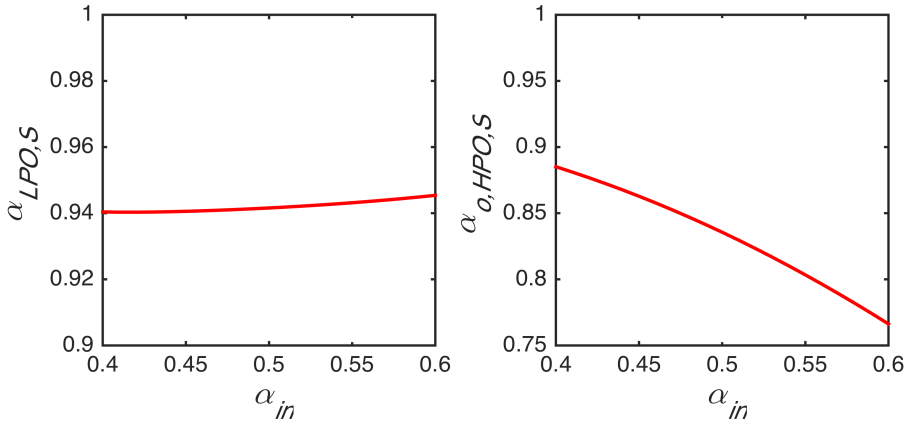

Figure 6.9: Gas volume fraction in the light phase outlet of the system, $\alpha_{LPO,S}$, and the liquid volume fraction in the heavy phase outlet of the system, $\alpha_{o,HPO,S}$, as a function of the inlet gas volume fraction, α_{in}, for a fixed flow split. The inlet flow rate is 265 m^3/h and the flow split is fixed to 0.8.

Figure 6.9 presents the gas volume fraction in the LPO of the system and the liquid volume fraction in the HPO of the system with a fixed flow split of the deliquidizer. The flow split was set to 0.8 because when the deliquidizer was designed and dimensions chosen, it was dimensioned with respect to this flow split. By comparing Figures 6.8 and 6.9 it is evident that the optimal flow split yields a better purity of oil in the HPO compared to the fixed stream, however the purity of gas in the LPO is marginally lower compared to the case with the fixed flow split. This is explained by the fact that the optimizer wants to maximize both the gas volume fraction in the LPO and the liquid volume fraction in the HPO and therefore a trade-off needs to be considered when maximizing both fractions. This trade-off can be adjusted by changing the values

of the weighting variables in Equation 5.2, Section 5.1 and depends on the objective of the system. It is however interesting to note that the single flow split manages to give decent purities in the LPO and the HPO of the system. It is however believed that having a flow split on the GLCC or introducing an inline degasser will improve the results and the controllability of the system.

6.2.2 Inlet Flow Rate

The optimal values for the flow split was also tested towards a change in the inlet flow rate, q_{in}. The interval for the inlet flow rate is between 220 and 280 m^3/h and is based on the design flow rate of $q_{in} = 265$ m^3/h mentioned in Section 6.2.1. The inlet gas fraction, α_{in}, was set to be 0.5, being in the middle of the interval where the GLCC has the poorest performance.

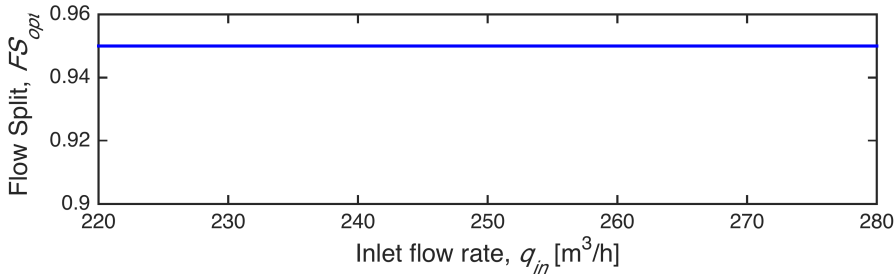

Figure 6.10: The optimal flow split, FS_{opt}, at the deliquidizer as a function of the inlet flow rate, q_{in}. The inlet gas volume fraction is 0.5.

In Figure 6.10 the optimal flow split for the deliquidizer, FS_{opt}, as a function of the inlet flow rate, q_{in}, is presented. As for the case with varying inlet gas volume fractions the flow split in this case also operates

at its maximum constraint, forcing most of the inlet flow to the deliquidizer out through the light phase outlet of the separator. This result can also be explained by the fact that the flow entering the deliquidizer contains a high amount of gas, see Table B.2 in Appendix B, and therefore a high flow will force more gas out through the LPO of the system and thus minimize the amount of gas flowing out through the HPO of the deliquidizer that will eventually flow out through the HPO of the system.

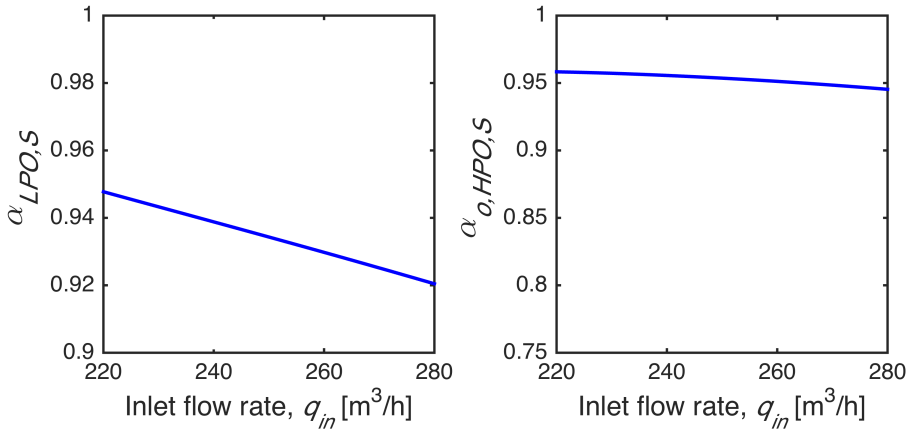

Figure 6.11: Gas volume fraction in the light phase outlet, of the system $\alpha_{LPO,S}$, and the liquid volume fraction in the heavy phase outlet of the system, $\alpha_{o,HPO,S}$, as a function of the inlet flow rate, q_{in}. The inlet gas volume fraction is 0.5.

Figure 6.10 presents the gas volume fraction in the LPO of the system, $\alpha_{LPO,S}$, and the liquid volume fraction in the HPO of the system, $\alpha_{o,HPO,S}$ as a function of the inlet flow rate, q_{in}. It is seen that the optimal flow split manages to contain a high purity of gas in the LPO and oil in the HPO. It can be noted that the gas volume fraction in the LPO decreases as the

inlet flow rate increases. This decrease is a result of an overall increased throughput in the system as well as the performance of the GLCC and the deliquidizer decreases with increasing flow rates.

The liquid volume fraction in the HPO, will due to the high flow split at the deliquidizer, mainly be affected by the performance of the GLCC. As mentioned, the performance of the GLCC decreases as the flow rate increases.This will yield lower values of liquid volume fraction in the HPO out of the GLCC, which will propagate to the liquid volume fraction in the HPO out of the system. As the performance of the deliquidizer also decreases, the amount of gas in the HPO out of the deliquidizer will increase and thus further lower the liquid volume fraction in the HPO of the system.

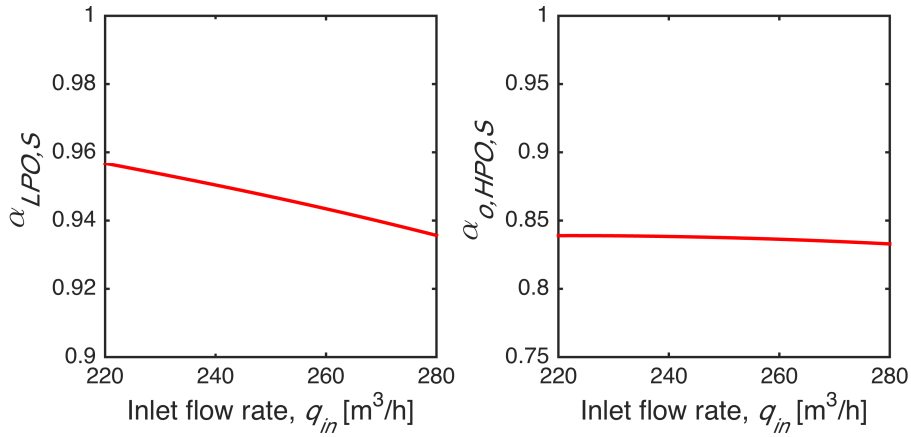

Figure 6.12: Gas volume fraction in the light phase outlet of the system, $\alpha_{LPO,S}$, and the liquid volume fraction in the heavy phase outlet of the system, $\alpha_{o,HPO,S}$, as a function of the inlet flow rate, q_{in}, for a fixed flow split. The inlet gas volume fraction is 0.5 and the flow split is fixed to 0.8.

The gas volume fraction in the LPO of the system, $\alpha_{LPO,S}$, and the liquid volume fraction in the HPO of the system, $\alpha_{HPO,S}$ as a function of the inlet flow rate, q_{in}, and with a fixed flow rate of 0.8 is presented in Figure 6.12. By comparing Figures 6.11 and 6.12 it is clear that the optimal deliquidizer flow split yields greater values for the liquid volume fraction in the HPO of the system, but the fixed split yields greater values for the gas volume fraction in the LPO of the system. This is due to the optimizer wants to maximize both fractions and not only one and therefore a trade-off needs to be considered, as described in Section 6.2.1.

7 Conclusion

The main objective for this thesis was to develop a model that determines the separation performance of a Gas-Liquid Cylindrical Cyclone separator (GLCC separator) for control and optimization purposes. The GLCC separator was split into three areas that were considered separate components, namely the inlet pipe, the upper part of the separator with gas as the continuous phase and the lower part of the separator with liquid as the continuous phase. The inlet area determines the entrainment of gas into the liquid stream and the entrainment of liquid into the gas stream, while the upper and lower part combined determine the separation performance for the GLCC separator. The model for the entrainment is based on Wallis' entrainment correlation, while the models determining the performance are based on an average droplet/bubble velocity estimated by the buoyancy and drag forces by assuming Stokes' law. The model needs a correlation describing the droplet and bubble size in the separator, which is dependent on the velocity of the gas and liquid respectively. A correlation describing the tangential velocity is also needed.

The model has not been validated by comparing the model results against experimental data, but the performance has been analysed against varying inlet flow rates and varying inlet gas volume fractions. The results show that the performance of the GLCC separator is highly dependent on these factors and that it obtains minimum gas recovery and split efficiency when the flow rate increases and the inlet gas volume fraction is about 0.5. The results also revealed that at a given set of flow rates and inlet gas fractions, the gas volume fraction in the downwards liquid flow exceeds 0.5, which results in a gas continuous phase. The model of the lower part

of the separator is generated for a liquid continuous phase and the model will therefore give inaccurate results when the gas entrainment exceeds a fraction 0.5.

The model also revealed an unexpected property in not being able to explicitly set the flow rates out of the separator. This is a result of the used entrainment model, where the entrainment calculations will determine the flow split out of the separator. For optimization and control purposes this is an unfortunate revelation due to the fact that a degree of freedom is lost.

The GLCC separator was then combined with a model for a deliquidizer to form a hypothetical compact subsea separation system. This system was then optimized with respect to maximizing the gas volume fraction in the light phase outlet of the stream and the liquid volume fraction in the heavy phase outlet. The variable used for the optimization was the flow split of the deliquidizer. The optimal flow split was found to be 0.95 for both cases. Compared to a fixed flow split, the optimal flow split generates higher values of the liquid volume fraction in the heavy phase outlet of the system but lower values for the gas volume fraction in the light phase outlet. This is a result of the objective of the optimizer and in order to maximize both values, a trade-off must be considered. This trade-off can however be adjusted according to what the objective of the optimization is. It is also believed that the introduction of a second flow split will improve the optimization of the system.

7.1 Further Work

The model for the GLCC separator has not been validated by any experimental data. In order to determine the accuracy of the model and adjust/improve the models based on the experimental results, this should be done.

As mentioned above, the way the model is built up excludes the possibility to explicitly determine the flow rates out of the GLCC separator by using a flow split. A new way of modelling the entrainment should be considered so that the outlet flows can be determined by a flow split. One approach could be to start the other way around by first determining the flow rates and make the entrainment calculations be dependent on these flow rates. Through the introduction of a flow split at the GLCC the optimization could be improved by having another variable that can be optimally tuned. The entrainment versus flow split seems to be a complex problem that will need further investigation.

In addition to removing the flow split at the GLCC, the entrainment model also causes the separator model to break down at given operating conditions by estimating the entrainment of gas into the liquid stream to exceed a fraction of 0.5. The entrainment of gas should therefore be calculated differently in order to expand the area in which the model works and to improve the separator model.

It can also be possible to introduce an inline degasser that separates out any gas residue from the heavy phase outlet at the GLCC to see if the overall system performance increases. This will introduce an extra flow split that can improve the optimization of the system.

The model could be improved by making the gas core radius dependent on

the axial direction from the inlet, which will give a more realistic picture of the conditions inside the separator. Including a pressure drop in the separator is also thought to improve the model.

Bibliography

[1] Algifri, A. H., Bhardwaj, R. K., and Rao, Y. V. N. Turbulence Measurements in Decaying Swirl Flow in a Pipe. *Applied Scientific Research 45* (1988), 233–250.

[2] Arpandi, I. A., Joshi, A. R., Shoham, O., Shirazi, S., and Kouba, G. E. Hydrodynamics of Two-Phase Flow in Gas-Liquid Cylindrical Cyclone Separators. In *SPE Annual Technical Conference & Exhibition* (1995).

[3] Azzopardi, B. J. Drop sizes in annular two-phase flow. *Experiments in Fluids 3*, 1 (1985), 53–59.

[4] Balakrishna, S., and Biegler, L. T. Targeting strategies for the synthesis and energy integration of nonisothermal reactor networks. *Industrial & Engineering Chemistry Research 38*, 3 (1992), 2152–2164.

[5] Bandyopadhya, P. R., and Gad-el Hak, M. Sensitivity of a Gas-Core Vortex in a Cyclone-Type Gas-Liquid Separator. *ASME Fed 192* (1994), 37–45.

[6] Bishop, T. Modeling a Multiphase Subsea Separation System. Tech. rep., Department of Chemical Engineering, Norwegian University of Science and Technology, 2015.

[7] Chang, F., and Dhir, V. K. Turbulent Flow Field in Tangentially Injected Swirl Flows in Tubes. *International Journal of Heat and Fluid Flow*, OCTOBER 1994 (1994), 346–356.

[8] Constantinides, A., and Mostoufi, N. *Numerical Methods for Chemical Engineers with MATLAB Applications*, 1 ed. Prentice Hall PTR, Upper Saddle River, N.J, 1999.

[9] Dirkzwager, M. *A New Axial Cyclone Design for Fluid-Fluid Separation.* Ph.d, Delft University of Technology, 1996.

[10] FMC-Technologies. Separation Systems-Subsea Separation. URL: `http://www.fmctechnologies.com/en/SeparationSystems/Solutions/SubseaSeparation.aspx`, Entered: 13.12.2015.

[11] Gao, X., Chen, J., Feng, J., and Peng, X. Numerical and experimental investigations of the effects of the breakup of oil droplets on the performance of oil e gas cyclone separators in oil-injected compressor systems. *International Journal of Refrigeration 36*, 7 (2013), 1894–1904.

[12] Giaiotti, D. B., and Stel, F. The Rankine Vortex Model. *October* (2006), 1–14.

[13] Gomez, L. *A State-of-the-Art Simulator and Field Application Design of Gas-Liquid Cylindrical Cyclone Separators.* Master thesis, University of Tulsa, 1998.

[14] Gomez, L., Mohan, R., and Shoham, O. Swirling Gas Liquid Two-Phase Flow Experiment and Modeling Part I : Swirling Flow Field. 935–942.

[15] Gomez, L., Mohan, R., Shoham, O., Marrelli, J., and Kouba, G. Aspect Ratio Modeling and Design Procedure for GLCC Compact Separators. *Journal of Energy Resources Technology 121*, March (1999).

[16] Hreiz, R., Gentric, C., Midoux, N., Lainé, R., and Fünfschilling, D. Chemical Engineering Research and Design Hydrodynamics and velocity measurements in gas liquid swirling flows in cylindrical cyclones . *Chemical Engineering Research and Design 92*, 11 (2014), 2231–2246.

[17] Hreiz, R., Lainé, R., Wu, J., Lemaitre, C., Gentric, C., and Fünfschilling, D. On the effect of the nozzle design on the performances of gas liquid cylindrical cyclone separators. *International Journal of Multiphase Flow 58* (2013), 15–26.

[18] Ishii, M., and Zuber, N. Drag coefficient and relative velocity in bubbly, droplet or particulate flows. *AIChE Journal 25*, 5 (1979), 843–855.

[19] Kouba, G., Shoham, O., and Shirazi, S. Design and Performance of Gas-Liquid Cylindrical Cyclone Separators. In *Multiphase 95* (1995).

[20] Kristiansen, O., Sørensen, Ø., and Nilssen, O. R. CompactSep - Compact Subsea Gas-Liquid Separator for High-Pressure. In *Offshore Technology Conference* (2016).

[21] Kurokawa, J., and Ohtaki, T. Gas-Liquid Flow Characteristics and Gas-Separation Efficiency in a Cyclone Separator. *ASME Fed 225* (1995), 51–56.

[22] Mantilla, I. *Bubble Trajectory Analysis in Gas-Liquid Cylindrical Cyclone Separators.* Master thesis, University of Tulsa, 1998.

[23] Marti, S., Erdal, F., Shoham, O., Shirazi, S., and Kouba, G. Analysis of Gas Carry-Under in Gas-Liquid Cylindrical Cyclones.

Tech. rep., 1996.

[24] Matovu, F. *Modelling and Optimization of Compact Sub-sea Separators*. Master thesis, Norwegian University of Science and Technology, Trondheim, 2015.

[25] Mcclimans, O. T., Fantoft, R., and Technologies, F. M. C. Status and New Developments in Subsea Processing. *Offshore Technology Conference* (2006), 1–10.

[26] Millington, B., and Thew, M. LDA Study of Component Velocities in Air-Water Models of Steam-Water Cyclone Separators. In *Multi-Phase Flow* (The Hauge, 1987), pp. 115–125.

[27] Molina, R., Gomez, L. E., and Mohan, R. S. Wet Gas Separation in Gas-Liquid. *Journal of Energy Resources Technology 130*, December 2008 (2008).

[28] Moreno-Trejo, J., and Markeset, T. Identifying Challenges in the Development of Subsea Petroleum Production Systems Field Development. In *The Proceedings of the international Conferece of Advances in Production Management System* (Stavanger, 2011), pp. 26–28.

[29] Mørk, P. *Overflate og kolloidkjemi: grunnleggende prinsipper og teorier*, 4th ed. Department of Chemical Engineering, Norwegian University of Science and Technology, 2004.

[30] Movafaghian, S., Jaua-marturet, J. A., Mohan, R. S., and Shoham, O. The Effects of Geometry, Fluid Properties and Pressure on teh Hydrodynamics of Gas-Liquid Cylindrical Cyclone Separators. 999–1018.

[31] Nocedal, J., and Wright, S. *Numerical Optimization*. Springer, 2006.

[32] Paleev, I., and Filippovich, B. Phenomena of Liquid Transfer in Two-Phase Dispersed Annular Flow. *International Journal of Heat and Mass Transfer 9* (1965), 1089–1093.

[33] Pan, L., and Hanratty, T. J. Correlation of entrainment for annular flow in horizontal pipes. *International Journal of Multiphase Flow 28*, 3 (2002), 385–408.

[34] Poling, B. E., Prausnitz, J. M., and O'Connell, J. P. *The Properties of GASES AND LIQUIDS*, 5th ed. McGraw-Hill, New York, 2007.

[35] Rosa, E. S., Franc, F. A., and Ribeiro, G. S. The cyclone gas liquid separator : operation and mechanistic modeling. *Journal of Petroleum Science and Engineering 32* (2001), 87–101.

[36] Skogestad, S. Sigurd Skogestad's Homepage. URL: `http://www.nt.ntnu.no/users/skoge/book-cep/matlab/srk-flash/`, Entered: 01.10.2015.

[37] Soave, G. Equilibrium constants from a modified Redlich-Kwong equation of state. *Chemical Engineering Sicence 27*, 6 (1972), 1197 – 1203.

[38] Statoil. Subsea Processing on Tordis. URL: `http://www.statoil.com/en/TechnologyInnovation/FieldDevelopment/AboutSubsea/SubseaProcessingOnTordisIOR/Pages/default.aspx`, Entered: 13.12.2015.

[39] Taitel, Y., and Dukler, A. A Model for Predicting Flow Regime Transitions in Horizontal and Near Horizontal Gas-Liquid Flow. *AICHe Journal 22*, 1 (1976), 47–55.

[40] Tatterson, D. F., Dallman, J. C., and Hanratty, T. J. Drop Sizes in Annular Gas-Liquid Flows. *AIChE Journal 23*, 1 (1977), 68–76.

[41] Tyvold, P. *Modeling and Optimization of a Subsea Oil-Water Separation System*. Master thesis, Norwegian University of Science and Technology, Trondheim, 2015.

[42] van Campen, L. *Bulk Dynamics of Droplets in Liquid-Liquid Axial Cyclones*. Ph.d, Delft University of Technology, 2014.

[43] Wallis, G. B. Phenomena of liquid transfer in two-phase dispersed annular flow. *International Journal of Heat and Mass Transfer 11*, 4 (1968), 783–785.

[44] Wallis, G. B. *One-dimensional Two-phase Flow*. McGraw-Hill, 1969.

A Derivation of Outlet Fraction Equations

The deviation for the expressions used to calculate the gas volume fraction in the heavy phase outlet, Equation 4.27 in Section 4.2.6, and the liquid volume fraction in the light phase outlet, Equation 4.30 in Section 4.2.7, are shown in this appendix. The general idea in how to determine these fractions is from Tyvold[41].

A.1 Gas Volume Fraction in HPO

The idea behind Equation 4.27 in Section 4.2.6, is that the flow of gas bubbles through the light blue area in Figure A.1, must be equal to the flow of gas bubbles out through the HPO. For this to be true it is assumed that no droplet trajectories cross each other and that at the inlet to the lower part of the separator there is an uniform distribution of the bubbles. This can be expressed as:

$$\alpha_{HPO}\, q_{LPO} = \alpha_{in\,L} \left(\frac{R_s^2 - r_{in}^2}{R_s^2 - R_{cap}^2} \right) q_{TL} \tag{A.1}$$

where α_{HPO} is the GVF in the HPO, $\alpha_{in\,L}$ is the gas volume fraction into the lower part of the separator, q_{TL} is the total volumetric flow into the lower part of the separator and q_{HPO} is the flow rate out through the HPO. Re-arranging Equation A.1 will yield the the expression used to calculate the GVF in the HPO:

$$\alpha_{HPO} = \alpha_{in\,L} \left(\frac{R_s^2 - r_{in}^2}{R_s^2 - R_{cap}^2} \right) \frac{q_{TL}}{q_{HPO}} \tag{A.2}$$

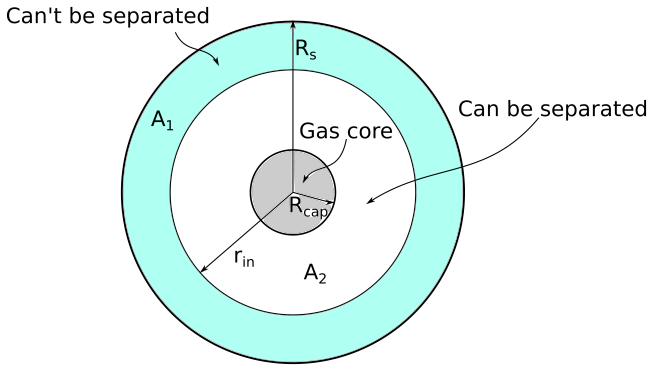

Figure A.1: Top-down cross-sectional of the view of the lower part of the GLCC, showing the cross-sectional area, A_1, in which the gas bubble will not separate and the cross-sectional area, A_2, where a gas bubble will separate.

A.2 Liquid Volume Fraction in LPO

The idea behind Equation 4.30 in Section 4.2.7 is the same as described above. The flow of oil droplets through the light blue area in Figure A.2 must be equal to the the flow of oil droplets out through the HPO. If the same assumptions mentioned above is considered in this case, the following expression can be formulated:

$$\alpha_{o,LPO}\, q_{LPO} = \alpha_{o,in\,U} \left(\frac{r_{in}^2}{R_s^2} \right) q_{TU} \tag{A.3}$$

where $\alpha_{o,LPO}$ is the LVF in the LPO, $\alpha in\, U$ is the GVF into the upper part of the separator, q_{TU} is the total volumetric flow to the upper part of the separator and q_{LPO} is the flow rate out through the LPO. Re-written, Equation A.3, will then yield the equation for the LVF in the LPO:

$$\alpha_{o,LPO} = \alpha_{o,in\, U} \left(\frac{r_{in}^2}{R_s^2} \right) \frac{q_{TU}}{q_{LPO}} \tag{A.4}$$

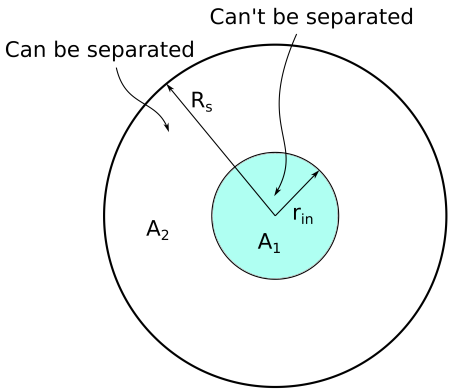

Figure A.2: Top-down cross-sectional of the view of the upper part of the GLCC, showing the cross-sectional area, A_1, in which the gas bubble will not separate and the cross-sectional area, A_2, where a gas bubble will separate.

B System Values from Optimization

The optimal values of the separation system are presented in this appendix. The values for a constant inlet flow rate of 265 m^3/h, with varying inlet gas volume fractions are presented in Table B.1. The values for a constant inlet gas volume fraction of 0.5, with varying inlet flow rates are presented in Table B.2.

Table B.1: Optimized system values for inlet gas volume fractions of 0.4, 0.5 and 0.6 for an inlet flow rate of $q_{in} = 265$.

Variable	$\alpha_{in} = 0.4$	$\alpha_{in} = 0.5$	$\alpha_{in} = 0.6$
$q_{LPO,GLCC}$	114 m^3/h	143 m^3/h	170 m^3/h
$\alpha_{LPO,GLCC}$	0.90	0.89	0.91
$q_{HPO,GLCC}$	151 m^3/h	122 m^3/h	95 m^3/h
$\alpha_{HPO,GLCC}$	0.02	0.03	0.04
$q_{LPO,S}$	109 m^3/h	136 m^3/h	162 m^3/h
$\alpha_{LPO,S}$	0.928	0.927	0.935
$q_{HPO,DL}$	5 m^3/h	7 m^3/h	9 m^3/h
$\alpha_{HPO,DL}$	0.33	0.27	0.41
$q_{HPO,S}$	156 m^3/h	129 m^3/h	103 m^3/h
$\alpha_{HPO,S}$	0.03	0.05	0.08

Table B.2: Optimized system values for inlet flow rates of 230, 265 and 280 m^3/h with an inlet gas volume fraction of $\alpha_{in} = 0.5$.

Variable	q_{in} = 230 m^3/h	q_{in} = 265 m^3/h	q_{in} = 280 m^3/h
$q_{LPO,GLCC}$	123 m^3/h	143 m^3/h	152 m^3/h
$\alpha_{LPO,GLCC}$	0.91	0.89	0.89
$q_{HPO,GLCC}$	107 m^3/h	122 m^3/h	128 m^3/h
$\alpha_{HPO,GLCC}$	0.02	0.04	0.05
$q_{LPO,S}$	117 m^3/h	136 m^3/h	144 m^3/h
$\alpha_{LPO,S}$	0.94	0.93	0.92
$q_{HPO,DL}$	6 m^3/h	7 m^3/h	8 m^3/h
$\alpha_{HPO,DL}$	0.45	0.27	0.22
$q_{HPO,S}$	113 m^3/h	129 m^3/h	136 m^3/h
$\alpha_{HPO,S}$	0.04	0.05	0.05

C GLCC Profiles

In this appendix plots illustrating the conditions inside the GLCC separator for different inlet flow rates and inlet gas volume fractions are given.

Figures C.1 and C.2 show how the entrainment of liquid into the upwards flowing gas stream is affected by the inlet gas volume fraction, α_{in}, and the inlet flow rate, q_{in}, respectively.

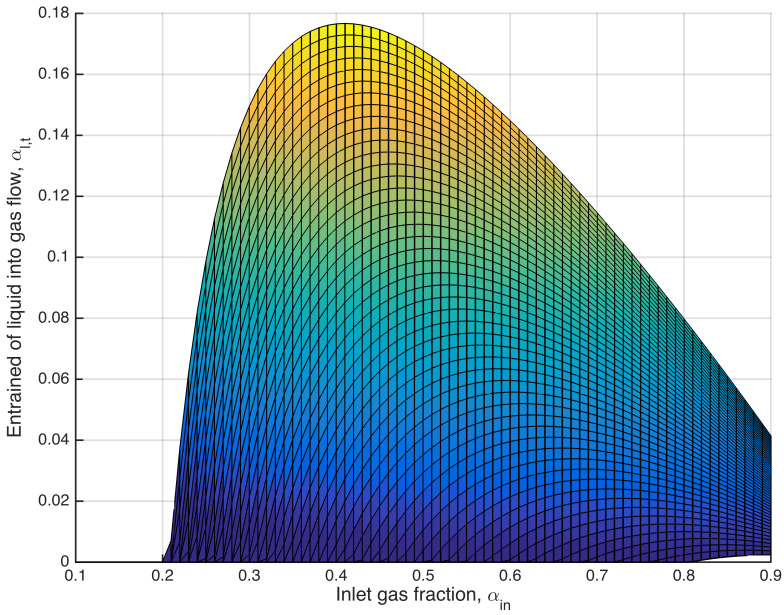

Figure C.1: X-Z view showing the entrainment of liquid into the upwards flow as a function of the inlet gas volume fraction, α_{in}.

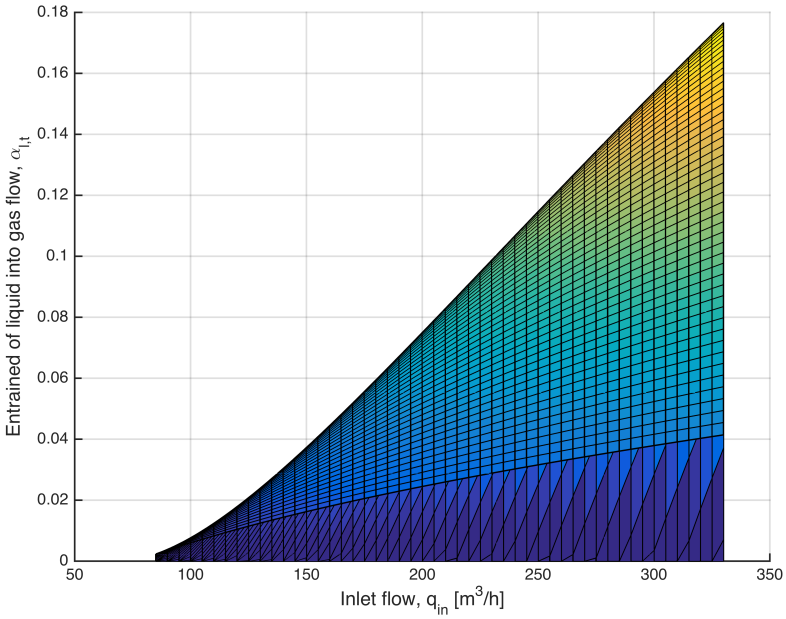

Figure C.2: Y-Z view showing the entrainment of liquid into the upwards flow as a function of the inlet gas volume fraction, q_{in}.

In Figures C.3 and C.4, the effect of the inlet gas volume fraction, α_{in}, and inlet flow rate, q_{in}, on the entrainment of gas into the downwards flowing liquid stream is shown. Note how the entrainment of gas at some point exceeds 0.5, thus highlighting the area where the model is not valid any more.

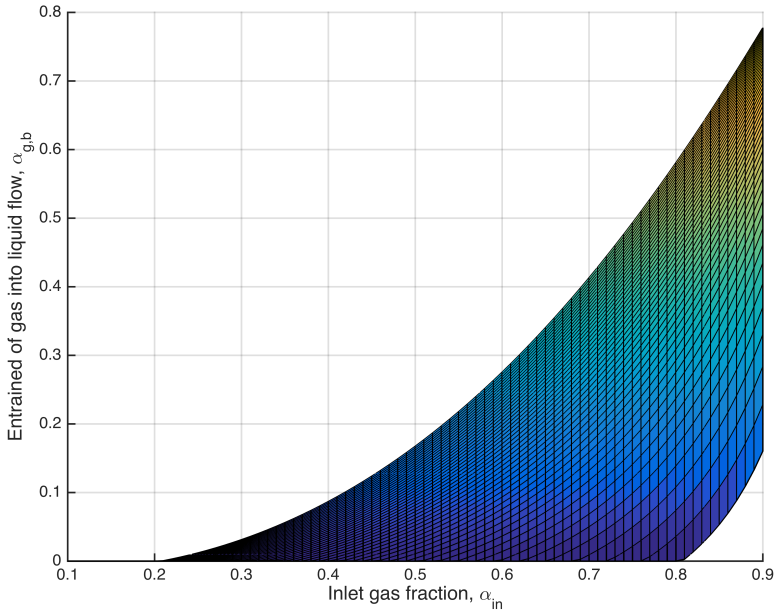

Figure C.3: X-Z view showing the entrainment of gas into the downwards flow as a function of the inlet gas volume fraction, α_{in}.

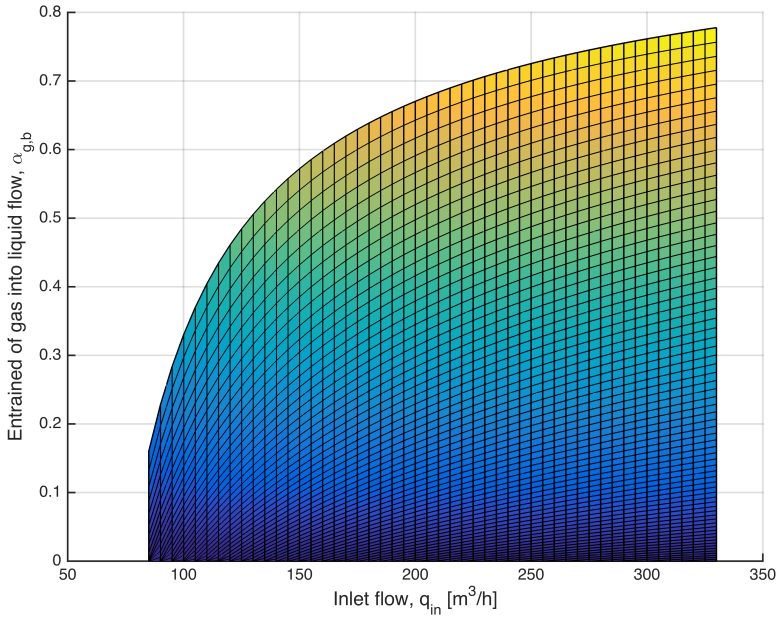

Figure C.4: Y-Z view showing the entrainment of gas into the downwards flow as a function of the inlet gas volume fraction, q_{in}.

Figure C.5 highlights the relationship between liquid, v_l, and gas, v_g, velocity and the inlet flow rate, q_{in}, and the inlet gas volume fraction, α_{in}.

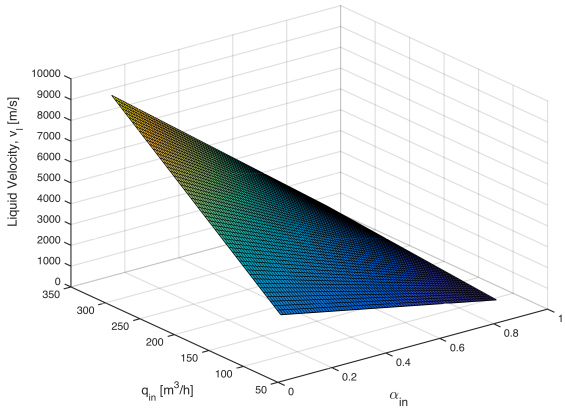

(a) Liquid Velocity

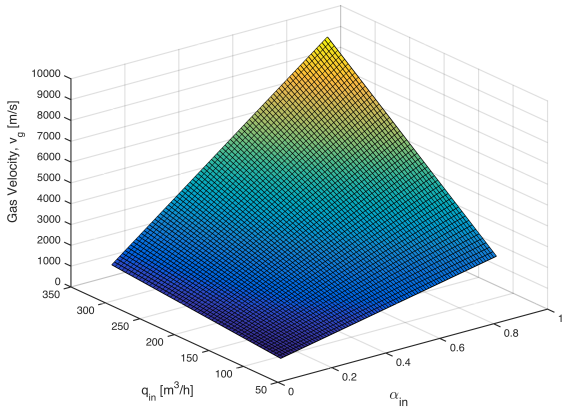

(b) Gas Velocity

Figure C.5: Liquid, v_l, and gas, v_g, velocity as a function of the inlet gas volume fraction, α_{in}, and the inlet flow rate, q_{in}.

In Figure C.6 the droplet and bubble size as a function of the inlet flow rate, q_{in}, and the inlet gas volume fraction, α_{in} is given.

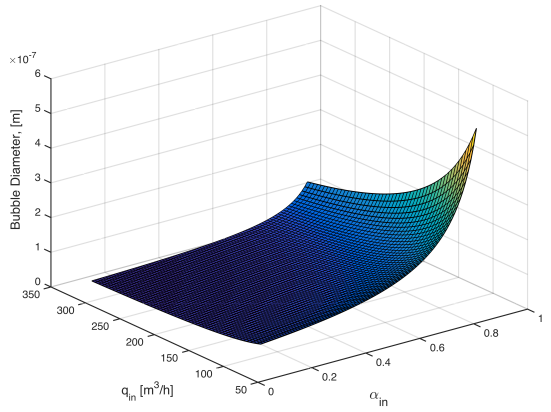

(a) Bubble Size

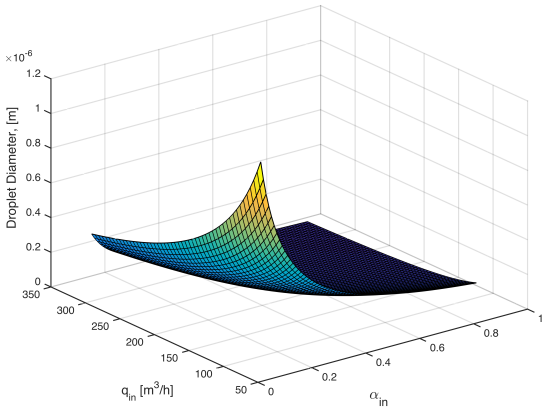

(b) Droplet Size

Figure C.6: Bubble and droplet size as a function of the inlet gas volume fraction, α_{in}, an the inlet flow rate, q_{in}.

D Deliquidizer Performance

In this appendix the results from the deliquidizer simulations conducted in the specialization project during the fall of 2015 are given. The results from the inlet flow rate analysis are given in Appendix D.1 and the results from the flow split analysis are given in Appendix D.2.

D.1 Flow Rate Analysis

Figure D.1 shows the results from the simulation testing the performance of the deliquidizer with varying inlet flow rates. The flow split for this case was 0.8 and the inlet gas volume fraction was 0.8.

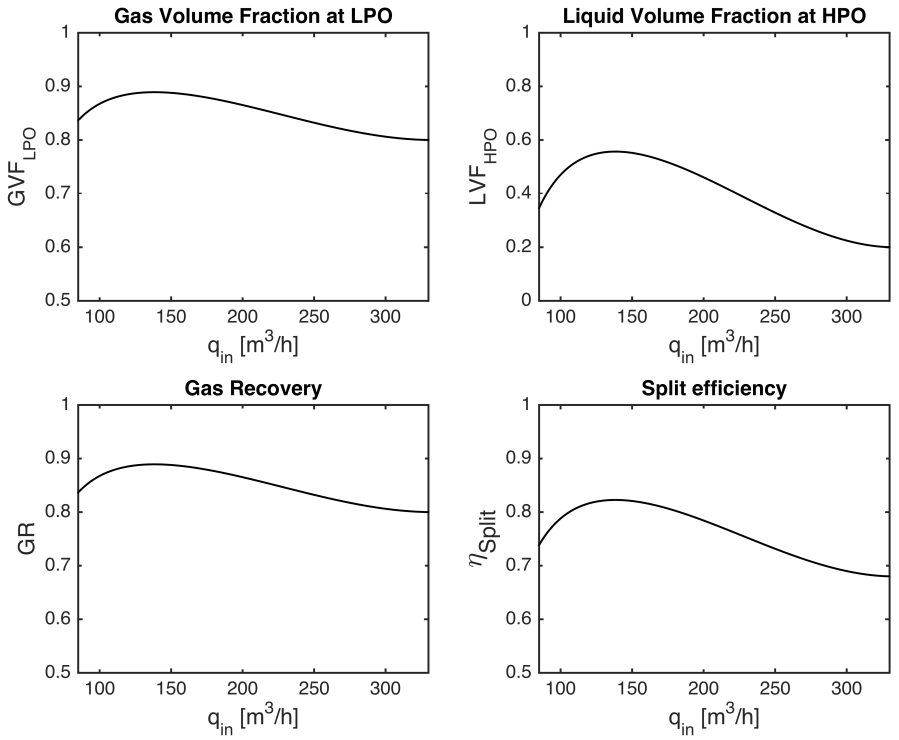

Figure D.1: Deliquidizer performance with inlet gas fraction of 0.8 and flow split of 0.8 as a function of inlet flow rate, q_{in}.

D.2 Flow Split Analysis

Figure D.2 shows the results from the simulation testing the performance of the deliquidizer with varying flow spilts. The inlet flow rate was 140 m^3/h and the inlet gas volume fraction was 0.8.

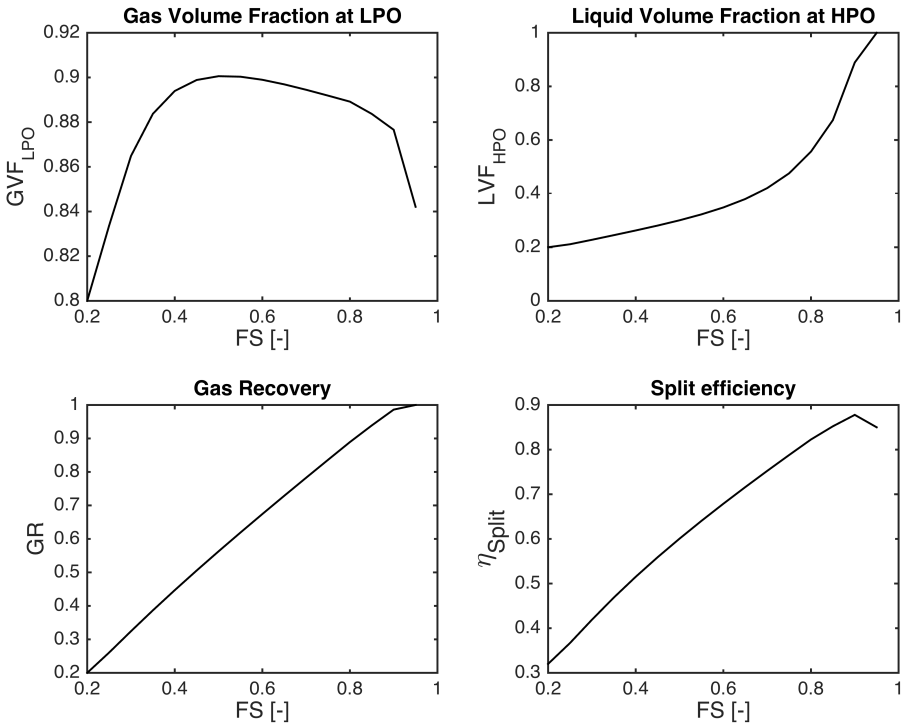

Figure D.2: Deliquidizer performance with inlet gas fraction of 0.8 and flow rate of 140 m^3/h as a function of flow split, FS.

E MATLAB Scripts

In this appendix the MATLAB codes that were used in the simulations are given. The scripts for the GLCC separator are given in Appendix E.1, the solvers used and the Soave-Redlich-Kwong Equation of State are given Appendix E.3 and the optimization procedure is given in Appendix E.4. The scripts for the deliquidizer are given in Appendix E.2.

E.1 GLCC Separator

The MATLAB scripts for the GLCC separator are presented in this section. The main function, in Appendix E.1.1, calls the function that calculates the entrainment in the streams, Appendix E.1.6, and the function where the separator performance is estimated, Appendix E.1.2. This function will in turn call the functions containing the governing equations, Appendix E.1.3 and E.1.4, and the function that estimates the composition in the streams leaving the GLCC.

E.1.1 Main Function

The script *GLCC_Driver* is the main script where all graphs and profiles are generated.

```
%%%%%%%%%%%%%%%%%%%%%%%%%%%%%%%%%%%%%%%%%%%%%%%%%%%%%%%%%%%%%%%%%%%%%%%%%%%%%%
% Author: Torstein Bishop
%
% Department of Chemical Engieneering, NTNU. Spring 2016.
%
```

```
%
%
% This is the main script running all the functions that are necessary in %
% in order to perform simulations of the GLCC. This script calls on the
%
% functions Flow_Split3 and GLCC_comb.
%
%
%
% Calls on the following functions:
%
%%%%%%%%%%%%%%%%%%%%%%%%%%%%%%%%%%%%%%%%%%%%%%%%%%%%%%%%%%%%%%%%%%%%%%%%%%%%
clc
clear all
tic

%% Parameters
Dim.Ls=5;%1.5;  %Separator length [m]
Dim.Li = 1; %Length of inlet pipe [m]
Dim.Lt = Dim.Ls/2;%0.75; %Length of upper part of the separator [m]
Dim.Lb = Dim.Ls/2;% 0.75; %Length of lower part of the separator [m]
Dim.theta = 27; %Inclination angle of inlet pipe [degrees]
Dim.Rs=0.1016;%0.075; %Separator radius [m]
Dim.Ds = Dim.Rs*2; %Separator diameter [m]

Dim.D_in = 0.2032; % Diameter of inlet pipe [m]
Dim.A_in = pi*(Dim.D_in)^2/4;%0.4 %Cross-sectional area of inlet pipe [m2]
Dim.A_is = 0.25*Dim.A_in;%0.1; %Cross-sectional are of inlet slot [m2]
Dim.D_is = 2*sqrt(Dim.A_is/pi); % Diameter of inlet pipe slot [m]

xg_in = [0.1:0.01:0.9];%0.40 %Gas fraction into separator
q_in = [85:5:330];%150 %Inlet flow-rate into separator [m3/h]
```

```
%% Calculating the density of the methane gas
% Filling in component data needed to calculate the density of the gas
% found from The properties of Gases and Liquids fifth edition.
compData.Pc = 45.99e5; % [Pa], Critical Pressure
compData.Tc = 190.56;  % [K], Critical Temperature
compData.w = 0.011;     % Acentric factor
compData.Cp = 0;       % Not used in any calculations yet
compData.Tref = 273.15; % [K]
compData.Mm = 16.043;   % [g/mol] Methane molar weight

P = 50e5; % [Pa] Pressure in separation system
T = 50+273; % [K] Assumed temperature in separation system
y = 1; % Assume only methane in gas phase

% Calling SRK-EOS for density calculations
[Z, RHO] = SRK(y, T, P, 'vapor', compData);

rhog=RHO; %kg/m^3, density for gas
rhoo=857;%881; %kg/m^3, density for oil

RHO = [rhog,rhoo]; %Vector of densities.

%% Estimate efficiency vs xg_in and q_in
q_t = zeros(length(q_in),length(xg_in)); %Empty q_t matrix
q_b = zeros(length(q_in),length(xg_in)); %Empty q_b matrix
x_ot = zeros(length(q_in),length(xg_in)); %Empty x_ot matrix
x_gb = zeros(length(q_in),length(xg_in)); %Empty x_gb matrix
xg_LPO = zeros(length(q_in),length(xg_in)); %Empty xg_LPO matrix
xo_HPO = zeros(length(q_in),length(xg_in)); %Empty xo_HPO matrix
GR = zeros(length(q_in),length(xg_in)); %Empty GR matrix
Esplit = zeros(length(q_in),length(xg_in)); %Empty Esplit matrix
count = 0;

n = 1;
for i = 1:length(q_in)
```

```
    for j = 1:length(xg_in)

% Calculating the flows and mole frac to upper and lower part of separator

[q_t(i,j), q_b(i,j), x_ot(i,j), x_gb(i,j)]=Flow_Split3(q_in(i)/3600 ...
                                                    ,xg_in(j), RHO, Dim);

% Performing the calculations of the separator

[xg_LPO(i,j),xo_HPO(i,j),GR(i,j),Esplit(i,j),q_LPO(i,j),q_HPO(i,j)]=...
    GLCC_comb(q_t(i,j),q_b(i,j),x_ot(i,j),x_gb(i,j),q_in(i)/3600,...
    xg_in(j),Dim,RHO,n);
count = count+1
    end
end

%% Generating plots for efficiency vs xg_in and q_in

figure (1)
set(gcf,'PaperPositionMode','auto')
subplot(2,1,1)
plot(xg_in,GR(1,:),'b',xg_in,GR(14,:),'g', xg_in, GR(24,:),'r',...
    xg_in, GR(44,:),'k','LineWidth',1.5)
xlabel('\alpha_{in}','FontSize',14)
ylabel('Gas Recovery','FontSize',12)
axis([0.1 0.9 0.94 1])
legend('q_{in}=85 m^{3}/h','q_{in}=150 m^{3}/h','q_{in}=200 m^{3}/h',...
    'q_{in}=300 m^{3}/h','location','west')


subplot(2,1,2)
plot(xg_in,Esplit(1,:),'b',xg_in,Esplit(14,:),'g', xg_in,Esplit(24,:)...
    ,'r', xg_in,Esplit(44,:),'k','LineWidth',1.5)
xlabel('\alpha_{in}','FontSize',14)
ylabel('\eta_{split}','FontSize',14)
```

```
axis([0.1 0.9 0.87 1])
legend('q_{in}=85 m^{3}/h','q_{in}=150 m^{3}/h','q_{in}=200 m^{3}/h',...
    'q_{in}=300 m^{3}/h','location','west')

%subplot(2,2,3)
figure (2)
set(gcf,'PaperPositionMode','auto')
plot(xg_in,xg_LPO(1,:),'b',xg_in,xg_LPO(14,:),'g',...
    xg_in,xg_LPO(24,:),'r', xg_in,xg_LPO(44,:),'k','Linewidth',1.5)
xlabel('\alpha_{\it in}','FontSize',14)
ylabel('\alpha_{\it LPO}','FontSize',14)
axis([0.1 0.9 0.85 1])
legend('q_{in}=85 m^{3}/h','q_{in}=150 m^{3}/h','q_{in}=200 m^{3}/h',...
    'q_{in}=300 m^{3}/h','location','southeast')

%subplot(2,2,4)
figure (3)
set(gcf,'PaperPositionMode','auto')
plot(xg_in,xo_HPO(1,:),'b',xg_in,xo_HPO(14,:),'g',...
    xg_in,xo_HPO(24,:),'r', xg_in,xo_HPO(44,:),'k','LineWidth',1.5)
xlabel('\alpha_{\it in}','FontSize',14)
ylabel('\alpha_{\it o,HPO}','FontSize',14)
axis([0.1 0.9 0.9 1])
legend('q_{in}=85 m^{3}/h','q_{in}=150 m^{3}/h','q_{in}=200 m^{3}/h',...
    'q_{in}=300 m^{3}/h','location','west')

%suptitle('\alpha_{in} analysis')


figure(4)
set(gcf,'PaperPositionMode','auto')
subplot(2,1,1)
plot(q_in,GR(:,1),'b', q_in,GR(:,31),'g',q_in, GR(:,41),'k',...
    q_in,GR(:,61),'r','LineWidth',1.5)
xlabel('\it q_{in} \rm[m^{3}/h]','FontSize',12)
```

```
ylabel('Gas Recovery','FontSize',12)
axis([85 330 0.86 1])
legend('\alpha_{in} = 0.1','\alpha_{in} = 0.4','\alpha_{in} = 0.5',...
    '\alpha_{in} = 0.7','location','southwest')

subplot(2,1,2)
plot(q_in,Esplit(:,1),'b', q_in,Esplit(:,31),'g',q_in,Esplit(:,41),'k',...
    q_in,Esplit(:,61),'r','LineWidth',1.5)
xlabel('\it q_{in} \rm[m^{3}/h]','FontSize',12)
ylabel('\eta_{split}','FontSize',14)
axis([85 330 0.86 1])
legend('\alpha_{in} = 0.1','\alpha_{in} = 0.4','\alpha_{in} = 0.5',...
    '\alpha_{in} = 0.7','location','southwest')

%subplot(2,2,3)
figure (5)
set(gcf,'PaperPositionMode','auto')
plot(q_in,xg_LPO(:,1),'b', q_in,xg_LPO(:,31),'g',q_in,xg_LPO(:,41),'k',...
    q_in,xg_LPO(:,61),'r','LineWidth',1.5)
xlabel('\it q_{in} \rm[m^{3}/h]','FontSize',12)
ylabel('\alpha_{\it LPO}','FontSize',14)
axis([85 330 0.86 1])
legend('\alpha_{in} = 0.1','\alpha_{in} = 0.4','\alpha_{in} = 0.5',...
    '\alpha_{in} = 0.7','location','southwest')

%subplot(2,2,4)
figure (6)
set(gcf,'PaperPositionMode','auto')
plot(q_in,xo_HPO(:,1),'b', q_in,xo_HPO(:,31),'g',q_in, xo_HPO(:,41),'k',...
    q_in,xo_HPO(:,61),'r','LineWidth',1.5)
xlabel('\it q_{in} \rm [m^{3}/h]','FontSize',12)
ylabel('\alpha_{\it o,HPO}','FontSize',14)
axis([85 330 0.85 1])
legend('\alpha_{in} = 0.1','\alpha_{in} = 0.4','\alpha_{in} = 0.5',...
    '\alpha_{in} = 0.7','location','southwest')
```

```
%suptitle('q_{in} analysis')

x = (1-xo_HPO');
figure (7)
set(gcf,'PaperPositionMode','auto')
surf(q_in,xg_in,x)
xlabel('Inlet flow, q_{in} [m^{3}/h]')
ylabel('Inlet gas fraction, \alpha_{in}')
zlabel('1-\alpha_{o,HPO}')

figure(8)
set(gcf,'PaperPositionMode','auto')
surf(xg_in,q_in, x_gb)
ylabel('Inlet flow, q_{in} [m^{3}/h]','FontSize',12)
xlabel('Inlet gas fraction, \alpha_{in}','FontSize',12)
zlabel('Entrained of gas into liquid flow, \alpha_{g,b}','FontSize',12)

figure(9)
set(gcf,'PaperPositionMode','auto')
surf(xg_in,q_in,x_ot)
ylabel('Inlet flow, q_{in} [m^{3}/h]','FontSize',12)
xlabel('Inlet gas fraction, \alpha_{in}','FontSize',12)
zlabel('Entrained of liquid into gas flow, \alpha_{l,t}','FontSize',12)

toc
```

E.1.2 Performance Function

The function *GLCC_comb* calculates the performance of the separator given a set of inlet conditions.

```
function [xg_LPO,xo_HPO,GR,Esplit,q_LPO,q_HPO]= GLCC_comb(q_t,q_b, x_ot,...
```

```
                                                    x_gb, q_in,xg_in,Dim,RHO,n)
%%%%%%%%%%%%%%%%%%%%%%%%%%%%%%%%%%%%%%%%%%%%%%%%%%%%%%%%%%%%%%%%%%%%%%%%%%%%
% Author: Torstein Bishop
%
% Department of Chemical Engineering, NTNU. Spring 2016.
%
%
%
% This function calls on the functions GLCC_LowerPart_Governing and
%
% GLCC_UpperPart_Governing in order to determine the smallest radius the
%
% droplets and bubbles can have in order to be separated. It also calls on%
% the function GLCC2 that calculates the outlet streams and the
%
% compositon between oil and gas in the stream.
%
%
%
%%%%%%%%%%%%%%%%%%%%%%%%%%%%%%%%%%%%%%%%%%%%%%%%%%%%%%%%%%%%%%%%%%%%%%%%%%%%

% Separator dimensions.
Ls=Dim.Ls;  %Separator length [m]
Rs=Dim.Rs; %Separator radius [m]
Ds = Dim.Ds; %Separator diameter [m]
Lt = Dim.Lt; %Length of upper part of the separator [m]
Lb = Dim.Lb; %Length of lower part of the separator [m]
theta = Dim.Lb; %Inclination angle of inlet pipe [degrees]
Li = Dim.Li; %Length of inlet pipe [m]
A_in = Dim.A_in; %Cross-sectional area of inlet pipe [m2]
A_is = Dim.A_is; %Cross-sectional are of inlet slot [m2]
z_l = 0.001; % Level of Liquid interface, inlet = 0. [m]

% Calculations of important parameters for the separator
q_gin = xg_in*q_in; %Inlet gas flow [m3/s]
```

```
q_oin = q_in-q_gin; %Inlet gas flow [m3/s]
%q_LPO = FS*q_in;    %Flow out through LPO [m3/s]
%q_HPO = (1-FS)*q_in; %Flow out through HPO [m3/s]
v_oin = q_oin/A_in; %Inlet velocity of oil [m/s]
v_gin = q_gin/A_in; %Inlet velocity of gas [m/s]
v_ltis = v_oin*(A_in/A_is)*cosd(theta); %Inlet tangential velocity of oil
v_gtis = v_gin*(A_in/A_is)*cosd(theta); %Inlet tangential velocity of gas

%% Calculations for the lower part of the separator

zD_ratio = 2; %Ratio of z/D
% Calculating Rcap, Omega, Mom and Uz_low by using fsolve, Lower part of
% separator
%x0 = [Rcap, Omega, Mom, Uz_low]
%       1      2     3     4


Eqn1 = @(x) x(1) - (0.5-(0.65/exp(0.6*x(2))))*Rs; %Gas-core radius
Eqn2 = @(x) x(2) - 1.48*(x(3))^(0.93)*exp(-0.113*(x(3))^(0.35)*...
    (zD_ratio)^(0.7)); %Equation for the swirl intensity at inlet
Eqn3 = @(x) x(3) - (v_ltis/x(4)); %Momentum flux ratio
Eqn4 = @(x) x(4) - (q_b/(pi*(Rs^2 - (x(1))^2))); %Equation for Uz_top

Eqns = @(x) [Eqn1(x); Eqn2(x); Eqn3(x); Eqn4(x)];

if n==1 %This is not used anymore
    x0 = [0.01 0.5 0.5 4];%Inital values for the variables
else
    %x0 = [0.01 0.01 0.01 0.01];
    x0 = [0.04 0.5 0.5 4];
end
lb = [0, 0, 0, 0]; %Lower bounds
ub = [1/2*Rs, inf, inf, inf]; %Upper bounds
options = optimoptions('lsqnonlin','Display','off');
%x = fsolve(Eqns,x0,options);
```

```
x = lsqnonlin(Eqns,x0,lb,ub,options);

%y = Eqns(x)
Rcap = real(x(1)); %Capture Radius [m]
Omega = real(x(2)); %Swirl intensity at inlet
Mom = real(x(3)); %Momentum flux
Uz_low = real(x(4)); %Axial velocity lower part [m/s]
%pause
if Rcap <=0 || Rcap > Rs
    Rcap
    return
end

t_b = (pi*(Rs^2 - Rcap^2)*(Lb-z_l))/q_b; %Residence time for lower part [s]

%Finding rin=r(t0) that gives r(ta)=Rcap
h = t_b/10; %Amount of steps
alpha_low = 0.001; %Relaxation factor
tol_low = 10E-6*Rcap; %Tolerance allowed in the iteration
in_low = [q_in, Uz_low, v_ltis, Ds, v_oin];
Rin_0low = 0.999*Rs;%0.999*Rs; %Initial guess of bubble position
Z_in = Lb; % Integrating upwards from bottom towards inlet
zF = z_l;%Lb;%0; %Final position for bubble

[T_low, r_low, z_low] = RK4_GLCC(@GLCC_LowerPart_Governing,[0,t_b],...
    Rcap, Z_in, h, in_low, RHO);
% r_low
% z_low
% pause
R_low = r_low(end,end); %Inlet radius for droplet
Z_low = z_low(end,end); %Inlet axial position for droplet

BigSep = 0;
if R_low > Rs
    disp('R_low > Rs = full separation')
```

```
    BigSep = BigSep +1; %Give the amount of Rsep >Rs
    R_low = Rs;
end

%% Calculations for the upper part of the separator

Uz_top = q_t/(pi*Rs^2); % Axial velocity upper part [m/s]

t_t = (pi*Rs^2*Lt)/q_t; %Residence time fo upper part [s]

z0 = 0; %Starting point for droplet

%Finding rin=r(t0) that gives r(ta)=Rs
h_top = t_t/10;
tol_top = 10E-10*Rs; %Tolerance allowed in iteration
in_top = [q_in, Uz_top, v_gtis, Ds, v_gin];
Rin_0top = 10E-2*Rs; %Initial guess of droplet position
zF = Lt; %Final axial position for droplet
alpha_top = 1; %Relaxation factor

[T_top, r_top, z_top] = shooting_GLCC(@GLCC_UpperPart_Governing, [0,t_t]...
    , h_top, Rs, Rin_0top, alpha_top, tol_top, z0,zF, in_top, RHO);
%[T_top, r_top, z_top] = RK4_GLCC(@GLCC_UpperPart_Governing, [0,t_t],...
%    Rs, zF, h_top, in_top, RHO);

%r_top
%z_top
R_top = r_top(1,1); %Inlet radius for bubble
Z_top = z_top(1,1); %Inlet axial position for bubble
%R_top = r_top(end,end);
%Z_top = z_top(end,end);

%pause
%% Determining the gas/oil fractions in LPO/HPO as well sep efficiency
```

```
%q = [q_LPO, q_HPO, q_b, q_t]; % Vector of flows
q = [q_b,q_t];
R = [Rs, Rcap, R_low, R_top]; % Vector of radii
[ xg_LPO, xo_LPO, xo_HPO,xg_HPO,q_LPO,q_HPO ] = GLCC2( q, R, x_gb, x_ot );

GR = (q_LPO*xg_LPO)/(xg_in*q_in); %Gas recovery
Esplit = 1-(xo_LPO*q_LPO + xg_HPO*q_HPO)/q_in; %Split efficiency
end
```

E.1.3 Governing Equation for Lower Part

The function *GLCC_LowerPart_Governing* contains the model equations for the lower part and will calculate the bubbles radial velocity. This velocity is integrated to find the bubble trajectory.

```
function [ vr, vz ] = GLCC_LowerPart_Governing(t, r, z, in, RHO)
%%%%%%%%%%%%%%%%%%%%%%%%%%%%%%%%%%%%%%%%%%%%%%%%%%%%%%%%%%%%%%%%%%%%%%%%%%%%%%%
% Author: Torstein Bishop
%
% Department of Chemical Engineering, NTNU. Spring 2016.
%
%
%
% This function contains the governing equations for the bubble trajectory%
% inside the lower part of a GLCC separator, where oil is the continuous
%
% phase and the methane gas is the dispersed face.
%
% The governing equations are made up from force balances on the bubble in%
% axial and radial direction.
%
%%%%%%%%%%%%%%%%%%%%%%%%%%%%%%%%%%%%%%%%%%%%%%%%%%%%%%%%%%%%%%%%%%%%%%%%%%%%%%%
```

```
%Input parameters
qin = in(1); %Total inlet volumetric flow [m3/h]
Uz = in(2); %Axial flow [m/s]
vtis = in(3); %Inlet tangential velocity of oil [m/s]
D = in(4); %Separator Diameter[m]
v_oin = in(5); %Inlet oil flow
Rs = D/2; %Separator Radius [m]
Visc_oil = 0.0051;%0.0088; %0.0088; % [Pa*s] Viscosity of oil
sigma = 0.0155; %0.0722; %Surface tension of oil [N/m] WATER in this case
g = 9.81;          % [m/s^2] Gravitational acceleration

rhog=RHO(1); %kg/m^3, density for gas
rhoo=RHO(2); %kg/m^3, density for oil

%Tangential velocity calculations
mom = vtis/Uz; %Momentum flux ratio between tangential and total flux

if z/D < 2 %Omega only valid for z/D >=2
    ratio = 2;
else
    ratio = z/D;
end

Omega = 1.48*mom^(0.93)*exp(-0.113*mom^0.35*(ratio)^(0.7));%Swirl intensity

B = 3.6 + 20*exp(-(Omega/0.6)); %Radial location of maximum velocity

Tm = 0.9*Omega - 0.05; %Maximum tangential velocity momentum

vt = (Tm/(r/Rs))*(1-exp(-B*(r/Rs)^2))*Uz; % Tangential velocity

% Droplet size correlation
%rd = (-0.6*(qin*3600)*1E-6+0.0002)/2;
lambda_bub = (sigma/(rhog*g))^(0.5);
```

```
d_bub = (1/v_oin)*((0.14*sigma*lambda_bub)/rhoo)^(0.5);
rd = d_bub/2;

% Radial velocity equation
vr = abs((2/9)*((rhog-rhoo)/Visc_oil)*((rd^2)*(vt^2))/r);

% Axial velocity
vz = -Uz;
end
```

E.1.4 Governing Equation for Upper Part

The function *GLCC_UpperPart_Governing* contains the model equations for the upper part and will calculate the droplets radial velocity. This velocity is integrated to find the droplet trajectory.

```
function [ vr, vz ] = GLCC_UpperPart_Governing( t, r, z, in, RHO )
%%%%%%%%%%%%%%%%%%%%%%%%%%%%%%%%%%%%%%%%%%%%%%%%%%%%%%%%%%%%%%%%%%%%%%%%%%%%%%%
% Author: Torstein Bishop
%
% Department of Chemical Engineering, NTNU. Spring 2016.
%
%
%
% This function contains the governing equations for the droplet
%
% trajectory inside the lower part of a GLCC separator, where methan gas
%
% is the continuous phase and oil is the dispersed phase.
%
% The governing equations are made up from force balances on the droplet
%
```

```
% in axial and radial direction.
%
%%%%%%%%%%%%%%%%%%%%%%%%%%%%%%%%%%%%%%%%%%%%%%%%%%%%%%%%%%%%%%%%%%%%%%%%%%%%%%%%

%Input parameters
qin = in(1); %Total inlet volumetric flow [m3/h]
Uz = in(2); %Axial flow [m/s]
vtis = in(3); %Inlet tangential velocity of gas [m/s]
D = in(4); %Separator diameter [m]
v_gin = in(5);
Rs = D/2; %Separator Radius [m]
Visc_gas =0.0000127;% 0.00001118; % [Pa*s] Viscosity of gas
sigma = 0.0155; %0.0722; %Surface tension of oil [N/m] WATER in this case
g = 9.81;          % [m/s^2] Gravitational acceleration

rhog=RHO(1); %kg/m^3, density for gas
rhoo=RHO(2); %kg/m^3, density for oil


%Tangential velocity calculations
mom = vtis/Uz; %Momentum flux ratio between tangential and total flux

if z/D < 2 %Omega only valid for z/D >=2
    ratio = 2;
else
    ratio = z/D;
end

Omega = 0.01*mom^(0.93)*exp(-0.113*mom^0.35*(ratio)^(0.7));%Swirl intensity

vt_max = (3/2)*Uz*Omega; % Maximum tangential velocity

vt = vt_max*(r/Rs); %Tangential velocity

% Bubble size correlation
```

```
%rd = (-0.6*(qin*3600)*1E-6+0.0002)/2;
lambda_drop = (sigma/(rhoo*g))^(0.5);
d_drop = (1/v_gin)*((0.14*sigma*lambda_drop)/rhog)^(0.5);
rd = d_drop/2;

% Radial velocity equation
vr = (2/9)*((rhoo-rhog)/Visc_gas)*rd^2*(vt^2)/r;

% Axial velocity
vz = Uz;
end
```

E.1.5 Composition Calculations

The function *GLCC2* calculates the conditions in the outlet streams given the radii that will ensure separation in the upper and lower part.

```
function [xg_LPO,xo_LPO,xo_HPO,xg_HPO,q_LPO,q_HPO]=GLCC2(q, R, x_gb, x_ot )
%%%%%%%%%%%%%%%%%%%%%%%%%%%%%%%%%%%%%%%%%%%%%%%%%%%%%%%%%%%%%%%%%%%%%%%%%%%%%%%
% Author: Torstein Bishop
%
% Department of Chemical Engineering, NTNU. Spring 2016.
%
%
%
% This script calculates the oil and gas volume fractions in the outlet
%
% streams.
%
%%%%%%%%%%%%%%%%%%%%%%%%%%%%%%%%%%%%%%%%%%%%%%%%%%%%%%%%%%%%%%%%%%%%%%%%%%%%%%%

Rs = R(1); % Separator radius [m]
Rcap = R(2); %Capture radius [m]
```

```
r_low = R(3); %inlet radius that gives bubble separation [m]
r_top = R(4); %inlet radius that gives droplet separation [m]
q_b = q(1);   %Inlet stream to lower part [m3/s]
q_t = q(2);   %Inlet stream to upper part [m3/s]

%x = [q_bt  q_o  q_tt  q_g  x_tgb  x_tot  xo_LPO  xg_HPO  q_HPO  q_LPO]
%      1     2    3     4    5      6      7       8      9      10

Eqn1= @(x) x(1) - (q_b + x(2));
Eqn2= @(x) x(3) - (q_t + x(4));
Eqn3= @(x) x(5) - ((x_gb*q_b)/x(1));
Eqn4= @(x) x(6) - ((x_ot*q_t)/x(3));
Eqn5= @(x) x(2) - (x(6)*x(3) - x(7)*x(10));
Eqn6= @(x) x(4) - (x(5)*x(1) - x(8)*x(9));
Eqn7= @(x) x(7) - x(6)*(r_top^2/Rs^(2))*(x(3)/x(10));
Eqn8= @(x) x(8)-x(5)*((Rs^(2) - r_low^(2))/(Rs^(2)-Rcap^(2)))*(x(1)/x(9));
Eqn9= @(x) x(9) - (x(1) - x(4));
Eqn10=@(x) x(10) - (x(3) - x(2));

Eqns=@(x)[Eqn1(x);Eqn2(x);Eqn3(x);Eqn4(x);Eqn5(x);Eqn6(x);Eqn7(x);...
    Eqn8(x);Eqn9(x);Eqn10(x)];

x0=[q_b,x_ot*q_t,q_t,x_gb*q_b,x_gb,x_ot,0.001,0.001,q_b,q_t];%Inital values
lb = [0, 0, 0, 0, 0, 0, 0, 0,]; %Lower bounds
ub = [inf, inf, inf, inf, 1, 1, 1, 1,]; %Upper bounds
%options = optimoptions('lsqnonlin','Display','off');
options = optimoptions('fsolve','Display','off');
%x = lsqnonlin(Eqns,x0,lb,ub,options);
[x,~,exitflag,output]= fsolve(Eqns,x0,options);

xo_LPO = real(x(7));
xg_LPO = 1-xo_LPO;
xg_HPO = real(x(8));
xo_HPO = 1-xg_HPO;
q_LPO = real(x(10));
```

```
q_HPO = real(x(9));

end
```

E.1.6 Entrainment Calculations

The function *Flow_Split3* calculates the entrainment of gas into the liquid stream entering the lower part of the separator and the entrainment of liquid into the gas stream entering the upper part of the separator.

```
function [ q_t, q_b, x_ot, x_gb ] = Flow_Split3( q_in, xg_in, RHO, Dim )
%%%%%%%%%%%%%%%%%%%%%%%%%%%%%%%%%%%%%%%%%%%%%%%%%%%%%%%%%%%%%%%%%%%%%%%%%%%%%%%
% Author: Torstein Bishop
%
% Department of Chemical Engineering, NTNU. Spring 2016.
%
%
%
% This function calculates the flow split at the inlet of the GLCC
%
% separator. It also determines the amount of liquid going upwards with
%
% the gas phase and the amount of gas that goes downwards with the liquid %
% phase. The calculations are done by using Wallis' correlation on
%
% Paleev's entrainment equation.
%
%
%
%%%%%%%%%%%%%%%%%%%%%%%%%%%%%%%%%%%%%%%%%%%%%%%%%%%%%%%%%%%%%%%%%%%%%%%%%%%%%%%

%% Parameters
```

```
rhog = RHO(1); %Density for the gas
rhoo = RHO(2); %Density for the oil
sigma = 0.0155; %Surface tension of oil [N/m]
Visc_gas = 0.0000127;%0.00001118; % [Pa*s] Viscosity of gas
A_in = Dim.A_in; %Cross-sectional area of inlet pipe [m2]
q_gi = xg_in*q_in; % Inlet gas flow [m3/s]
q_oi = (1-xg_in)*q_in; %Inlet oil flow [m3/s]
v_gin = q_gi/A_in; % Superficial/inlet gas velocity [m/s]


%% Paleevs equation w/ Wallis' correlation

phi = ((v_gin*Visc_gas)/sigma)*(rhog/rhoo)^(1/2); %Wallis' correlation

Eo = 1 - (0.985 - 0.44*log10(phi*10^(4))); %Paleevs entr equation

if Eo < 0
   Eo = 0;
end

Eg = Eo;

%% Calculation of flow streams and mole fractions
q_ot = Eo*q_oi; %Upwards oil-flow [m3/s]

q_gb = Eg*q_gi; %Downwards gas-flow [m3/s]

q_t = q_gi*(1-Eg) + q_ot; %Total flow to the upper part of the GLCC [m3/s]

q_b = q_oi*(1-Eo) + q_gb; %Total flow to the lower part of the GLCC [m3/s]

x_ot = q_ot/q_t; % Oil-fraction in the upper part of the GLCC

x_gb = q_gb/q_b; % Gas-fraction in the lower part of the GLCC
end
```

E.2 Deliquidizer

The MATLAB scripts for the deliquidizer are given in this section. The main function, Appendix E.2.1, calls the function containing the governing equations, Appendix E.2.2, and the function calculating the conditions in the outlet streams, Appendix E.2.2.

E.2.1 Main Function

The function *swirl_func3_deliq* will calculate, for given inlet conditions, the performance of the deliquidizer.

```
function [Vg_LPO,Vg_HPO,GR,Esplit,qen]=...
    swirl_func3_deliq(Vg_in,qin,FS)
Lsw=1.5;  %Separator length
Ro=0.075; %Separator radius
Ri= sqrt(4/5)*Ro; %Radius for gas-extraction pipe

qi=FS*qin;      %Light phase out flow
qo=qin-qi;      %Heavy phase out flow
ta=(pi*Ri^2*Lsw)/qi; % Residence time

%%
%Finding rin=r(t0) that gives r(ta)=Ri
h=ta/10;%Amount of steps
rin_0= 0.00001;% Initial guess
in=[qin,Ro,Ri,Vg_in,ta,rin_0,FS];
rho=1; %Under-relaxation parameter
tol=10^-10*Ri; %Tolerance allowed in interation
[T,X]=shooting_deliq(@swirl_sep2_deliq,[0,ta],h,Ri,rin_0,rho,tol,in);

rin=X(1,1); %Inlet radius for droplet
```

```
[Vg_LPO,Vg_HPO,qen]=DeLiquidizer(qin,Vg_in,FS,rin,[Lsw;Ro;Ri]);
Vo_LPO=1-Vg_LPO; Vo_HPO=1-Vg_HPO;


GR=Vg_LPO*qi/((Vg_in)*qin);              % Gas Recovery
Esplit=1-((1-Vg_LPO)*qi+Vg_HPO*qo)/qin; % Split efficiency
```

E.2.2 Governing Equation

The governing model equations for the deliquidizer are given in the function *swirl_sep2_deliq*. It will calculate the radial velocity of the droplet given a set of inlet conditions.

```
function [vr]=swirl_sep2_deliq(t,x,in)
qin=in(1);
Ro=in(2);
Ri=in(3);
Vg_in=in(4);
ta=in(5);
rin=in(6);
FS=in(7);

% Filling in component data needed to calculate the density of the gas
% found from The properties of Gases and Liquids fifth edition.
compData.Pc = 45.99e5; % [Pa], Critical Pressure
compData.Tc = 190.56;  % [K], Critical Temperature
compData.w = 0.011;     % Acentric factor
compData.Cp = 0;       % Not used in any calculations yet
compData.Tref = 273.15; % [K]
compData.Mm = 16.043;   % [g/mol]
```

```
P = 50e5; % [Pa] Pressure in separation system
T = 50+273; % [K] Assumed temperature in separation system
y = 1; % Assume only methane in gas phase

% Calling SRK-EOS for density calculations
[Z, RHO] = SRK(y, T, P, 'vapor', compData);

rhog=RHO; %kg/m^3, density for gas
rhoo=857;%881; %kg/m^3, density for oil


r=x(1);

Rc=0.25*Ro; %Critical radius
va=qin/(pi*Ro^2); % Initial axial velocity

k= 0.1; % Swirl number

vt0=k*va; %Initial tangential velocity

rd = (-0.6*(qin*3600)*1E-6+0.0002)/2; % Droplet size

% if vt0>4.45%28
%     rd=(-8*vt0+160)/2*10^-6;
% else
%     rd=(-107*vt0+600)/2*10^-6;
% end

Visc_gas = 0.0000127; % Gas viscosity

mum=Visc_gas;

%Smooth centrifugal acceleration
f2=(vt0*exp(-0.04*va*t/(2*Ro)))^2/r;
```

```
f1=(vt0*exp(-0.04*va*t/(2*Ro))/Rc)^2*r;
f=f2-f1;
beta=1; %Smoothing parameter
ac=f2-0.5*((f^2+beta^2)^.5+f); %Centrifugal acceleration


%Radial velocity of droplet
 vr=(2/9*(rhoo-rhog)*rd^2/mum)*ac; %Original model

end
```

E.2.3 Composition Calculations

The function *DeLiquidizer* will calculate the conditions in the outlet streams of the separator given an inlet radius that yields separation.

```
function [Vg_LPO,Vg_HPO,qen]=DeLiquidizer(qin,Vg_in,FS,rin,p3)

Ro=p3(2);Ri=p3(3);

qi=FS*qin;      %Light phase out flow
qo=qin-qi;      %Heavy phase out flow

% Volume fraction of oil in outlets before
% the re-entrainment is accounted for
Vo_HPO=(1-Vg_in)*(((1-FS)*Ri^2+FS*(Ri^2-rin^2))/((1-FS)*Ri^2));
Vo_LPO=((1-Vg_in)*qin-Vo_HPO*qo)/qi;

% Velocities needed for re-entrainment
u_LPO=qi/(pi*Ri^2);
u_HPO=qo/(pi*(Ro^2-Ri^2));
du=u_LPO-u_HPO;
k=2*10^-4; % Re-entrainment proportionality coefficient
```

```
qen=k*du;

%Adding re-entrainment to fraction equations
if du>=0
    Vo_LPO=(Vo_LPO*(qi-qen)+Vo_HPO*qen)/qi;
    Vo_HPO=((1-Vg_in)*qin-Vo_LPO*qi)/qo;
else
    Vo_HPO=(Vo_HPO*(qi+qen)-Vo_LPO*qen)/qi;
end

% Restrict oil volume fraction in HPO
% to range Vw_in->1
if Vo_HPO>1
    Vo_HPO=1;
elseif Vo_HPO<(1-Vg_in)
    Vo_HPO=(1-Vg_in);
end

Vo_LPO=((1-Vg_in)*qin-Vo_HPO*qo)/qi;%Oil composition in LPO

Vg_LPO=1-Vo_LPO; %Gas composition in LPO
Vg_HPO=1-Vo_HPO; %Gas composition in HPO
end
```

E.3 Solvers and SRK-EOS

In this section the solvers and the SRK equation of state used for the simulations are given. The Runge-Kutta integrator is given in Appendix E.3.1, the shooting method is given in Appendix E.3.2 and the SRK-EOS is given in Appendix E.3.3

E.3.1 Runge-Kutta

The *RK4_GLCC* function is a fourth order Runge-Kutta integrator that is used to integrate the droplet/bubble velocities for the GLCC and the deliquidizer so that their trajectories can be determined.

```
function [t,y,z] = RK4_GLCC( ODEfile,tspan,yi,z0,h,in, RHO )
%%%%%%%%%%%%%%%%%%%%%%%%%%%%%%%%%%%%%%%%%%%%%%%%%%%%%%%%%%%%%%%%%%%%%%%%%%%%%%%
% Author: Torstein Bishop
%
% Department of Chemical Engineering, NTNU. Spring 2016.
%
%
%
% This function is used, combined with the shooting_GLCC to solve the
%
% the governing equations for the upper and lower part of the GLCC, by
%
% integrating the radial and axial position of the droplet/buble.
%
%%%%%%%%%%%%%%%%%%%%%%%%%%%%%%%%%%%%%%%%%%%%%%%%%%%%%%%%%%%%%%%%%%%%%%%%%%%%%%%

t=tspan(1):h:tspan(2); %Vector of t-values
if t(end)~=tspan(2)
    t(end+1)=tspan(2);
end

d=diff(t); %Vector of t-increments
yi=(yi(:).')'; %Makes sure it is a column vector
z0 = (z0(:).')'; %Column vector

y(:,1)=yi; % Initial condition
z(:,1)=z0; % Initial condition
```

```
for i = 1:length(t) - 1

    [k1,l1] = feval(ODEfile,t(i),y(:,i), z(:,i),in,RHO);

    [k2,l2] = feval(ODEfile,t(i)+d(i)/2,y(:,i)+k1/2,z(:,i)+l1/2,in,RHO);

    [k3,l3] = feval(ODEfile,t(i)+d(i)/2,y(:,i)+k2/2,z(:,i)+l2/2,in,RHO);

    [k4,l4] = feval(ODEfile,t(i)+d(i),y(:,i)+k3,z(:,i)+l3,in,RHO);

    y(:,i+1) = y(:,i)+d(i)*(k1+2*k2+2*k3+k4)/6;
    z(:,i+1) = z(:,i)+d(i)*(l1+2*l2+2*l3+l4)/6;

end


z=z';
y=y';
t=t';
end
```

E.3.2 Shooting Method

The function *shooting_GLCC* is used to solve the boundary value problems that arises in the model for the GLCC and the deliquidizer.

```
function [t, r, z] = shooting_GLCC( ODEfile, tspan, h, yf, gamma0, ...
                                    alpha, tol, z0, zF,in, RHO)
%%%%%%%%%%%%%%%%%%%%%%%%%%%%%%%%%%%%%%%%%%%%%%%%%%%%%%%%%%%%%%%%%%%%%%%%%%%%%%%
% Author: Torstein Bishop
%
% Department of Chemical Engineering, NTNU. Spring 2016.
%
```

```
%
%
% Function used to solve the initial value problem to find the radius of
%
% of a bubble/droplet that will leave the separator at Rcap.
%
%%%%%%%%%%%%%%%%%%%%%%%%%%%%%%%%%%%%%%%%%%%%%%%%%%%%%%%%%%%%%%%%%%%%%%%%%%%%%%%
gammanew=gamma0;
iter=0; %Iteration variable
maxiter= 100; %Maximum iteration
fnk=10*yf; %Random number to get iteration started
zi = z0; %Iteration variable for the z-direction

while max(abs(yf - fnk)) > tol && iter < maxiter
    iter = iter+1;
    gamma1 = gammanew;
    [t,r,z] = RK4_GLCC(ODEfile,tspan,gamma1,z0,h,in,RHO);
    fnk = r(end,1);
    zi = abs(z(end));

    % Setting dgamma for the derivative term
    if gamma1~=0
       dgamma = gamma1/100;
    else
        dgamma= 0.01;
    end

    %Calculating the Jacobian
    a = gamma1 + dgamma;
    [ta,ra,za] = RK4_GLCC(ODEfile,tspan,a,z0,h,in, RHO);
    fnka = ra(end,1);
    jacob = (fnka-fnk)/dgamma;
    a = gamma1-dgamma;

    %Next approximation of the roots
```

```
    if jacob==0;
        gammanew=gamma1+max([abs(dgamma),1.1*tol]);
    else
        gammanew=gamma1-alpha*inv(jacob)*(fnk-yf);
    end


end


if  iter >= maxiter
    disp(['Warning: Maximum iterations reached.',num2str((fnk-yf)/yf)])
    disp(ODEfile)
end

end
```

E.3.3 Soave-Redlich-Kwong Equation of State

The function *SRK* calculate the density of the gas given the temperature, pressure and the composition of the gas. Important gas parameters are also needed. The code is an adaption of Professor Sigurd Skogestad's code published on his web page [36].

```
function [ Z, RHO, V ] = SRK(x,T,P,Phase,compData )
% This is a remake of Andreas Linhart and Sigurd Skogestads
% implementation of the SRK-EOS and is adapted for specialization project
% fall 2015.

%Author: Torstein Bishop, Department of Chemical Engineering, NTNU. Fall
%2015.
```

```
% IN: molefraction of mixture (x), Pressure (P) [Pa], Temperature [K],
% phase of mixture and various component data (Tc,Pc, CP, w).

%OUT: Compressibility, Z, and density, rho, [kg/m3].

% Checking for number of components and gathering compData
NC = length(x);

%Checking for consistent mole fractions
if NC == 1 && sum(x) <1
    disp('Inconsistent mole fractions')
end

%Here: SRK binary interaction parameters set to zero
kinteraction=zeros(NC,NC);

% initialize
% liquid=1;vapor=2; Not sure if this part is needed
R = 8.314; % [J/K*mol]

Pc=compData.Pc; %Critical Pressure
Tc=compData.Tc; %Critical Temperature
w=compData.w;   % Acentric factor
ZRA=0.29056-0.08775*w;  % Rackett compressibility factor.
Cp=compData.Cp;
Tref=compData.Tref; % Reference temperature
Mm=compData.Mm/1000; % Molar mass for the components

% Calculating important parameters needed to solve system
Tre=T./Tc;
Pre=P./Pc;
m=0.480+1.574.*w-0.176.*w.^2;
a=(1+m.*(1-Tre.^0.5)).^2;
Ap=0.42747.*a.*Pre./Tre.^2;
Bp=0.08664.*Pre./Tre;
```

```
% Start calculations
% Binary a's:
Ab=zeros(NC,NC);
for i=1:NC
    for j=1:NC
        Ab(i,j)=(Ap(i)*Ap(j))^0.5;
    end
end
% Mixture a and b
A=0;
for i=1:NC
    for j=1:NC
        A=A+x(i)*x(j)*Ab(i,j)*(1-kinteraction(i,j));
    end
end
B=0;
for i=1:NC
    B=B+x(i)*Bp(i);
end

% Solve cubic equation to find compressibility Z = P*V/(R*T)
Zall=roots([1 -1 A-B-B^2 -A*B]);
% use real roots only
        Zreal=[];
    for i=1:3
      if isreal(Zall(i))==1
            Zreal=[Zreal Zall(i)];
      end
    end

    %disp(Zreal)
% Select right root depending on phase
if     strcmp(Phase,'liquid')
```

```
    Z=min(Zreal);
elseif strcmp(Phase,'vapor')
    Z=max(Zreal);
else
    disp('error in specifying phase')
end


% Density (more precisely: molar volume)
MM = 0;
if strcmp(Phase,'liquid')%Correct liquid SRK-volume using Peneleoux...
    %correction
     c=0;
     for i=1:NC
     c=c+x(i) * (0.40768 * (0.29441 - ZRA(i)) * (R * Tc(i)) / (Pc(i))) ;
     end
   V = ((Z * R * T / P)- c);
     for i = 1:NC % Loop to calculate average Molar Mass
         MM = MM + x(i)*Mm(i);
     end

     RHO = MM/V;

else  % vapor
   V = Z * R * T / P;

    for i = 1:NC % Loop to calculate average Molar Mass
         MM = MM + x(i)*Mm(i);
    end

   RHO = MM/V; %Calculating the density
end
end
```

E.4 Optimization

By using the script for the optimization, Appendix E.4.1, the system is optimized. The optimization script calls the cost function, Appendix E.4.2, which is minimized while the constraints given by the constraint function, Appendix E.4.3, are satisfied. The script that calculates the performance of the system for a fixed flow rate is given in Appendix E.4.4.

E.4.1 Main Script

The *Optimization* script optimizes the system by minimizing the cost function, given in Appendix E.4.2, while satisfying the system constraints, given in Appendix E.4.3.

```
%%%%%%%%%%%%%%%%%%%%%%%%%%%%%%%%%%%%%%%%%%%%%%%%%%%%%%%%%%%%%%%%%%%%%%%%%%%%%%%
% Author: Torstein Bishop
%
% Department of Chemical Engineering, NTNU. Spring 2016.
%
%
%
% This is the main script for the optimization procedure. It calcukates
%
% the initial values and calls on the fmincon function for the
%
% optimization procedure. Fmincon will in addition call the cost function %
% and the constraint fucntion. The flow split is also called uppon.
%
%%%%%%%%%%%%%%%%%%%%%%%%%%%%%%%%%%%%%%%%%%%%%%%%%%%%%%%%%%%%%%%%%%%%%%%%%%%%%%%
clc
clear all
```

```
addpath('Deliquidizer')
addpath('GLCC')
tic

q_in = [220:1:280]/3600;%265/3600; %Inlet flow rate to system [m3/s]
xg_in = [0.4:0.01:0.6];%0.5; %Inlet gas volume fraction

L_U = 2.5; %Length upper part of GLCC [m]
L_L = 2.5; %Length lower part of GLCC [m]
R_G = 0.1016; %GLCC radius [m]
Dim.Ls=5;%1.5;  %Separator length [m]
Dim.Li = 1; %Length of inlet pipe [m]
Dim.Lt = Dim.Ls/2;%0.75; %Length of upper part of the separator [m]
Dim.Lb = Dim.Ls/2;% 0.75; %Length of lower part of the separator [m]
Dim.theta = 27; %Inclination angle of inlet pipe [degrees]
Dim.Rs=0.1016;%0.075; %Separator radius [m]
Dim.Ds = Dim.Rs*2; %Separator diameter [m]

Dim.D_in = 0.2032; % Diameter of inlet pipe [m]
Dim.A_in = pi*(Dim.D_in)^2/4;%0.4 %Cross-sectional area of inlet pipe [m2]
Dim.A_is = 0.25*Dim.A_in;%0.1; %Cross-sectional are of inlet slot [m2]
Dim.D_is = 2*sqrt(Dim.A_is/pi); % Diameter of inlet pipe slot [m]
GLCC_Param = [L_L,L_U,R_G]; %Parameter vector for GLCC

L_D = 1.5;% Length of GLCC [m]
R_Do = 0.075; %Deliquidizer radius [m]
R_Di = sqrt(4/5)*R_Do; %Radius for gas-extraction pipe [m]
Deliq_Param = [L_D,R_Do,R_Di]; %Paramter vector for deliq
CostG = 2;%0.30; %Cost of gas [$/m3]
CostO = 1;%313; %Cost of oil [$/m3]31.2


x=zeros(length(q_in),length(xg_in),8); %Array of state values
exitflag=zeros(length(q_in),length(xg_in)); %Matrix for the exitflag
Cost1=zeros(length(q_in),length(xg_in)); %Matrix of the cost
```

```
%output = zeros(length(q_in),length(xg_in));
options =optimset('Algorithm','sqp','Display','off');
A = [];b=[];Aeq=[];beq=[];%Empty linear ineguality and equality constraints

%% Calculating the density of the methane gas
% Filling in component data needed to calculate the density of the gas
% found from The properties of Gases and Liquids fifth edition.
compData.Pc = 45.99e5; % [Pa], Critical Pressure
compData.Tc = 190.56;  % [K], Critical Temperature
compData.w = 0.011;     % Acentric factor
compData.Cp = 0;       % Not used in any calculations yet
compData.Tref = 273.15; % [K]
compData.Mm = 16.043;   % [g/mol] Methane molar weight

P = 50e5; % [Pa] Pressure in separation system
T = 50+273; % [K] Assumed temperature in separation system
y = 1; % Assume only methane in gas phase

% Calling SRK-EOS for density calculations
[Z, RHO] = SRK(y, T, P, 'vapor', compData);

rhog=RHO; %kg/m^3, density for gas
rhoo=857;%881; %kg/m^3, density for oil

RHO = [rhog,rhoo]; %Vector of densities.

%% Optimalization proceedure
count = 0;

for i = 1:length(q_in)
    for j =1:length(xg_in)


         %Flow split calculations
        [q_t, q_b, x_ot, x_gb]=Flow_Split3(q_in(i), xg_in(j), RHO, Dim);
```

```
[xg_LPOGLCC(i,j),xo_HPOGLCC(i,j), ~, ~, q_LPOGLCC(i,j), q_HPOGLCC(i,j)]=...
 GLCC_comb(q_t,q_b, x_ot, x_gb, q_in(i),xg_in(j),Dim,RHO,1);


  xg_HPOGLCC(i,j) = 1-xo_HPOGLCC(i,j);


        %Defining the upper and lower bounds
        lb = [0.6;0;zeros(6,1)]; %Vector of lower bounds
        ub = [0.95;R_Di;zeros(6,1)]; %Upper bounds vector

        for k=3:length(ub) %Filling in the rest of the ub
            if mod(k,2) == 0; %Even numbers = gas fractions
                ub(k) = 1;
            else % Even numbers = flows
                ub(k) = q_in(i);
            end
        end

        %Checking for entrainment
        if x_ot==0 && x_gb==0
            x(i,j,:)=0;
            Cost1(i,j)=0;
            disp('No entrainment')
        else

        %Value of initial conditions
        x0 = [0.8;1E-4*R_Di; 0.8*q_LPOGLCC(i,j);xg_LPOGLCC(i,j);...
            0.2*q_LPOGLCC(i,j);xg_LPOGLCC(i,j);q_HPOGLCC(i,j);...
            xo_HPOGLCC(i,j)];

        p = [q_LPOGLCC(i,j);q_HPOGLCC(i,j);xg_LPOGLCC(i,j);...
            xg_HPOGLCC(i,j)]; %Parameter vector
```

```
        [x(i,j,:),Cost1(i,j),exitflag(i,j),output(i,j)] = fmincon(...
          @(x)Cost_Func(x,CostG,CostO),x0,A,b,Aeq,beq,lb,ub,...
          @(x)Opt_Constraints(x,p,Deliq_Param),options);

        if exitflag(i,j)==1 || exitflag(i,j)==2
            x0 = squeeze(x(i,j,:));
        end
        end

        count = count + 1
    end
end
Cost2 = -1*Cost1; %To get the maximum cost

%% Plots

FSvecqin = squeeze(x(:,11,1)); %Vector of the flow splits for xg_in=0.5

Q = q_in*3600;
figure (1)
set(gcf,'PaperPositionMode','auto')
plot(Q, FSvecqin,'b','LineWidth',1.5)
axis([220 280 0.90 0.96])
xlabel('Inlet flow rate,\it q_{in}\rm [m^{3}/h]','FontSize',12)
ylabel(' Flow Split,\it FS_{opt}','FontSize',12)

% CostVecqin = Cost2(:,11)*3600; %Vector of the cost [$/h] fo xg_in = 0.5
%
% figure (2)
% set(gcf,'PaperPositionMode','auto')
% plot(Q,CostVecqin)
% xlabel('Inlet flow rate,\it q_{in}\rm [m^{3}/h]','FontSize',12)
% ylabel('Gas profit [$/h]','FontSize',12)
%
```

```
xg_LPOoutqin = squeeze(x(:,11,4)); %Vector for gas in LPO out xg_in=0.5
xg_HPOoutqin = squeeze(x(:,11,8)); %Vector for gas in HPO out xg_in=0.5
xo_HPOoutqin = 1 - xg_HPOoutqin;

figure(3)
set(gcf,'PaperPositionMode','auto')
subplot(1,2,1)
plot(Q,xg_LPOoutqin,'b','LineWidth',1.5)
xlabel('Inlet flow rate,\it q_{in}\rm [m^{3}/h]','FontSize',12)
ylabel('\it \alpha_{LPO,S}','FontSize',14)
axis([220 280 0.90 1])

subplot(1,2,2)
plot(Q,xo_HPOoutqin,'b','LineWidth',1.5)
xlabel('Inlet flow rate,\it q_{in}\rm [m^{3}/h]','FontSize',12)
ylabel('\it \alpha_{o,HPO,S}','FontSize',14)
axis([220 280 0.75 1])


FSvecxgin = squeeze(x(46,:,1));% Flow split for qin=265

figure (4)
set(gcf,'PaperPositionMode','auto')
plot(xg_in, FSvecxgin,'b','LineWidth',1.5)
axis([0.4 0.6 0.90 0.96])
xlabel('\it \alpha_{in}','FontSize',14)
ylabel(' Flow Split,\it FS_{opt}','FontSize',12)

xg_LPOoutxgin = squeeze(x(46,:,4)); %Gas in LPO out at qin=265
xg_HPOoutxgin = squeeze(x(46,:,8)); %Gas in HPO out at qin=265
xo_HPOoutxgin = 1 - xg_HPOoutxgin;

figure(5)
set(gcf,'PaperPositionMode','auto')
subplot(1,2,1)
```

```
plot(xg_in,xg_LPOoutxgin,'b','LineWidth',1.5)
xlabel('\it \alpha_{in}','FontSize',14)
ylabel('\it \alpha_{LPO,S}','FontSize',14)
axis([0.4 0.6 0.90 1])

subplot(1,2,2)
plot(xg_in,xo_HPOoutxgin,'b','LineWidth',1.5)
xlabel('\it \alpha_{in}','FontSize',14)
ylabel('\it \alpha_{o,HPO,S}','FontSize',14)
axis([0.4 0.6 0.75 1])

%Plotting the fractions from unoptimized case
xg_LPODL_UnOpt = load('xg_LPODL_UnOpt.mat');
xg_HPOout_UnOpt = load('xg_HPOout_UnOpt.mat');


xg_LPODL_Unxgin = xg_LPODL_UnOpt.xg_LPODL(46,:); %qin = 265
xo_HPOout_Unxgin = 1-(xg_HPOout_UnOpt.xg_HPOout(46,:)); %qin = 265
xg_LPODL_Unqin = xg_LPODL_UnOpt.xg_LPODL(:,11); %xgin = 0.5
xo_HPOout_Unqin = 1-xg_HPOout_UnOpt.xg_HPOout(:,11); %xgin = 0.5

figure(6)
set(gcf,'PaperPositionMode','auto')
subplot(1,2,1)
plot(Q,xg_LPODL_Unqin,'r','LineWidth',1.5)
xlabel('Inlet flow rate,\it q_{in}\rm [m^{3}/h]','FontSize',12)
ylabel('\it \alpha_{LPO,S}','FontSize',14)
axis([220 280 0.90 1])

subplot(1,2,2)
plot(Q,xo_HPOout_Unqin,'r','LineWidth',1.5)
xlabel('Inlet flow rate,\it q_{in}\rm [m^{3}/h]','FontSize',12)
ylabel('\it \alpha_{o,HPO,S}','FontSize',14)
axis([220 280 0.75 1])
```

```
figure(7)
set(gcf,'PaperPositionMode','auto')
subplot(1,2,1)
plot(xg_in,xg_LPODL_Unxgin,'r','LineWidth',1.5)
xlabel('\it \alpha_{in}','FontSize',14)
ylabel('\it \alpha_{LPO,S}','FontSize',14)
axis([0.4 0.6 0.9 1])

subplot(1,2,2)
plot(xg_in,xo_HPOout_Unxgin,'r','LineWidth',1.5)
xlabel('\it \alpha_{in}','FontSize',14)
ylabel('\it \alpha_{o,HPO,S}','FontSize',14)
axis([0.4 0.6 0.75 1])

toc
```

E.4.2 Cost Function

The function *Cost_Fuc* contains the cost function of the optimization problem and is minimized by the main script.

```
function [ C ] = Cost_Func(x,CostG,CostO )
%This function contains the cost function for the optimization procedure
xg_LPODL = x(4);
q_LPODL = x(3);
q_HPOout = x(7);
xg_HPOout = x(8);

%C = -(CostG*xg_LPODL*q_LPODL + CostO*(1-xg_HPOout)*q_HPOout);
C = -(CostG*xg_LPODL + CostO*(1-xg_HPOout));
%C = (1-xg_LPODL) - xg_LPODL;
end
```

E.4.3 Constraints

The *Opt_Constraints* function determines the the equality and inequality constraints for the optimization problem. It include all the model equations as well as any additional inequality constraints that are explicitly set.

```
function [C,Ceq] = Opt_Constraints( x1,p,Deliq_Param)
%%%%%%%%%%%%%%%%%%%%%%%%%%%%%%%%%%%%%%%%%%%%%%%%%%%%%%%%%%%%%%%%%%%%%%%%%%%%%%%
% Author: Torstein Bishop
%
% Department of Chemical Engineering, NTNU. Spring 2016.
%
%
%
% This function calculates the non-linear equality and inequality
%
% constraints for the optimization. It calls on the functions RK4,
%
% RK4_GLCC, swirl_sep2_deliq, GLCC_LowerPart_Governing,
%
% GLCC_UpperPart_Governing, Deliquidizer and GLCC2.
%
%%%%%%%%%%%%%%%%%%%%%%%%%%%%%%%%%%%%%%%%%%%%%%%%%%%%%%%%%%%%%%%%%%%%%%%%%%%%%%%

FS = x1(1); %Deliq flow split
rin_D = x1(2); %Droplet inlet in deliquidizer

q_LPOGLCC = p(1); %LPO flow out of GLCC
q_HPOGLCC = p(2); %HPO flow out of Deliq
xg_LPOGLCC = p(3); %GVF out of LPO in GLCC
xg_HPOGLCC = p(4); %GVF out of HPO in GLCC
```

```
%% Deliquidizer
L_D = Deliq_Param(1);
R_Do = Deliq_Param(2);
R_Di = Deliq_Param(3);


q_LPODL = q_LPOGLCC*FS; %LPO in deliq
q_HPODL = q_LPOGLCC - q_LPODL; %HPO in deliq

ta=(pi*R_Di^2*L_D)/q_LPODL;
h_D=ta/10;%Amount of steps
in_D=[q_LPOGLCC,R_Do,R_Di,xg_LPOGLCC,ta,rin_D,FS];

[T,X]=RK4(@swirl_sep2_deliq,[0 ta],rin_D,h_D,in_D);

rout_D = X(end,1);

[xg_LPODL,xg_HPODL]=DeLiquidizer(q_LPOGLCC,xg_LPOGLCC,FS,rin_D,...
                                        Deliq_Param);

%% Oil product

q_HPOout = q_HPODL + q_HPOGLCC; %Oil stream out of separation system
xg_HPOout = (xg_HPOGLCC*q_HPOGLCC + xg_HPODL*q_HPODL)/q_HPOout;%outlet GVF


%% Constraints
Eq = [q_LPODL;xg_LPODL;q_HPODL;xg_HPODL;q_HPOout;xg_HPOout] - x1(3:8);

%Eq = [q_LPOGLCC;xg_LPOGLCC;q_HPOGLCC;xg_HPOGLCC;q_LPODL;xg_LPODL;...
%      q_HPODL; xg_HPODL; q_HPOout; xg_HPOout]-x1(5:14);

Ceq = [(R_Di-rout_D)/R_Di;Eq];
```

```
C = [];
end
```

E.4.4 Combined Separation System

The script *Combined* calculates the performance of the separation system for a fixed flow split, which is used as a comparison towards the performance of the optimized system.

```
%%%%%%%%%%%%%%%%%%%%%%%%%%%%%%%%%%%%%%%%%%%%%%%%%%%%%%%%%%%%%%%%%%%%%%%%%%%
% Author: Torstein Bishop
%
% Department of Chemical Engineering, NTNU. Spring 2016.
%
%
%
% A script that runs the combined system to generate values that can be
%
% compared to the values from the optimized values.
%
%%%%%%%%%%%%%%%%%%%%%%%%%%%%%%%%%%%%%%%%%%%%%%%%%%%%%%%%%%%%%%%%%%%%%%%%%%%

clc
clear all
addpath('Deliquidizer')
addpath('GLCC')
tic

%% Parameters for GLCC
Dim.Ls=5;%1.5;  %Separator length [m]
Dim.Li = 1; %Length of inlet pipe [m]
Dim.Lt = Dim.Ls/2;%0.75; %Length of upper part of the separator [m]
```

```
Dim.Lb = Dim.Ls/2;% 0.75; %Length of lower part of the separator [m]
Dim.theta = 27; %Inclination angle of inlet pipe [degrees]
Dim.Rs=0.1016;%0.075; %Separator radius [m]
Dim.Ds = Dim.Rs*2; %Separator diameter [m]

Dim.D_in = 0.2032; % Diameter of inlet pipe [m]
Dim.A_in = pi*(Dim.D_in)^2/4;%0.4 %Cross-sectional area of inlet pipe [m2]
Dim.A_is = 0.25*Dim.A_in;%0.1; %Cross-sectional are of inlet slot [m2]
Dim.D_is = 2*sqrt(Dim.A_is/pi); % Diameter of inlet pipe slot [m]

%% Calculating the density of the methane gas
% Filling in component data needed to calculate the density of the gas
% found from The properties of Gases and Liquids fifth edition.
compData.Pc = 45.99e5; % [Pa], Critical Pressure
compData.Tc = 190.56;  % [K], Critical Temperature
compData.w = 0.011;     % Acentric factor
compData.Cp = 0;       % Not used in any calculations yet
compData.Tref = 273.15; % [K]
compData.Mm = 16.043;   % [g/mol] Methane molar weight

P = 50e5; % [Pa] Pressure in separation system
T = 50+273; % [K] Assumed temperature in separation system
y = 1; % Assume only methane in gas phase

% Calling SRK-EOS for density calculations
[Z, RHO] = SRK(y, T, P, 'vapor', compData);

rhog=RHO; %kg/m^3, density for gas
rhoo=857;%881; %kg/m^3, density for oil

RHO = [rhog,rhoo]; %Vector of densities.

%% Calculations
q_in = [220:1:280];%265/3600; %Inlet flow rate to system [m3/s]
xg_in = [0.4:0.01:0.6];%0.5; %Inlet gas volume fraction
```

```
FS = 0.8;

q_t = zeros(length(q_in),length(xg_in)); %Empty q_t matrix
q_b = zeros(length(q_in),length(xg_in)); %Empty q_b matrix
x_ot = zeros(length(q_in),length(xg_in)); %Empty x_ot matrix
x_gb = zeros(length(q_in),length(xg_in)); %Empty x_gb matrix


count = 0;

n = 1;
for i = 1:length(q_in)
    for j = 1:length(xg_in)

% GLCC
[q_t(i,j), q_b(i,j), x_ot(i,j), x_gb(i,j)]=Flow_Split3(q_in(i)/3600 ...
                                                ,xg_in(j), RHO, Dim);

[xg_LPOGLCC(i,j),xo_HPOGLCC(i,j),GR(i,j),Esplit(i,j),q_LPOGLCC(i,j),q_HPOGLCC(i
 =GLCC_comb(q_t(i,j),q_b(i,j), x_ot(i,j), x_gb(i,j), ...
 q_in(i)/3600,xg_in(j),Dim,RHO,n);


xg_HPOGLCC(i,j) = 1-xo_HPOGLCC(i,j);

% Deliquidizer
[xg_LPODL(i,j),xg_HPODL(i,j),GRDL(i,j),EsplitDL(i,j),qenDL(i,j)]...
            = swirl_func3_deliq(xg_LPOGLCC(i,j),q_LPOGLCC(i,j),FS);

q_LPODL(i,j) = q_LPOGLCC(i,j)*FS;
q_HPODL(i,j) =  q_LPOGLCC(i,j) - q_LPODL(i,j);

% Oil product
q_HPOout(i,j) = q_HPODL(i,j) + ...
    q_HPOGLCC(i,j); %Oil stream out of separation system
```

```
xg_HPOout(i,j) = (xg_HPOGLCC(i,j)*q_HPOGLCC(i,j) +...
    xg_HPODL(i,j)*q_HPODL(i,j))/q_HPOout(i,j);%outlet GVF

count = count + 1
    end
end
```